

Original research

# ESE3/EHF, a promising target of rosiglitazone, suppresses pancreatic cancer stemness by downregulating CXCR4

Tianxing Zhou,<sup>1</sup> Jing Liu ,<sup>1,2</sup> Yongjie Xie,<sup>1</sup> Shuai Yuan,<sup>1</sup> Yu Guo,<sup>3</sup> Weiwei Bai,<sup>1</sup> Kaili Zhao,<sup>1</sup> Wenna Jiang,<sup>1</sup> Hongwei Wang,<sup>1</sup> Haotian Wang,<sup>1</sup> Tiansuo Zhao,<sup>1</sup> Chongbiao Huang,<sup>1</sup> Song Gao,<sup>1</sup> Xiuchao Wang,<sup>1</sup> Shengyu Yang,<sup>4</sup> Jihui Hao <sup>1</sup>

► Additional material is published online only. To view please visit the journal online (<http://dx.doi.org/10.1136/gutjnl-2020-321952>).

For numbered affiliations see end of article.

## Correspondence to

Professor Jihui Hao, Department of Pancreatic Cancer, Tianjin Medical University Cancer Institute and Hospital, Tianjin 300060, PR China; haojihui@tjmuch.com

TZ, JL and YX contributed equally.

Received 23 May 2020

Revised 2 February 2021

Accepted 20 February 2021

## ABSTRACT

**Background and aims** The crosstalk between cancer stem cells (CSCs) and their niche is required for the maintenance of stem cell-like phenotypes of CSCs. Here, we identified E26 transformation-specific homologous factor (EHF) as a key molecule in decreasing the sensitivity of pancreatic cancer (PC) cells to CSCs' niche stimulus. We also explored a therapeutic strategy to restore the expression of EHF.

**Design** We used a LSL-Kras<sup>G12D/+</sup> mice, LSL-Trp53<sup>R172H/+</sup> and Pdx1-Cre (KPC) mouse model and samples from patients with PC. Immunostaining, flow cytometry, sphere formation assays, anchorage-independent growth assay, in vivo tumorigenicity, reverse transcription PCR, chromatin immunoprecipitation (ChIP) and luciferase analyses were conducted in this study.

**Results** CXCL12 derived from pancreatic stellate cells (PSCs) mediates the crosstalk between PC cells and PSCs to promote PC stemness. Tumorous EHF suppressed CSC stemness by decreasing the sensitivity of PC to CXCL12 stimulus and inhibiting the crosstalk between PC and CSC-supportive niches. Mechanically, EHF suppressed the transcription of the CXCL12 receptor CXCR4. EHF had a cell autonomous role in suppressing cancer stemness by inhibiting the transcription of *Sox9*, *Sox2*, *Oct4* and *Nanog*. Rosiglitazone suppressed PC stemness and inhibited the crosstalk between PC and PSCs by upregulating EHF. Preclinical KPC mouse cohorts demonstrated that rosiglitazone sensitised PDAC to gemcitabine therapy.

**Conclusions** EHF decreased the sensitivity of PC to the stimulus from PSC-derived CSC-supportive niche by negatively regulating tumorous CXCR4. Rosiglitazone could be used to target PC stem cells and the crosstalk between CSCs and their niche by upregulating EHF.

## INTRODUCTION

Pancreatic ductal adenocarcinoma (PDAC) is a highly lethal tumour with aggressive clinical courses, poor prognosis and limited treatment options. Chemotherapy resistance and tumour relapse are still two unresolved problems in PDAC treatment.<sup>1,2</sup> Cancer stem cells (CSCs) contribute to PDAC recurrence and metastasis and cause resistance to chemotherapy.<sup>3-6</sup>

## Significance of this study

### What is already known on this subject?

- Pancreatic cancer (PC) is one of the leading causes of cancer-related death and is projected to become the second most lethal tumour by the year 2030.
- Cancer stem cells (CSCs) contributed to PC recurrence and metastasis.
- PC stemness is regulated by the aberrant activation of cell-intrinsic signal pathways and the crosstalk between CSCs and their niche.
- Patients with PC and low tumorous E26 transformation-specific homologous factor (EHF) expression gained poor overall and relapse-free survival.

### What are the new findings?

- Tumorous EHF decreased the sensitivity of PC to pancreatic stellate cell (PSC)-derived CXCL12 stimulus, which suppressed cancer stemness by inhibiting the crosstalk between PC and CSC-supportive niches.
- EHF transcriptionally suppressed CXCR4, which is the receptor of CXCL12.
- EHF also suppressed cancer stemness in a cell autonomous manner by transcriptionally suppressing *Sox9*, *Sox2*, *Oct4* and *Nanog*.
- Rosiglitazone suppressed PC stemness and inhibited the crosstalk between PC and PSCs by upregulating EHF.

### How might it impact on clinical practice in the foreseeable future?

- Our study identified that EHF suppressed cancer stemness from intrinsic and extrinsic pathways, which could be a promising target in PC therapy.
- Rosiglitazone could be used as a new therapeutic method in clinical practice to target pancreatic cancer stem cells and the crosstalk between CSCs and their niche.

CSCs are regulated by the aberrant activation of cell-intrinsic signal pathways, including NOTCH, WNT and STAT3 pathways, and the overexpression of OCT4, SOX2, NANOG, KLF4, c-MYC



© Author(s) (or their employer(s)) 2021. No commercial re-use. See rights and permissions. Published by BMJ.

**To cite:** Zhou T, Liu J, Xie Y, et al. *Gut* Epub ahead of print: [please include Day Month Year]. doi:10.1136/gutjnl-2020-321952

among others.<sup>3,7</sup> The recent insights into the complex nature of cancer stemness reveal that CSC phenotype is also regulated by cell-extrinsic factors derived from stromal cells.<sup>8–11</sup> The major cell types of PDAC stroma are pancreatic stellate cells (PSCs).<sup>9,12,13</sup> PSCs can secrete prostemness cytokines, such as interleukin (IL)-6, IL-8, tumour growth factor beta 1 (TGF- $\beta$ 1) and CXCL12, which form the CSC niche and participate in the active crosstalk with cancer cells within the tumour microenvironment.<sup>14–16</sup> The majority of anti-CSC therapeutic strategies focus on targeting cell-intrinsic stemness-associated genes. However, most of these genes are shared between CSCs and normal stem cells. Therefore, the side effect of anti-CSC therapy remains a major concern that restricts its clinical application.<sup>17</sup> Targeting the crosstalk between pancreatic cancer (PC) and its stemness-supporting niche may provide new therapeutic strategies for the prevention of PC progression.

Epithelium-specific E26 transformation-specific (ETS) factor family member 3 or ESE3/E26 transformation-specific homologous factor (EHF) is a member of the ETS gene superfamily.<sup>18</sup> Our previous work has demonstrated EHF as a tumour suppressor in PDAC. In PDAC, EHF promotes E-cadherin expression and suppresses epithelial–mesenchymal transition.<sup>19</sup> Furthermore, EHF deficiency induces the conversion and expansion of regulatory T cells (Treg) and myeloid-derived suppressor cells (MDSCs) by inhibiting TGF- $\beta$ 1 and granulocyte-macrophage colony stimulating factor (GM-CSF) secretion.<sup>20</sup> In prostate cancer, EHF plays a vital role in the inhibition of cell-intrinsic CSC signal by suppressing STAT3 and repressing the expression of TWIST1, ZEB2, BMI1 and POU5F1.<sup>21–23</sup> However, the role of EHF in pancreatic CSC regulation is not fully understood. Although the critical function of EHF has been verified in different tumour types,<sup>19–25</sup> no clinical and translational research involving EHF as a therapeutic target has been conducted.

In this study, we demonstrated that EHF could play a cell autonomous function and inhibit PDAC stemness by disrupting the crosstalk between CSCs and their PSC niche. Tumorous EHF decreased the sensitivity of PDAC to PSC-derived CXCL12 by repressing the CXCR4 expression. Moreover, we identified peroxisome proliferator-activated receptor gamma (PPAR- $\gamma$ ) ligand rosiglitazone as a promising suppressor of PDAC stemness by upregulating EHF.

## RESULTS

### Tumorous EHF is negatively correlated with stemness profiles in PDAC tissue

An immunohistochemical multiplex assay was conducted in archived tissues from a retrospective cohort of 93 patients with PDAC to examine the correlation between the expression of tumorous EHF and the proportion of pancreatic cancer stem cells (PCSCs). The frequencies of CD133<sup>+</sup> and aldehyde dehydrogenase 1 (ALDH1<sup>+</sup>) cells in the high-EHF group were significantly decreased compared with those in the low-EHF group (both  $p < 0.0001$ ; [figure 1A,B](#) and online supplemental figure S1A). Furthermore, fresh PDAC tissues from a prospective cohort of 39 patients were collected and analysed ([figure 1C](#)). As shown in [figure 1D–F](#) and online supplemental figure S1B, tumorous EHF IHC score was inversely correlated with the proportion of tumorous CD133<sup>+</sup>, ALDH1<sup>+</sup> and ESA<sup>+</sup>CD44<sup>+</sup>CD24<sup>+</sup> cells in the prospective cohort. These results confirmed the findings from the archived PDAC tissues. Therefore, our results suggested that tumorous EHF negatively correlated with stemness profiles in PDAC tissues. Besides, the clinical significance of EHF expression and PCSCs is shown in [figure 1G,H](#), online supplemental figure S1C–F and online supplemental tables S1 and S2).

### Tumorous EHF negatively regulates PC stemness

PDAC-EHF/short hairpin EHF (shEHF) cell lines were established (online supplemental figure S2A) to determine whether tumorous EHF regulated PDAC stemness. The percentage of CD44<sup>+</sup>CD24<sup>+</sup> cells in PDAC-EHF significantly decreased compared with that in the PDAC-vector control group ([figure 2A](#)). By contrast, the percentage of CD44<sup>+</sup>CD24<sup>+</sup> cells in PDAC-shEHF significantly increased compared with that of PDAC-scramble ([figure 2B](#)). Similarly, EHF negatively regulated the ALDH activity ([figure 2C,D](#)) and the proportions of CD133<sup>+</sup> cells ([figure 2E,F](#)). In vitro sphere formation assay demonstrated that EHF negatively regulated the cellular sphere formation capacity of PDAC ([figure 2G,H](#)). In in vivo limited dilution assay, the ectopic expression of EHF significantly reduced, whereas the knockdown of EHF increased the tumour incidence ([figure 2I](#)). This result suggested that EHF suppressed CSC stemness in PDAC. Quantitative PCR (Q-PCR) and western blot demonstrated that EHF negatively regulated stemness-related genes (*Sox9*, *Sox2*, *Oct4* and *Nanog*) ([figure 2J,K](#)) while increasing the expression of differentiation markers (online supplemental figure S2B). These findings were further confirmed in the other PC cell lines and two PDX cell lines (online supplemental figures S3 and S4). Chromatin immunoprecipitation (ChIP) analyses revealed that EHF directly bound to the promoter region of *Sox9*, *Sox2*, *Oct4* and *Nanog* ([figure 2L](#)).

### Tumorous EHF suppresses the crosstalk between PDAC and PSCs

PSCs can support PDAC stemness through paracrine mechanisms.<sup>16,26,27</sup> In vivo limited dilution assay was conducted to evaluate the role of tumorous EHF on the crosstalk between PDACs and PSCs. As shown in [figure 3A,B](#), the peritumorous injection of PSC-CM notably increased the tumour incidence in the PANC-1-vector group compared with that in the mice that received the control medium. However, the effect of PSC-CM was robustly suppressed in the PANC-1-EHF group.

PANC-1-vector, PANC-1-EHF, PANC-1-scramble and PANC-1-shEHF were incubated with the control medium or PSC-CM for 48 hours to determine whether EHF might regulate the crosstalk between PDAC cells and PSCs, and the proportions of CSCs were determined through flow cytometry. A PSC-CM stimulus could increase the proportion of CSC populations compared with those treated with the control medium ([figure 3C–H](#)). The abilities of PSC-CM to increase the CSC population were significantly enhanced by the short hairpin RNA knockdown of EHF and suppressed by the ectopic expression of EHF. Sphere formation and soft agar formation assays were also conducted. As shown in [figure 3I–L](#), the promoting effects of PSC-CM on the self-renewal and anchorage-independent growth of CSCs were inhibited by the ectopic expression of EHF and remarkably increased by EHF depletion. These results were confirmed in multiple PDAC cell lines (online supplemental figures S5 and S6). Therefore, our results indicated that tumorous EHF decreased the sensitivity of PDACs to PSC stimulus.

### Tumorous EHF abrogates the sensitivity of PDAC to PSC-derived CXCL12 stimulus

Blocking antibodies for cytokines secreted by PSCs were added to PSC-CM to identify the mechanism by which EHF regulated the PDAC–PSC crosstalk. CXCL12 was found to be the potential cytokine that induced the different reaction of PDACs to PSC-derived stimulus, depending on the EHF expression (online supplemental figure S7).

In in vivo limited dilution assay, CXCL12 notably increased the tumour incidence of PANC-1-vector group compared with that in the control medium group. However, the effect of CXCL12 was

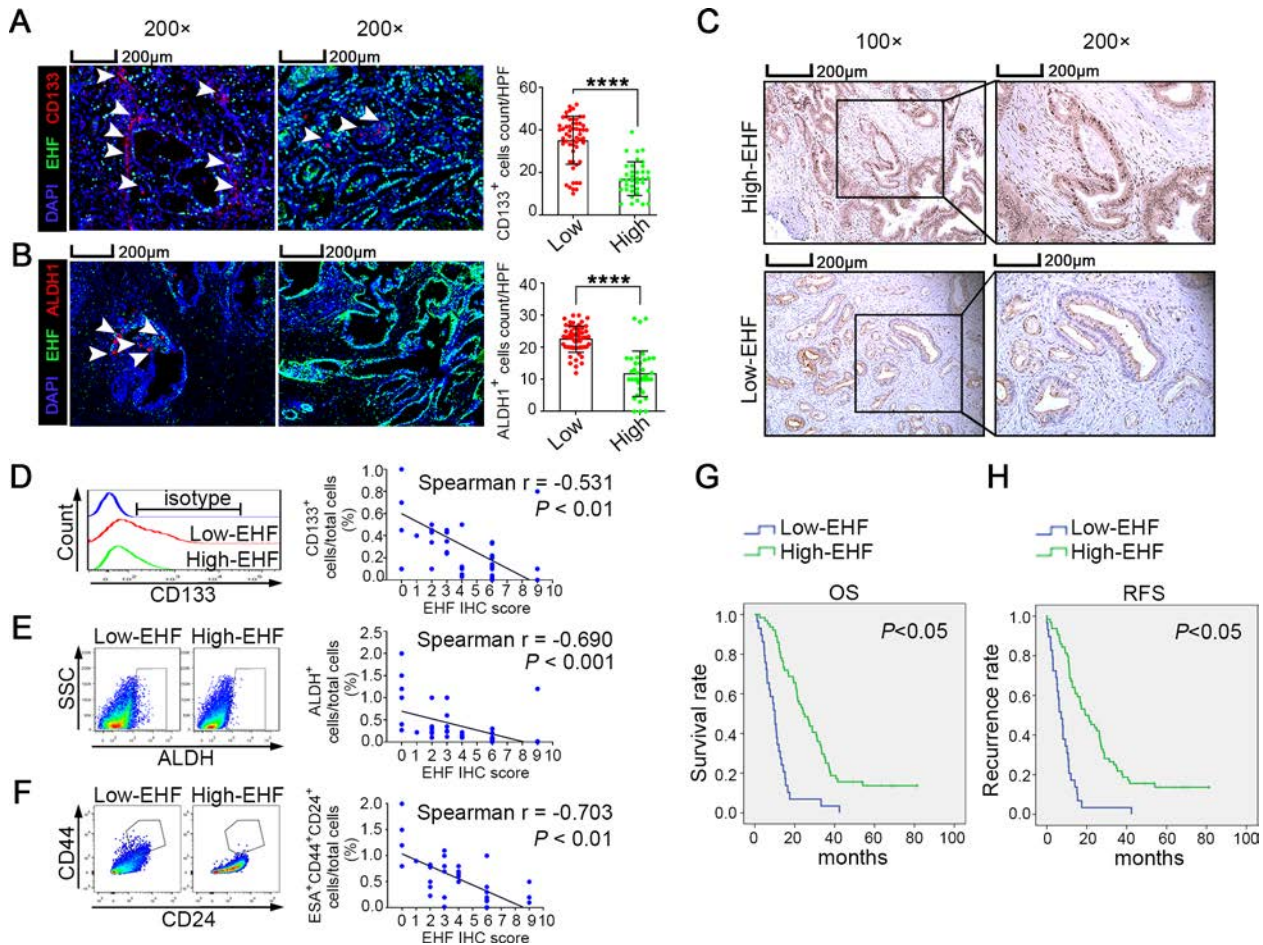


**Figure 1** Tumorous EHF is negatively correlated with stemness profiles in PDAC tissue. (A,B) Multiplex fluorescent IHC staining (left) of EHF expression and the accumulation of CD133<sup>+</sup> cells (A) and ALDH1<sup>+</sup> cells (B) in tumour tissues. The representative images from 93 pancreatic cancer cases are shown. The arrowheads indicate CD133<sup>+</sup> cells and ALDH1<sup>+</sup> cells. Bars, 200  $\mu$ m. Non-paired Student's t-test was used as statistical analysis;  $n=93$ , \*\*\*\* $p<0.0001$ . (C–F) Single-cell suspensions were prepared from 39 cases of fresh PDAC tissues and stained with ALDEFLUOR or specific antibodies against three CSC subsets (ALDH<sup>+</sup> cells, CD133<sup>+</sup> cells and CD44<sup>+</sup> CD24<sup>+</sup> cells). Representative IHC staining of EHF is shown (C). Bars, 200  $\mu$ m. Representative histogram and dot plots of CD133<sup>+</sup> cells (D, left), ALDH<sup>+</sup> cells (E, left) and CD44<sup>+</sup>CD24<sup>+</sup> cells (gated on ESA<sup>+</sup> epithelial cells; F, left). Spearman correlation analysis between EHF IHC score and the proportions of CD133<sup>+</sup> cells (D, right), ALDH<sup>+</sup> cells (E, right) and ESA<sup>+</sup>CD44<sup>+</sup>CD24<sup>+</sup> cells (F, right);  $n=39$ . Kaplan-Meier OS (G) and RFS (H) for different levels of EHF based on the log-rank statistic test ( $p<0.05$ ). Patients were divided into EHF-low and EHF-high groups based on the multiplex fluorescent IHC results. ALDH, aldehyde dehydrogenase; CSC, cancer stem cell; DAPI, 4',6-diamidino-2-phenylindole; EHF, E26 transformation-specific homologous factor; IHC, immunohistochemistry; OS, overall survival; PDAC, pancreatic ductal adenocarcinoma; RFS, relapse free survival; SSC, side scatter.

robustly suppressed in the PANC-1-EHF group (figure 4A,B). Then, the cell lines of PANC-1-vector, PANC-1-EHF, PANC-1-scramble and PANC-1-shEHF were treated with recombinant CXCL12 and the control medium. The CXCL12 treatment sharply increased the proportions of CSCs in low-EHF-expressing cell lines; the ectopic EHF overexpression remarkably suppressed the response to CXCL12 (figure 4C–H). Sphere formation and soft agar formation assays were also conducted. As shown in figure 4I–L, the CXCL12 treatment robustly increased tumour sphere formation and anchorage-independent growth, and the stimulating effects of CXCL12 were inhibited by the ectopic expression of EHF. Similar results were observed in other PDAC cell lines (online supplemental figures S8 and S9). Therefore, tumorous EHF abrogated the sensitivity of PDAC to the CXCL12 stimulus.

#### CXCR4 is transcriptionally repressed by EHF in PDAC

CXCR4 and CXCR7 are the receptors of CXCL12. Tumorous EHF did not regulate the secretion of CXCL12 in PSCs in

coculture experiments (online supplemental figure S10A,B), so we investigated whether EHF regulated the CXCR4/CXCR7 expression in PDACs. The expression of CXCR7 was not modulated by EHF (online supplemental figure S10C). Q-PCR, western blot and flow cytometry showed that the expression of CXCR4 was negatively regulated by EHF in the PDAC cell culture (figure 5A–D and online supplemental figure S11) and confirmed via western blot by using the harvested xenograft tumour tissues from the experiments in figure 2I (figure 5E). Importantly, the EHF expression was negatively correlated with the CXCR4 expression in human PDAC tumour tissues (figure 5F–I).

In silico analysis showed one high-confidence EHF-binding site (EBS) within the promoter region of CXCR4 in the JASPAR database (figure 5J,K). ChIP was conducted in the PANC-1 cell line and revealed that EHF markedly bound to the promoter of human CXCR4 (figure 5L). The luciferase analysis of PANC-1 and 293T showed that the EHF overexpression significantly

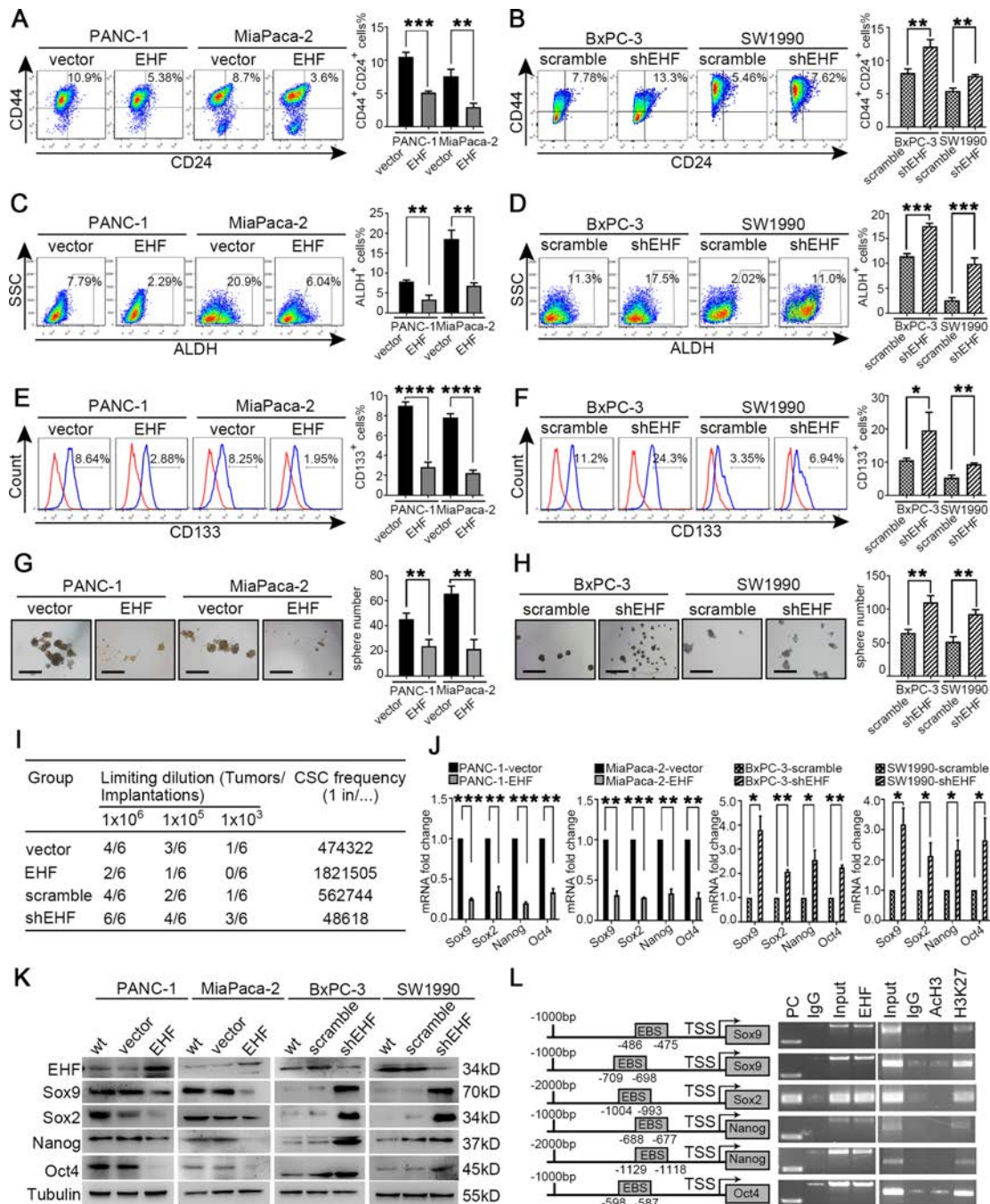


**Figure 2** Tumorous EHF negatively regulates pancreatic cancer stemness. (A,B) The proportion of CD44<sup>+</sup>CD24<sup>+</sup> cells in PANC-1-vector/EHF, MiaPaca-2-vector/EHF, BxPC-3-scramble/shEHF and SW1990-scramble/shEHF cells were analysed using flow cytometry. Representative dot plots (A, left; B, left) and percentage of CD44<sup>+</sup>CD24<sup>+</sup> cells (A, right; B, right) are shown. (C,D) The proportion of ALDH<sup>+</sup> cells in indicated cells were analysed using flow cytometry. Representative dot plots (C, left; D, left) and percentage of ALDH<sup>+</sup> cells (C, right; D, right) are shown. (E,F) The proportion of CD133<sup>+</sup> cells in indicated cells were analysed using flow cytometry. Representative histograms (E, left; F, left) and percentage of CD133<sup>+</sup> cells (E, right; F, right) are shown. (G,H) Sphere formation assays were performed in indicated cell lines. Representative images (G, left; H, left) and sphere number analysis (G, right; H, right) are shown. Bars:100  $\mu$ m. (I) In vivo limited dilution assays were performed to determine the effects of EHF overexpression or EHF depletion on CSC self-renewal of PANC-1 cells. Representative tumour incidence and CSC probabilities are shown. (J) Q-PCR on EHF and the stemness markers of Sox9, Sox2, Nanog and Oct4 were performed in indicated cells. Actin was used as internal control. (K) Western blot on EHF, Sox9, Sox2, Nanog and Oct4 were analysed in indicated cell lines.  $\beta$ -Tubulin was used as loading control. representative results are shown. (L) ChIP assay was performed to validate transcriptional regulation on Sox9, Sox2, Nanog and Oct4 by EHF. Predicted EBSs in the promoters of human Sox9, Sox2, Nanog and Oct4 (L, left). Binding of EHF to the promoters of the indicated genes in PANC-1 cells determined by ChIP (L, medium). IgG was used as negative control and anti-RNA polymerase II was used as PC. AcH3 and H3K27me3 occupancy on the identified EBSs in the promoters of the indicated genes in PANC-1 cells determined by ChIP (L, right). Representative results are shown. All experiments were repeated three times independently. Paired Student's t-test was used for statistical analysis. \*P<0.05, \*\*P<0.01, \*\*\*P<0.001, \*\*\*\*P<0.0001. ALDH, aldehyde dehydrogenase; ChIP, chromatin immunoprecipitation; CSC, cancer stem cell; EBS, EHF-binding site; EHF, E26 transformation-specific homologous factor; PC, positive control; Q-PCR, quantitative PCR; short hairpin EHF, shEHF; SSC, side scatter; TSS, transcriptional start site.

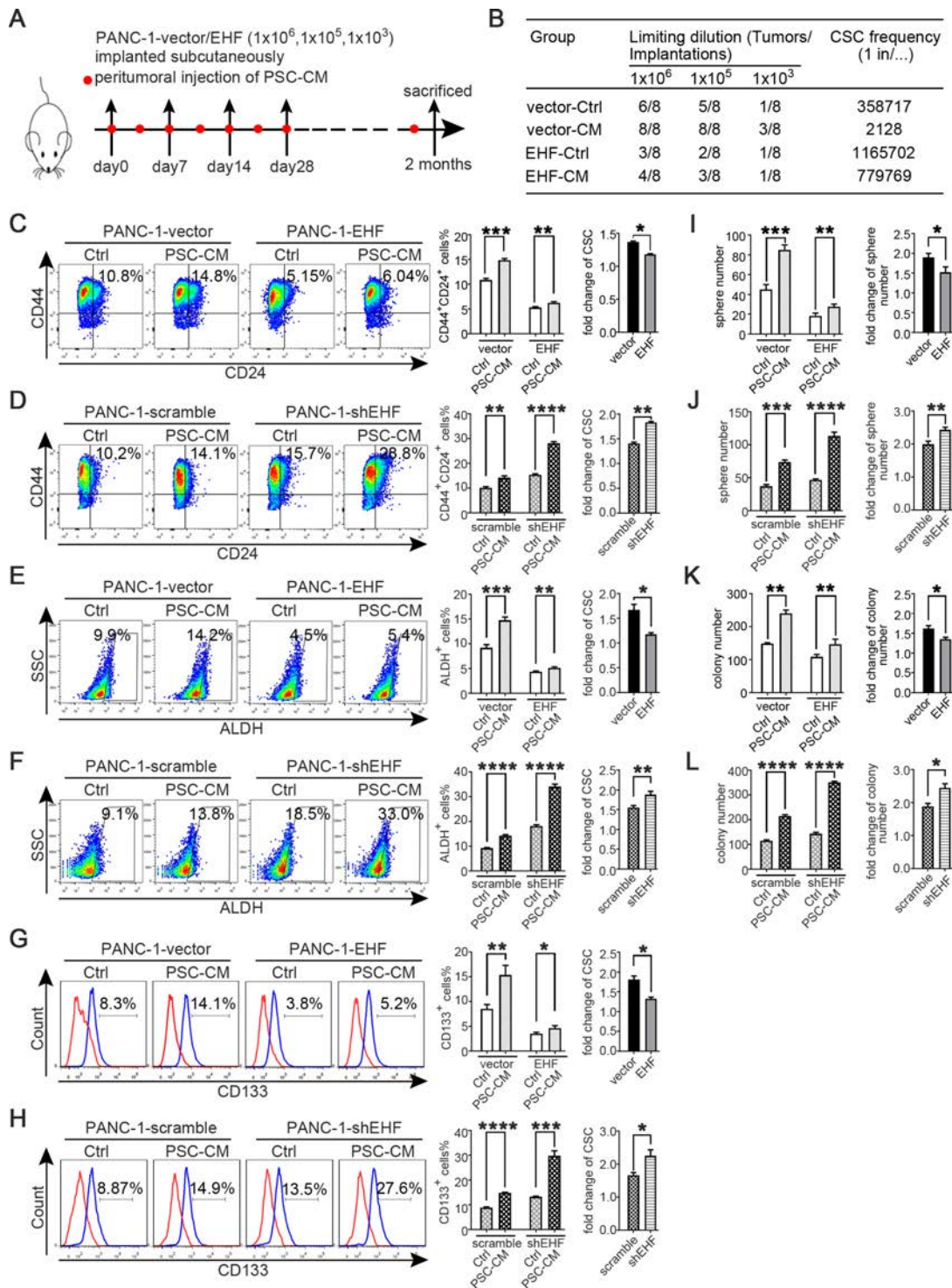


**Figure 3** Tumorous EHF suppresses the crosstalk between PDAC and PSCs. (A, B) In vivo limited dilution assay was performed to determine the effects of PSC-CM on CSC self-renewal of PANC-1-vector/EHF. Representative tumour incidence and CSCs probabilities are shown. All experiments were repeated three times independently. (C–H) PANC-1-vector, PANC-1-EHF, PANC-1-scramble and PANC-1-shEHF were cultured with PSC-CM or the Ctrl medium. The percentages of PCSCs in each cell line under each treatment are shown; the fold change of the percentage of PCSCs in each cell line after culturing with PSC-CM was calculated: (C, D) CD24<sup>+</sup>CD44<sup>+</sup> cells, (E, F) ALDH<sup>+</sup> cells and (G, H) CD133<sup>+</sup> cells. Representative dot plots/histogram (left), the statistical analysis of CSC percentage of each group (middle) and the statistical analysis of the fold change in each cell line (right). (I, J) Statistical analysis of the sphere number of each cell line under the treatment of serum-free medium and serum-free medium with PSC-CM added (left), statistical analysis of the fold change of sphere number after culturing with serum-free medium containing PSC-CM in each cell line (right). (K, L) Statistical analysis of the soft agar colony number of each cell line under the treatment of Ctrl medium and PSC-CM (left). Statistical analysis of the fold change of colony number after culturing with PSC-CM in each cell line (right). Paired Student's t-test was used for statistical analysis. \* $P < 0.05$ , \*\* $P < 0.01$ , \*\*\* $P < 0.001$ , \*\*\*\* $P < 0.0001$ . ALDH, aldehyde dehydrogenase; CM, conditioned medium; CSC, cancer stem cells; Ctrl, control; EHF, E26 transformation-specific homologous factor; PCSCs, pancreatic cancer stem cells; PDAC, pancreatic ductal adenocarcinoma; PSC, pancreatic stellate cell; shEHF, short hairpin EHF; SSC, side scatter.

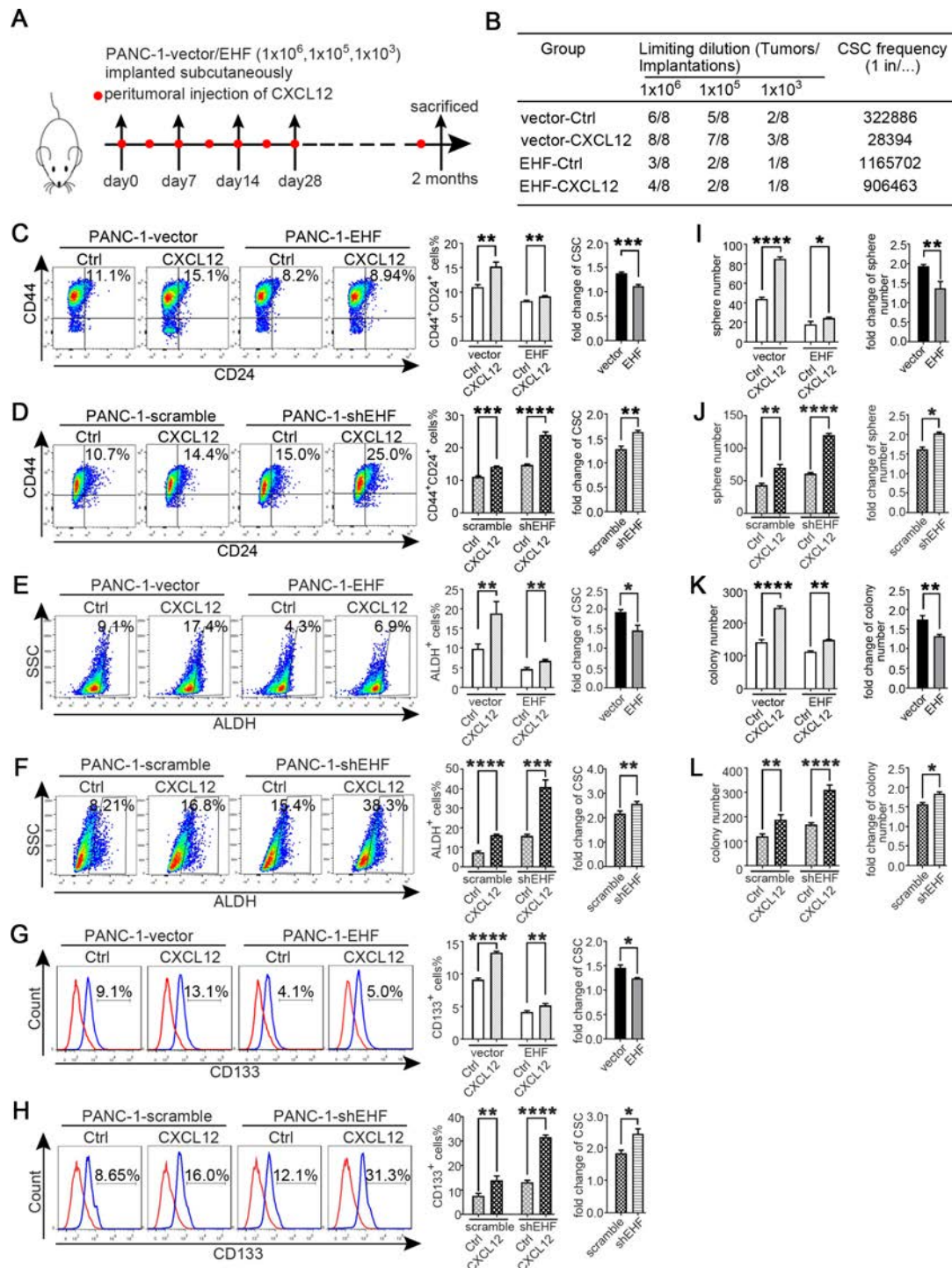


**Figure 4** Tumorous EHF abrogates the sensitivity of PDAC to PSC-derived CXCL12 stimulus. (A,B) In vivo limited dilution assay was performed to determine the effects of human recombinant CXCL12 on CSC self-renewal of PANC-1-vector/EHF. Ctrl medium was used as the control of CXCL12. Tumour incidence and CSC probabilities were shown. (C–H) PANC-1-vector, PANC-1-EHF, PANC-1-scramble and PANC-1-shEHF were cultured with medium containing CXCL12 or the Ctrl medium. The percentages of PCSCs in each cell line under each treatment are shown; the fold change of the percentage of PCSCs in each cell line after culturing with medium containing CXCL12 was calculated: (C,D) CD24<sup>+</sup>CD44<sup>+</sup> cells, (E,F) ALDH<sup>+</sup> cells and (G,H) CD133<sup>+</sup> cells. Representative dot plots/histogram (left), the statistical analysis of CSC percentage of each group (medium) and the statistical analysis of the fold change in each cell line (right). (I,J) Statistical analysis of the sphere number of each cell line under the treatment of serum-free medium and serum-free medium with CXCL12 added (left), statistical analysis of the fold change of sphere number after culturing with serum-free medium containing CXCL12 in each cell line (right). (K,L) Statistical analysis of the soft agar colony number of each cell line under the treatment of Ctrl medium and medium containing CXCL12 (left), statistical analysis of the fold change of colony number after culturing with medium containing CXCL12 in each cell line (right). All experiments were repeated three times independently. Paired Student's t-test was used for statistical analysis. \* $P < 0.05$ , \*\* $P < 0.01$ , \*\*\* $P < 0.001$ , \*\*\*\* $P < 0.0001$ . ALDH, aldehyde dehydrogenase; CSC, cancer stem cell; Ctrl, control; EHF, E26 transformation-specific homologous factor; PCSCs, pancreatic cancer stem cells; PDAC, pancreatic ductal adenocarcinoma; PSC, pancreatic stellate cell; shEHF, short hairpin EHF; SSC, side scatter.

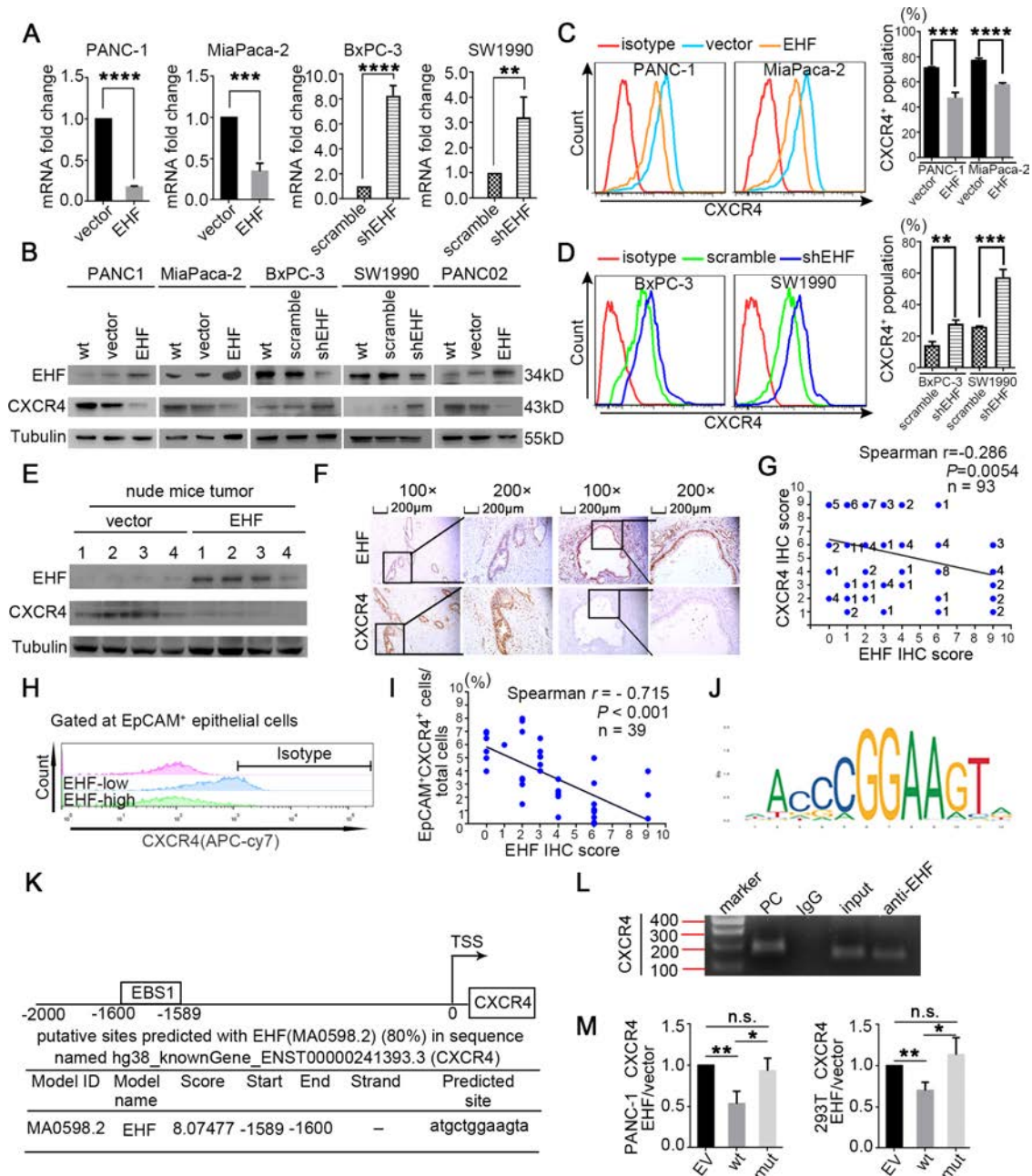


**Figure 5** CXCR4 is transcriptionally repressed by EHF in PDAC. (A) Q-PCR on CXCR4 mRNA were performed in indicated cell lines. Actin was used as internal control. (B) Western blot on EHF and CXCR4 proteins in indicated cell lines was performed. Representative results are shown. (C,D) Percentages of CXCR4<sup>+</sup> population in indicated cell lines were determined by flow cytometry. Representative histograms (C, left; D, left) and percentage of CXCR4<sup>+</sup> population (C, right; D, right) are shown. (E) Western blot on EHF and CXCR4 proteins in harvested mice subcutaneous tumour tissues (tumour tissues were from [figure 2I](#)).  $\beta$ -Tubulin was used as loading control. Representative results are shown. (F,G) Representative IHC images of EHF and CXCR4 expression using human PDAC tissue sections (n=93) (F). Bars, 200  $\mu$ m. Spearman rank correlation analysis was used to evaluate the correlation between tumorous EHF and CXCR4 expression (n=93) (G). The number at the right side of the plots represented the case number. (H,I) Single-cell suspensions were made from 39 cases of fresh PDAC tissues and stained with antibodies against CXCR4. Tumorous CXCR4<sup>+</sup> cells were determined by flow cytometry. Gated on EpCAM<sup>+</sup> cells to exclude non-epithelial cells. Representative histograms are shown (H). Spearman correlation analysis between EHF IHC score and the proportion of EpCAM<sup>+</sup>CXCR4<sup>+</sup> population are shown (I); n=39, p<0.001. (J) EHF scanned motif logo. (K) Predicted EBSs on the human CXCR4 promoter. Position relative to the transcription start site of CXCR4, EBS sequence and corresponding JASPAR score. (L) Binding of EHF to the promoter of CXCR4 was determined by chromatin immunoprecipitation. IgG was used as negative control. Anti-RNA polymerase II was used as positive control. Representative results are shown. (M) PANC-1 (left) and 293 T cells (right) were transfected with either vector control or pCDH-EHF in conjunction with the luciferase reporter pGL3-empty vector, pGL3-CXCR4-EBS1-wt or pGL3-CXCR4-EBS1-mut. Results were expressed as fold induction relative to that of the corresponding cells transfected with the control vector after normalisation of firefly luciferase activity according to Renilla luciferase activity. All experiments were repeated three times independently. Paired Student's t-test was used for statistical analysis. \*P<0.05, \*\*P<0.01, \*\*\*P<0.001, \*\*\*\*P<0.0001. EBS, EHF-binding site; EHF, E26 transformation-specific homologous factor; IHC, immunohistochemistry; n.s., not significant; PC, positive control; PDAC, pancreatic ductal adenocarcinoma; Q-PCR, quantitative PCR; shEHF, short hairpin EHF; wt, wild type.

decreased the transcription of CXCR4 (PANC-1,  $p=0.0065$ ; 293T,  $p=0.0061$ ) and the mutation of EBS1 substantially abrogated the trans-suppression of the CXCR4 promoter induced by EHF (PANC-1,  $p=0.3295$ ; 293T,  $p=0.4918$ ; [figure 5M](#)).

#### EHF decreases the sensitivity of PDACs to PSC-derived CSC-supporting stimulus by suppressing CXCR4

BxPC-3-scramble-scramble, BxPC-3-scramble-shCXCR4, BxPC-3-shEHF-scramble and BxPC-3-shEHF-shCXCR4 were established (online supplemental figure S12A,B) and treated with the control medium or PSC-CM to evaluate whether EHF decreased the sensitivity of PDACs to PSC-CM stimulus by suppressing CXCR4. As we previously observed, EHF depletion with shRNA increased the pro-CSC effects of PSC-CM ([figure 6A–C](#)). However, knocking down CXCR4 in BxPC-3-shEHF cells almost abrogated the effects of PSC-CM treatment ([figure 6A–C](#)). Similarly, the shRNA depletion of CXCR4 in PDAC cells abrogated the abilities of PSC-CM to promote the sphere formation of PDAC tumour ([figure 6D](#)). In vivo limited dilution assay demonstrated that PSC-CM significantly increased the CSC frequency in PDAC cells (from 1/779769 to 1/245406), and the effects of PSC-CM were dramatically enhanced after EHF knockdown (CSC frequency increased from 1/210828 in the 1640 group to 1/1443 in the PSC-CM group; [figure 6E](#)). Strikingly, CXCR4 knockdown abrogated the pro-CSC effects of the conditioned medium from PSC ([figure 6E](#)). Collectively, our data supported that tumorous EHF decreased the sensitivity of PDACs to PSC-derived CSC stimulus by suppressing the CXCR4 expression.

#### Identification of compounds that induce EHF overexpression

EHF is a promising therapeutic target of PDAC, so 190 compounds from a drug library in our laboratory were screened to determine their effects on regulating the EHF expression (online supplemental table S3 and online supplemental figure S13A). Among these 190 compounds, 14 could induce the EHF overexpression (online supplemental figure S13B). Considering the efficacy on the EHF upregulation and the safety profile, we chose rosiglitazone as a candidate for further studies. As shown in [figure 7A,B](#), rosiglitazone significantly induced the mRNA and protein expression of EHF in PDAC cells and PDX-derived PDAC cells in a concentration-dependent manner.

PPAR- $\gamma$  is a ligand-activated nuclear transcription factor. Rosiglitazone is a specific PPAR- $\gamma$  agonist that improves glycaemic control and insulin sensitivity in patients with diabetes by selectively activating PPAR- $\gamma$ . Computational analysis showed two high-confidence PPAR- $\gamma$  response elements (PPREs) corresponding to the promoter regions of EHF in the JASPAR database ([figure 7C,D](#)). ChIP primers were designed to investigate the binding site through the ChIP assay and evaluate whether PPAR- $\gamma$  directly bound to the promoter of EHF. As shown in [figure 7E](#), PPAR- $\gamma$  antibody could precipitate the PPRE sequence, which indicated the direct binding of PPAR- $\gamma$  to the EHF promoter. Luciferase analysis showed that rosiglitazone significantly increased the transcriptional activity of the EHF promoter ( $p=0.0423$ ), suggesting that rosiglitazone induced the EHF overexpression through PPAR- $\gamma$  activation ([figure 7F](#)).

#### Rosiglitazone inhibits PDAC stemness and suppresses the sensitivity to the stemness-promoting stimulus by upregulating the EHF expression

As shown in [figure 8A,B](#), rosiglitazone treatment inhibited the sphere formation capacity of PDACs and essentially blocked the

CXCL12-mediated increase in the sphere formation of PDAC tumour. This finding suggested that rosiglitazone could be used to abrogate CXCL12 and PSC-mediated PDAC CSC self-renewal. To rigorously evaluate this hypothesis, we performed in vivo limited dilution tumorigenicity assay. As shown in [figure 8C](#), rosiglitazone significantly reduced tumour initiation and CSC frequency. Moreover, no significant difference in tumour incidence could be observed in the PANC-1-CXCL12-rosiglitazone and PANC-1-ctrl-rosiglitazone groups. This result indicated that the stemness-promoting effect of CXCL12 was blocked by rosiglitazone. We also observed that rosiglitazone significantly decreased the percentage of the CXCR4<sup>+</sup> population in PDAC cells ([figure 8D](#)). In the orthotopic BALB/C tumour mouse model, the mice in the rosiglitazone group survived significantly longer than those in the dimethyl sulfoxide (DMSO) control group ( $p=0.031$ ; [figure 8E,F](#)). The normalised BLI in the rosiglitazone group was notably lower than that in the DMSO control group, suggesting that orthotopic tumour growth was inhibited ([figure 8G,H](#)). The harvested tumours from the orthotopic mouse model were analysed through flow cytometry. As shown in online supplemental figure S14A, rosiglitazone significantly decreased the proportion of ALDH<sup>+</sup> cells. Western blot and IHC indicated that rosiglitazone increased the expression of EHF and decreased the expression of stemness genes (online supplemental figure S14B,C).

EHF was knocked out in PANC-1, BxPC-3 and PANC02 cells via the CRISPR/dCas9 system to determine whether rosiglitazone inhibited the stemness of PDACs via the PPAR- $\gamma$ -EHF pathway (online supplemental figure S15). As shown in [figure 8I,J](#), EHF-KO could abrogate the abilities of rosiglitazone to inhibit tumour sphere formation. In the orthotopic tumour mouse model ([figure 8K–M](#)), rosiglitazone significantly reduced the tumour burden in the PANC02-vector group but not in the EHF-KO group. Importantly, rosiglitazone could improve survival in the vector control group but not in the EHF-KO group ([figure 8N](#)).

Ibuprofen and allopurinol, two other compounds that upregulated the EHF expression, could similarly suppress CSC stemness in PDAC (online supplemental figures S16 and S17).

#### Rosiglitazone sensitises PDAC to gemcitabine therapy in the KPC mouse model

Given the role of CSCs in chemotherapy resistance and the function of rosiglitazone on suppressing PDAC stemness, KPC mouse models were used to evaluate the therapeutic effects of gemcitabine plus rosiglitazone. When the tumour volumes reached 20–60 mm<sup>3</sup>, the KPC mice were randomised into four groups: vehicle, GEM, rosiglitazone and GEM plus rosiglitazone groups ([figure 9A](#) and online supplemental figure S18). Ultrasonic imaging showed that the tumour burdens significantly decreased in the GEM plus rosiglitazone group compared with those in the GEM group alone on day 30 ([figure 9B](#)). Consistently, GEM plus rosiglitazone reduced the weight of pancreas compared with that of GEM monotherapy ([figure 9C](#)). The proportion of ALDH<sup>+</sup> cells significantly decreased when rosiglitazone was administered ([figure 9D,E](#)). The IHC of ki-67 indicated that GEM plus rosiglitazone combination therapy more significantly reduced cancer cell proliferation compared with that with GEM monotherapy ([figure 9F,G](#)). The western blot of pancreatic tumour tissues from the KPC mice further confirmed that rosiglitazone could induce the expression of EHF and suppress the expression of stemness marker genes ([figure 9H](#)). Finally, obvious survival benefits were observed in the GEM plus rosiglitazone group compared with

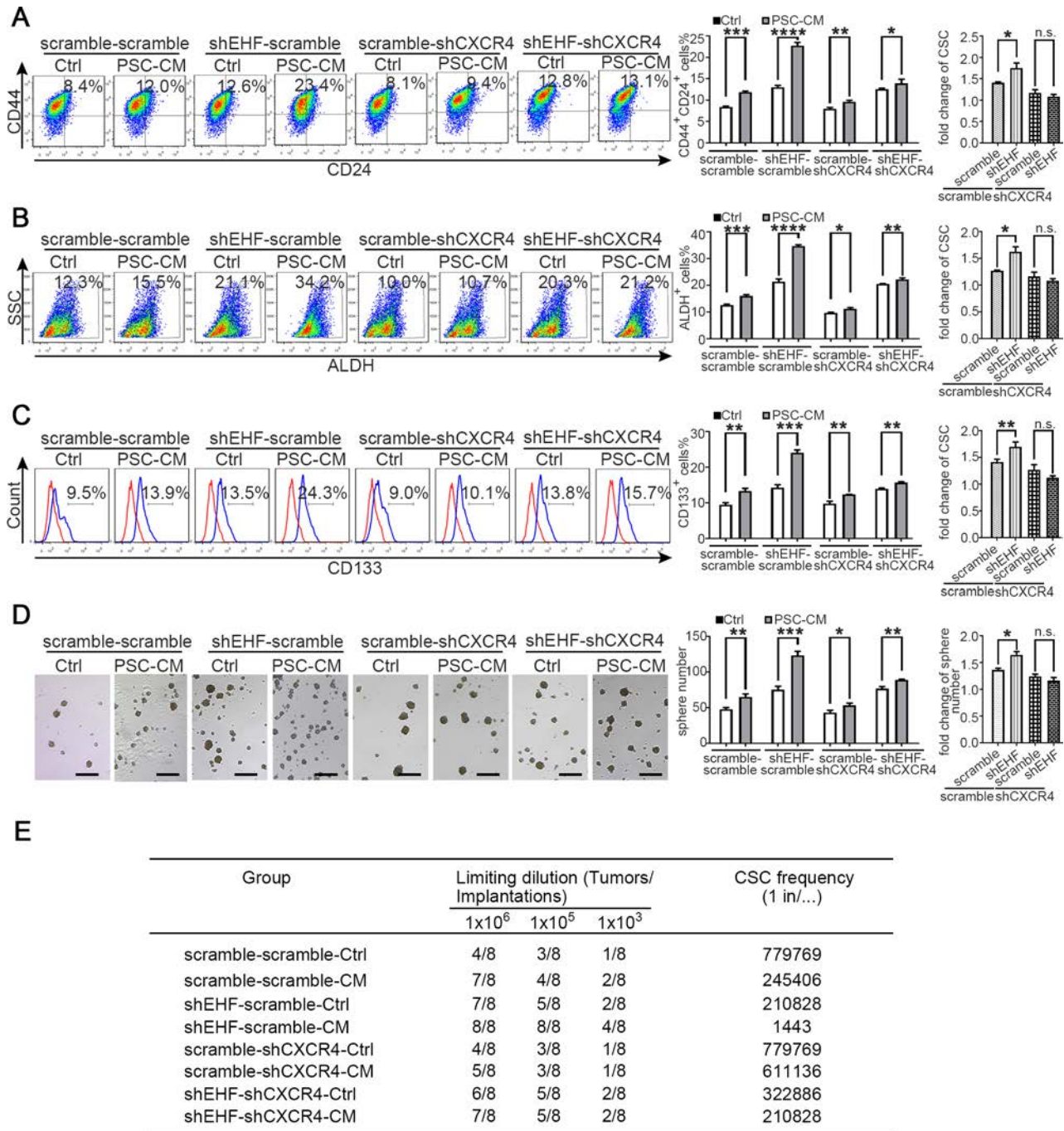


**Figure 6** EHF decreases the sensitivity of PDACs to PSCs derived CSC-supporting stimulus by suppressing CXCR4. (A–C) BxPC-3-scramble/shEHF-scramble and BxPC-3-scramble/shEHF-shCXCR4 were cultured with PSC-CM or the Ctrl medium. The percentages of PCSCs in each cell line under each treatment are shown; the fold change of the percentage of PCSCs in each cell line after culturing with PSC-CM was calculated: (A) CD24<sup>+</sup>CD44<sup>+</sup> cells, (B) ALDH<sup>+</sup> cells, (C) CD133<sup>+</sup> cells. representative dot plots/ histogram (left), the statistical analysis of CSC percentage of each group (medium) and the statistical analysis of the fold change in each cell line (right). (D) Statistical analysis of the sphere number of each cell line under the treatment of serum-free medium and serum-free medium with PSC-CM added (left), statistical analysis of the fold change of sphere number after culturing with serum-free medium containing PSC-CM in each cell line (right). (E) In vivo limited dilution assay was performed to determine the effects of PSC-CM on CSC self-renewal of BxPC-3-scramble/shEHF-scramble and BxPC-3-scramble/shEHF-shCXCR4. Tumour incidence and CSCs probabilities are shown. All experiments were repeated three times independently. Paired Student's t-test was used for statistical analysis. \*P<0.05, \*\*P<0.01, \*\*\*P<0.001, \*\*\*\*P<0.0001. ALDH, aldehyde dehydrogenase; CM, conditioned medium; CSC, cancer stem cell; Ctrl, control; EHF, E26 transformation-specific homologous factor; n.s., non-significant; PDAC, pancreatic ductal adenocarcinoma; PSC, pancreatic stellate cell; SSC, side scatter.

those in the GEM group (figure 9I). Therefore, rosiglitazone suppressed PC stemness and could be used as a new therapeutic method in the clinical practice of PDAC treatment (figure 10).

## DISCUSSION

CSCs play a significant role in disease recurrence and treatment failure in PC. The crosstalk between CSCs and its niche is

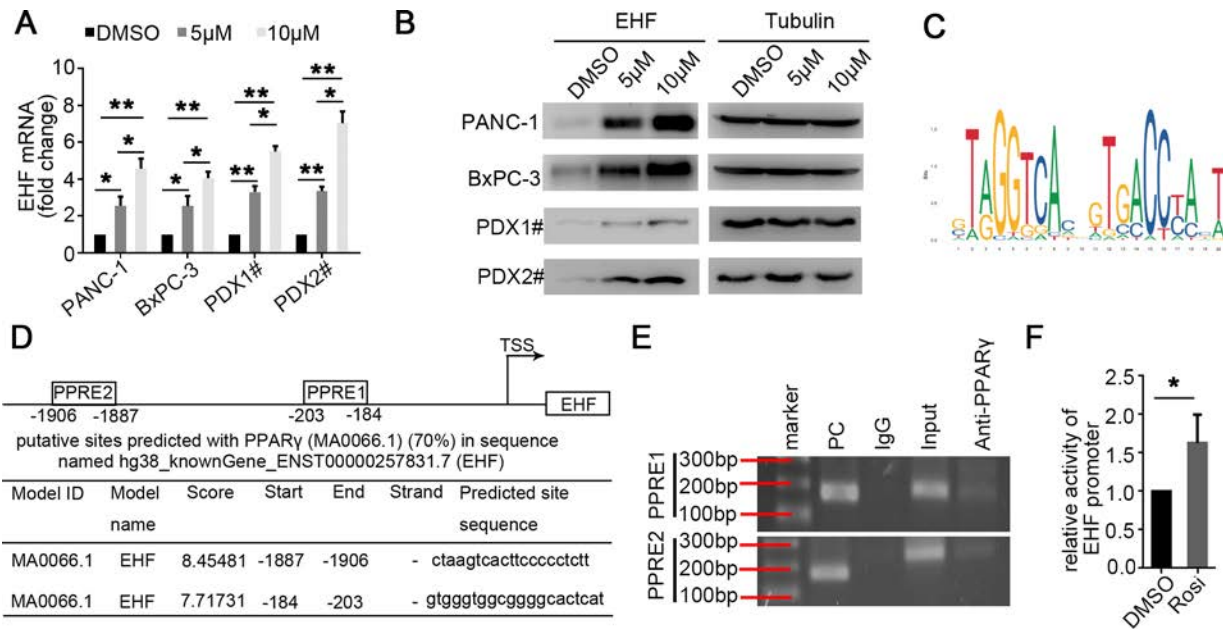


**Figure 7** Identification of compounds that induce EHF overexpression. (A,B). PANC-1, BxPC-3 and two primary cancer cell lines PDX1# and PDX2# were treated with rosiglitazone (5 and 10 µM, 24 hours). DMSO was used as control. (A) Q-PCR was conducted to detect for EHF mRNA expression. (B) Western blot for EHF expression was performed. Representative results are shown. (C) PPAR-γ-scanned motif logo (D) predicted PPREs on the human EHF promoter. position relative to the transcription start site of Ehf, PPRE sequences and corresponding JASPAR scores. (E) binding of PPAR-γ to the promoter of EHF was determined by chromatin immunoprecipitation. IgG was used as negative control. Anti-RNA Polymerase II was used as positive control. representative results were shown. (F) The promoter activity of EHF after treated with rosiglitazone. PANC-1 transfected with either luciferase reporter pGL3-empty vector or wild type pGL3-ESE3/EHF promoter were treated with rosiglitazone (10 µM, 24h). Forty-eight hours later, cells were collected for dual luciferase assay. results were expressed as fold induction relative to those of the corresponding cells transfected with pGL3-empty vector after normalisation of firefly luciferase activity according to Renilla luciferase activity. All experiments were repeated three times independently. Paired Student's t-test was used as statistical analysis. \* $p < 0.05$  and \*\* $p < 0.01$ . DMSO, dimethyl sulfoxide; EHF, E26 transformation-specific homologous factor; PC, positive control; PPRE, PPAR-γ response element; PPAR-γ, peroxisome proliferator-activated receptor gamma; Q-PCR, quantitative PCR; TSS, transcriptional start site.

essential for stemness maintenance, cancer initiation and progression.<sup>3, 28</sup> Seino *et al*<sup>29</sup> revealed that cancer-associated fibroblasts transmit a protumorigenic niche signal to PDACs through the juxtacrine production of stromal Wnt ligands. Öhlund *et al*<sup>30</sup> reported that tumour organoids need PSC-secreted ligands for surviving. Our study supported that the cytokines IL-6, IL-8 and CXCL12 secreted by PSCs significantly increase the cancer stemness of PDAC.<sup>30-32</sup> A PSC-derived CSCs niche shows potential for applications that promote cancer stemness, so targeting the crosstalk between CSCs and PSCs can be an efficient modality for the prevention of tumour recurrence.

EHF is a member of a highly diverse ETS superfamily. Our group first demonstrated EHF as a tumour suppressor that directly inhibits PDAC progression by upregulating E-cadherin while downregulating TGF-β1 and GM-CSF.<sup>19, 20</sup> The role of EHF in CSCs regulation was first identified in prostate cancer. Albino *et al*<sup>33</sup> reported that EHF directly controls the activity of the Lin28/let-7 axis, a key pathway involved in CSC expansion. EHF also represses the expression of the key CSC genes TWIST1, ZEB2, BMI1 and POU5F1.<sup>23</sup> Furthermore, the loss of EHF leads to the upregulation of IL-6 and the activation of the JAK/STAT3 pathway.<sup>21</sup> Our data indicated that EHF not only plays a cell autonomous role in regulating CSC stemness but also has important functions in regulating the sensitivity to a pro-CSC stimulus from the PSC niche.

PSCs within the tumour microenvironment represent the principal source of CXCL12, which binds to its two receptors, CXCR4 and CXCR7, to activate a number of signalling pathways

in PC cells, such as the PKCα/NFκB, MAPK, PI3K-Akt-mTOR and JAK/STAT pathways.<sup>34, 35</sup> Moreover, Hermann *et al*<sup>6</sup> defined a subpopulation of migrating CSCs that are characterised by the expression of the CXCR4 receptor and critically involved in tumour metastasis. Khan *et al*<sup>16</sup> reported that CXCR4/CXCL12 and hedgehog signalling pathways mediate the chemoresistance of PC cells on coculturing with PSCs. We found that tumorous EHF repressed the CXCR4 expression but not the CXCR7 expression. ChIP and dual-luciferase assays revealed that EHF directly bound to the promoter regions of CXCR4 to suppress its transcription. Our blocking experiment revealed that EHF decreased the sensitivity of cancer cells to the PSC stimulus by repressing the CXCR4 expression.

Our findings suggested that restoring the CSC-suppressing functions of EHF could be a promising approach in PDAC treatment. Here, we screened 190 compounds from our drug library on the basis of their effects on the EHF expression. These 190 compounds are commonly used drugs in clinical work and easily obtained. Rosiglitazone, a high-affinity synthetic agonist for nuclear PPAR-γ, was identified as the most potent activator of the EHF expression with limited side effects. On activation with specific ligands, PPAR-γ binds to PPREs, which then mediate the target gene expression.<sup>36</sup> Recently, studies have indicated that rosiglitazone and related thiazolidinediones may play inhibitory roles in various types of cancer cells, including PC, such as enhancing radiosensitivity,<sup>37</sup> reducing immune suppression<sup>38</sup> and inhibiting cell invasion and metastasis.<sup>39-41</sup> In our current work, rosiglitazone-activated PPAR-γ bound to the promoter

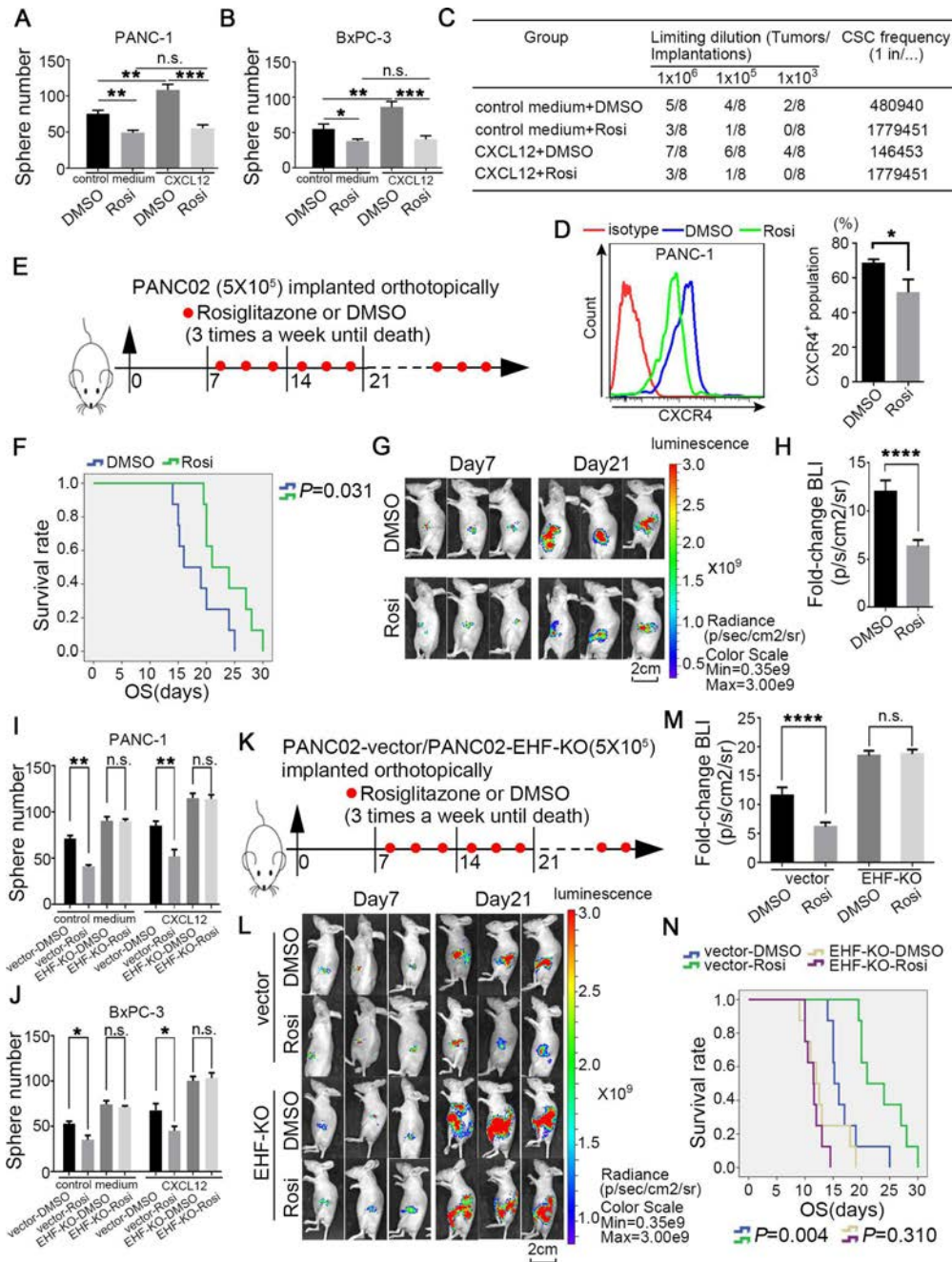


**Figure 8** Rosiglitazone inhibits PDAC stemness and suppresses the sensitivity to the stemness-promoting stimulus by upregulating the EHF expression. (A,B) Adherent cells were pretreated with 5  $\mu$ M rosiglitazone for 48 hours, and then cells were collected and cultured with serum-free medium containing 100 ng/mL human recombinant CXCL12 in low-adherent six-well plates. Representative results are shown (PANC-1, A; BxPC-3, B). (C) In vivo limiting dilution assays were performed to determine the effects of rosiglitazone on CSC self-renewal of PANC-1 cells with or without CXCL12 stimulus. Tumour incidences and CSCs probabilities are shown. (D) Rosiglitazone reduced the percentage of CXCR4<sup>+</sup> population (5  $\mu$ M, 24 hours). representative results are shown. (E) Schematic illustration for in vivo rosiglitazone therapeutic experiment in an orthotopic mice model. (F) Kaplan-Meier survival curves with log-rank test (PANC02-DMSO vs PANC02-rosiglitazone  $p=0.031$ ). (G,H) Representative bioluminescent images of two groups on days 7 and 21 after tumour implantation (G). Statistical analysis of the fold change of BLI after drug treatment (BLI on day 21 to BLI on day 7; H) ( $n=8$  per group). (I,J) Adherent PDAC-vector/EHF-KO cells were pretreated with 5  $\mu$ M rosiglitazone for 48 hours; and then cells were collected and cultured with serum-free medium with or without 100 ng/mL human recombinant CXCL12 in low-adherent six-well plates for the following sphere formation assays. Sphere number analysis was shown (PANC-1, I; BxPC-3, J). (K) Schematic illustration for in vivo rosiglitazone therapeutic experiment using PANC02-vector/EHF-KO cell lines in an orthotopic mice model. (L,M) Representative bioluminescent images of the two groups on days 7 and 21 after tumour implantation are shown (L). Statistical analysis of the fold change of BLI after drug administration (BLI on day 21 to BLI on day 7, M) ( $n=8$  per group). (N) Kaplan-Meier survival curves with log-rank test were used to analyse the different effect after treating with DMSO and rosiglitazone. All experiments were repeated three times independently. Paired Student's t-test was used for statistical analysis for in vitro experiments and unpaired Student's t-test was used for animal experiments. \* $P<0.05$ , \*\* $P<0.01$ , \*\*\* $P<0.001$ , \*\*\*\* $P<0.0001$ . BLI, bioluminescent intensity; CSC, cancer stem cell; DMSO, dimethyl sulfoxide; EHF, E26 transformation-specific homologous factor; KO, knock out; n.s., non-significance; PDAC, pancreatic ductal adenocarcinoma.

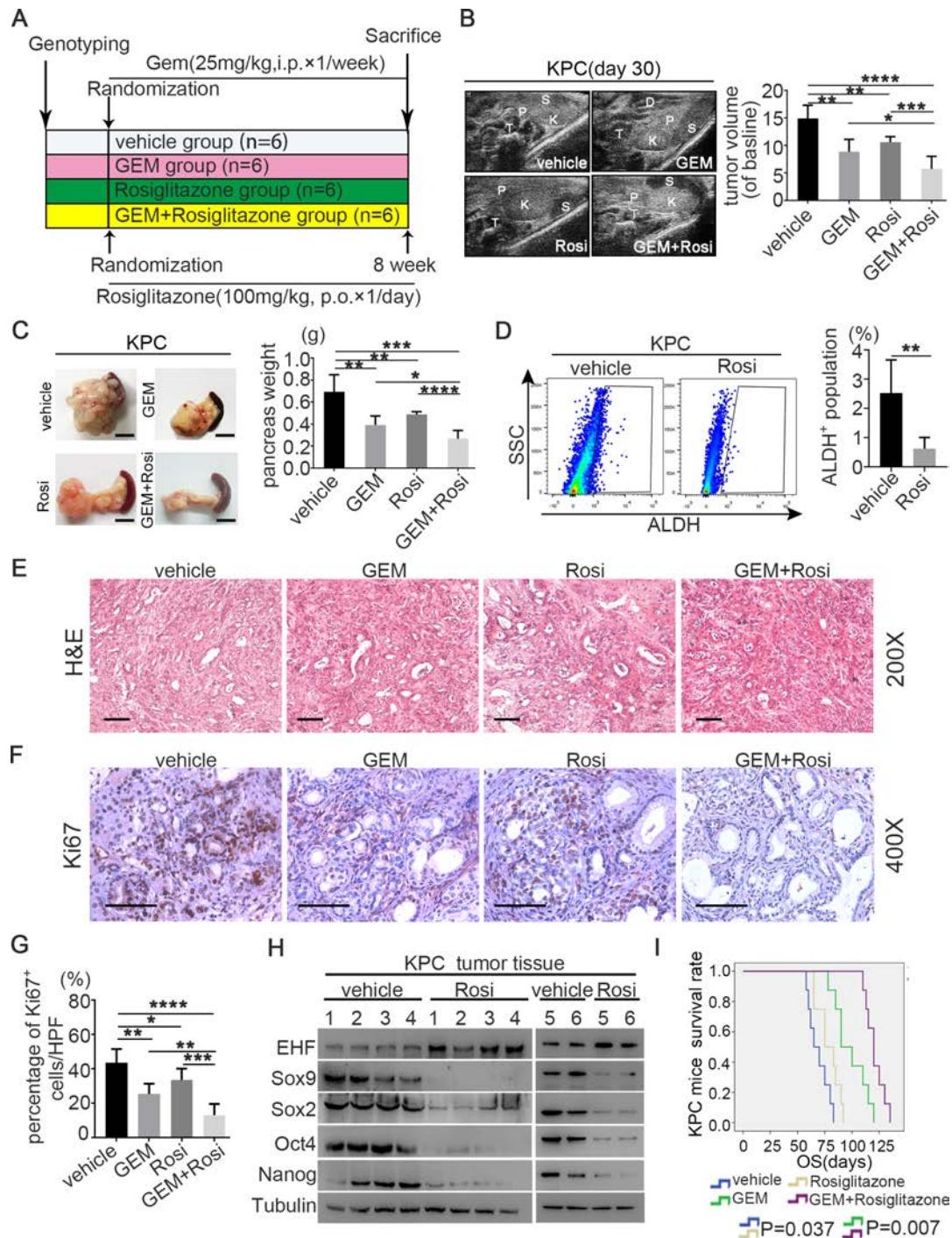


**Figure 9** Rosi sensitises PDAC to gemcitabine therapy in the KPC mouse model. (A) Experimental design programme. (B) Representative ultrasound images of KPC mice treated with vehicle (n=6), GEM (n=6), Rosi (n=6) and GEM+Rosi (n=6) at day 30 after drug treatment (left). Pancreatic T, P, S, K and D. Statistical analysis for the fold change of pancreatic T volumes measured by ultrasound system at day 30 after drug treatment (volumes in day 0 were used as baseline) (right). (C) Representative macroscopic images of pancreatic T in KPC mice treated with vehicle, GEM, Rosi and GEM+Rosi after sacrifice (left). Statistical analysis for P weight of KPC mice from different groups (right). (D) Rosi reduced the percentage of ALDH<sup>+</sup> population in PDAC in the KPC model. PI was used to exclude dead cells; CD45 was used to exclude leucocytes; and DEAB was used as negative control. Representative dot plots (left) and statistical analysis (right) are shown. (E) Representative images of H&E slides from tumours of four groups. Scale bars: 200  $\mu$ m. (F) Representative images of KPC pancreatic tumour IHC for Ki-67 staining. Scale bars: 400  $\mu$ m. (G) Statistical analysis for percentage of Ki-67-positive cells in different groups. (H) Protein expression of EHF and stemness markers (SOX9, Sox2, Nanog and Oct4) were detected in pancreatic T tissues of KPC mice by western blot. Tubulin was used as loading control. Representative results are shown. (I) Kaplan-Meier survival curves with log-rank test for KPC mice treated with vehicle (n=8), GEM (n=8), Rosi (n=8) and GEM+Rosi (n=8). The mouse experiments were repeated three times independently, and non-paired Student's t-test was used for statistical analysis. \*P<0.05, \*\*P<0.01, \*\*\*P<0.001, \*\*\*\*P<0.0001. ALDH, aldehyde dehydrogenase; D, duodenum; DEAB, diethylamino benzaldehyde; EHF, E26 transformation-specific homologous factor; GEM, gemcitabine; K, kidney; OS, overall survival; P, pancreas; PDAC, pancreatic ductal adenocarcinoma; PI, propidium iodide; Rosi, rosiglitazone; S, spleen; SSC, side scatter; T, tumour.

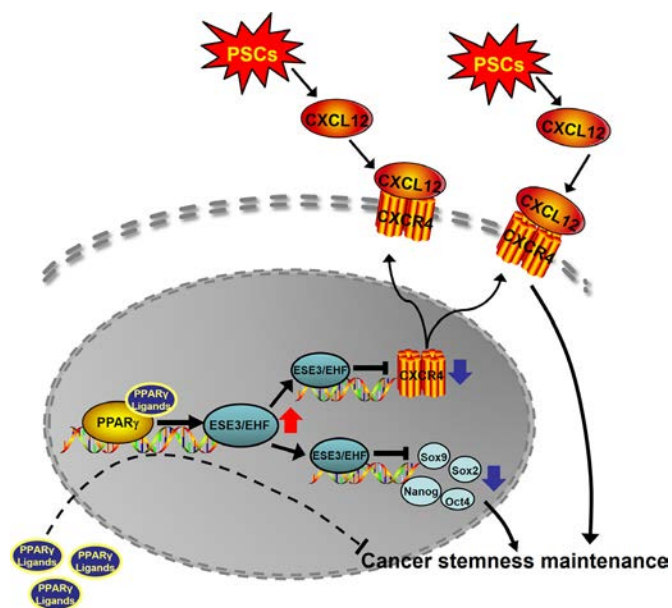


**Figure 10** Schematic of the research. ESE3/EHF regulated PDAC CSCs property through cell-intrinsic and extrinsic pathway. Rosiglitazone suppressed PC stemness and inhibited the cross-talk between PC and PSCs by upregulating ESE3/EHF. CSC cancer stem cell; EHF, E26 transformation-specific homologous factor; PC, positive control; PDAC, pancreatic ductal adenocarcinoma; PPAR- $\gamma$ , peroxisome proliferator-activated receptor gamma; PSC, pancreatic stellate cell.

region of EHF and upregulated its expression. In vivo and in vitro studies demonstrated that rosiglitazone decreased the sensitivity of PDAC to PSCs' stimulus and inhibited tumour stemness properties by inducing tumorous EHF expression. Our results suggested that the effects of rosiglitazone on EHF upregulation could be translated into the development of targeted therapy against cancer stemness.

Our study first reported that EHF suppressed cancer stemness from intrinsic and extrinsic pathways. For the intrinsic pathway, EHF repressed the expression of SOX9, SOX2, OCT4 and Nanog. For the extrinsic pathway, EHF decreased the sensitivity of PDACs to the stimulus from the PSC-derived CSC-supportive niche by negatively regulating the tumorous CXCR4 expression. Conceivably, rosiglitazone could be used to target pancreatic stem cells and the crosstalk between CSCs and its niche by upregulating EHF.

## MATERIALS AND METHODS

### Patient and sample collection

A total of 93 sequential PDAC tissues were retrospectively collected from patients who received radical surgery R0 resection at the Tianjin Medical University Cancer Institute and Hospital from July 2011 to January 2015. The follow-up rate was 100% until the last follow-up on 23 October 2019. Then, 39 consecutive cases of fresh PDAC tissues were prospectively collected during operation from January 2018 to November 2019.

### Primary human PC cells

Human pancreatic tumours were obtained during surgery with written informed consent from all the patients. Low-passage (<10 passages) primary cancer cells were used for later experiments. Information of patients and cellular genomic background was listed in online supplemental tables S4, S5.

## Cell culture and transfection

The PC cell lines PANC-1, MiaPaca-2, BxPC-3, SW1990 and PANC02 were maintained as previously described.<sup>20 42</sup> The human PSCs were set up as reported by Jesnowski *et al.*<sup>43</sup> PDAC-vector, PDAC-EHF, PDAC-scramble and PDAC-shEHF were established as previously described, and related sequence information is listed in online supplemental table S6.<sup>20</sup> Mycoplasma contamination was excluded in these cell lines. The cells were cultured at 37°C in a humidified atmosphere of 95% air and 5% CO<sub>2</sub> with Dulbecco's Modified Eagle Medium (DMEM) and Roswell Park Memorial Institute-1640 (RPMI-1640) basic medium supplemented with 10% fetal bovine serum (FBS) as a medium.

## Animals

Female NOD/SCID, BALB/C nude and KPC mouse models (4–6 weeks old) were used. All the mice were maintained in specific pathogen-free conditions.

## In vivo tumorigenicity assay

The cohorts of NOD/SCID mice were randomised into different groups. In each group, cancer cells at different dilutions were subcutaneously injected into the contralateral flanks of the NOD/SCID mice. Stem cell frequency was calculated via the website (<http://bioinf.wehi.edu.au/software/elda/>).

## Orthotopic mouse model

The cohorts of BALB/C nude mice were randomised into different groups. An orthotopic model was established using  $5 \times 10^5$  luciferase-expressing PDAC tumour cells. Tumour growth was analysed through BLI.

## KPC mouse model and preclinical animal cohorts

LSL-Kras<sup>G12D/+</sup>, LSL-Trp53<sup>R172H/+</sup> and Pdx1-Cre mouse models were generated in-house. Primers and PCR conditions for genotyping were listed in online supplemental tables S7, S8. Preclinical studies were conducted with a KPC mouse model.

## Immunohistochemistry (IHC) and multiplex fluorescent IHC

IHC score was determined by two independent pathologists who were blinded to the patients' clinicopathological features and prognosis. For multiplex fluorescent IHC, stained tissues were scanned and captured using a Vectra Polaris system (PerkinElmer). Images captured were analysed using the inForm cell analysis software (PerkinElmer).

## Flow cytometry

Primary pancreatic cells, PC cell lines and cells from tumour tissue digestions were stained with anti-hCD133, anti-hCD24, anti-hCD44, anti-ESA, anti-hCXCR4 or appropriate control antibodies. Detailed information of antibodies used is listed in online supplemental table S9. The ALDH activity was detected with ALDEFLUOR kits. Isotype controls were used as negative controls. Data were analysed using FlowJo V.10.0.

## Reverse transcription PCR (RT-PCR)

The total RNA of the cells was extracted with TRizol and converted to cDNAs by using an RT-PCR system. Then, real-time fluorescent Q-PCR was conducted to analyse the cDNA levels. Related primers are listed in online supplemental table S10.

## Western blot

Target proteins were detected through western blot with primary antibodies as follows: anti-EHF, anti-Sox9, anti-Sox2, anti-Nanog, anti-Oct4, anti-CXCR4, anti-E-cadherin, anti-CK19, anti-CAII and anti-tubulin.

## Anchorage-independent growth assay

Each six-well plate was coated with 1 mL of bottom agar, and 5000 cells were suspended in 1 mL of the top agar. Cells were incubated for 21 days, and colonies were analysed.

## Sphere formation assay

Cells (5000 cells/mL) were cultured in ultralow adhesion plates in a serum-free medium. After the cells were cultured for 2 weeks, tumour spheres with a diameter of >75 µm were counted.

## ChIP and luciferase analysis

ChIP assays were performed using a ChIP kit. The immunoprecipitated products were detected through PCR assays. Luciferase analysis was performed on the basis of the binding sites identified through ChIP analysis. Related sequences are listed in online supplemental table S11.

## Preparation of PSC-CM

PSCs were grown to 70%–80% confluence in 10 cm dishes in complete culture media. Then, the medium was replaced with FBS-free DMEM/F12 (1:1), and the cells were cultured for additional 48 hours.

## Stimulation of PSC-CM/CXCL12

For in vitro studies, PSC-CM was added to the culture medium at a ratio of 1:1, and CXCL12 was added to the culture system at a final concentration of 100 ng/mL. For in vivo studies, 200 µL of PSC-CM or 200 µL of CXCL12 was intratumourally injected three times a week.

## Treatment of rosiglitazone

For in vitro studies, adherent PDAC cells were pretreated with 5 µM rosiglitazone for 48 hours and were collected for further experiments. For in vivo tumorigenicity studies, rosiglitazone (100 mg/kg/day) was peritumorously injected three times a week. For orthotopic tumour models, rosiglitazone (100 mg/kg/day) was injected intraperitoneally three times a week.

## Statistical analysis

Statistical analysis was performed with IBM SPSS Statistics V21.0. Each experiment was conducted in triplicate, and data were presented as mean±SD unless otherwise stated. The variance between the groups was statistically compared. Student's t test was conducted to compare the mean values. Kaplan–Meier curves were analysed for median survival. A log-rank test was carried out to analyse the differences in survival times among the patient subgroups. \*P<0.05, \*\*P<0.01 and \*\*\*P<0.001 indicated significant differences, and n.s. meant non-significant. See online supplemental Methods for details.

## Author affiliations

<sup>1</sup>Department of Pancreatic Cancer, Tianjin Medical University Cancer Institute and Hospital, National Clinical Research Center for Cancer; Key Laboratory of Cancer Prevention and Therapy, Tianjin's Clinical Research Center for Cancer, Tianjin, PR China

<sup>2</sup>Department of Breast Oncoplastic Surgery, Tianjin Medical University Cancer Institute and Hospital, National Clinical Research Center for Cancer, Key Laboratory of Cancer Prevention and Therapy, Tianjin, Tianjin's Clinical Research Center for

Cancer, Key Laboratory of Breast Cancer Prevention and Therapy, Tianjin Medical University, Ministry of Education, Tianjin, China

<sup>3</sup>State Key Laboratory of Medicinal Chemical Biology and College of Pharmacy, Nankai University, Tianjin, China

<sup>4</sup>Department of Cellular and Molecular Physiology, Penn State College of Medicine, Hershey, PA, USA

**Acknowledgements** We thank Professor Xueli Bai and Professor Qi Zhang (Department of Surgery, the Second Affiliated Hospital, Zhejiang University, China) for their technical assistance.

**Contributors** JH and JL conceived and designed the experiments; TZ and YX performed most of the experiments; JL, WB, KZ, WJ, SY, HoWang and HaWang performed some experiments; YG, CH and SY provided technical support; TZ, SG, XW provided patient samples and technical support. JH, JL, TZ and YX analysed and discussed the data. JL and TZ wrote and completed the paper. JH supervised the entire project.

**Funding** This work was supported by the National Natural Science Foundation of China (grants 82030092, 81720108028, 82072657, 81802432, 82072716, 81802433, 82072659, 81871968 and 81871978), the programmes of Tianjin Prominent Talents, Tianjin Eminent Scholars, Tianjin Natural Science Foundation (20JCQNJC01330, 18JCQJC47800, 19JCQJC63100 and 19JCYBJC26200), Tianjin Postgraduate Research and Innovation Project (2019YJSB104), and Tianjin Research Innovation Project for Postgraduate Students (2019YJSB104). The research in S. Yang's laboratory is supported by the National Cancer Institute (R01 CA175741) and the Elsa U. Pardee Foundation (R01 CA175741)

**Competing interests** None declared.

**Patient consent for publication** Not required.

**Ethics approval** All the patients provided written consent for the use of their specimens and disease information for future investigations according to the ethics committee of Tianjin Medical University Cancer Institute and Hospital, China, and in accordance with the recognised ethical guidelines of Helsinki (ID number of the ethics approval: Ek2017141). Animal experiment procedures were approved by the ethics committee of Tianjin Medical University Cancer Institute and Hospital, in compliance with the principles and procedures of the NIH Guide for the Care and Use of Laboratory Animals.

**Provenance and peer review** Not commissioned; externally peer reviewed.

**Data availability statement** All data relevant to the study are included in the article or uploaded as supplementary information.

**Supplemental material** This content has been supplied by the author(s). It has not been vetted by BMJ Publishing Group Limited (BMJ) and may not have been peer-reviewed. Any opinions or recommendations discussed are solely those of the author(s) and are not endorsed by BMJ. BMJ disclaims all liability and responsibility arising from any reliance placed on the content. Where the content includes any translated material, BMJ does not warrant the accuracy and reliability of the translations (including but not limited to local regulations, clinical guidelines, terminology, drug names and drug dosages), and is not responsible for any error and/or omissions arising from translation and adaptation or otherwise.

## ORCID iDs

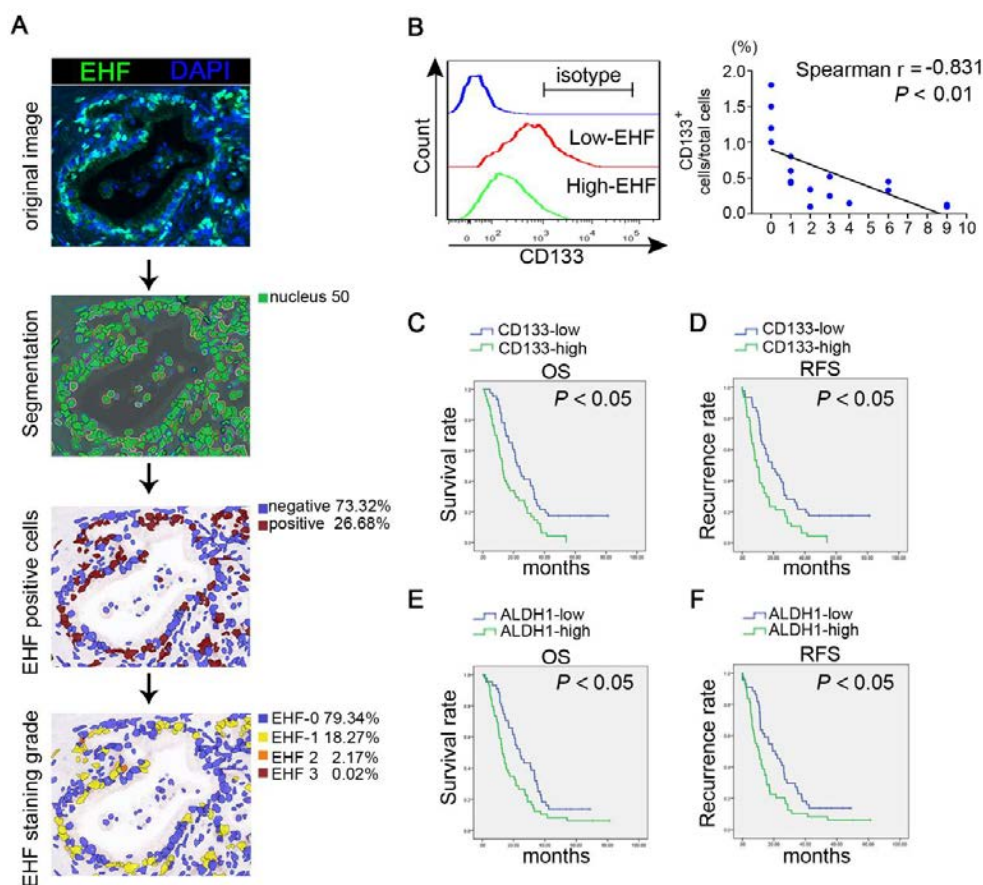
Jing Liu <http://orcid.org/0000-0002-8181-8159>

Jihui Hao <http://orcid.org/0000-0002-1607-1730>

## REFERENCES

- 1 Siegel RL, Miller KD, Jemal A. Cancer statistics, 2019. *CA Cancer J Clin* 2019;69:7–34.
- 2 Christenson ES, Jaffee E, Azad NS. Current and emerging therapies for patients with advanced pancreatic ductal adenocarcinoma: a bright future. *Lancet Oncol* 2020;21:e135–45.
- 3 Crawford HC, Pasca di Magliano M, Banerjee S. Signaling networks that control cellular plasticity in pancreatic tumorigenesis, progression, and metastasis. *Gastroenterology* 2019;156:2073–84.
- 4 Garcia-Maya Y, Mir C, Masson F, et al. Insights into new mechanisms and models of cancer stem cell multidrug resistance. *Semin Cancer Biol* 2020;60:166–80.
- 5 Li C, Heidt DG, Dalerba P, et al. Identification of pancreatic cancer stem cells. *Cancer Res* 2007;67:1030–7.
- 6 Hermann PC, Huber SL, Herrler T, et al. Distinct populations of cancer stem cells determine tumor growth and metastatic activity in human pancreatic cancer. *Cell Stem Cell* 2007;1:313–23.
- 7 Rodriguez-Aznar E, Wiesmüller L, Sainz B, et al. EMT and Stemness-Key players in pancreatic cancer stem cells. *Cancers* 2019;11:1136.
- 8 Fabian A, Stegner S, Miarka L, et al. Metastasis of pancreatic cancer: an uninfamed liver microenvironment controls cell growth and cancer stem cell properties by oxidative phosphorylation in pancreatic ductal epithelial cells. *Cancer Lett* 2019;453:95–106.
- 9 Mizutani Y, Kobayashi H, Iida T, et al. Meflin-Positive cancer-associated fibroblasts inhibit pancreatic carcinogenesis. *Cancer Res* 2019;79:5367–81.

- 10 Chan T-S, Shaked Y, Tsai KK. Targeting the interplay between cancer fibroblasts, mesenchymal stem cells, and cancer stem cells in desmoplastic cancers. *Front Oncol* 2019;9:688.
- 11 Begum A, McMillan RH, Chang Y-T, et al. Direct interactions with cancer-associated fibroblasts lead to enhanced pancreatic cancer stem cell function. *Pancreas* 2019;48:329–34.
- 12 Wilson JS, Pirola RC, Apte MV. Stars and stripes in pancreatic cancer: role of stellate cells and stroma in cancer progression. *Front Physiol* 2014;5:52.
- 13 Farran B, Nagaraju GP. The dynamic interactions between the stroma, pancreatic stellate cells and pancreatic tumor development: novel therapeutic targets. *Cytokine Growth Factor Rev* 2019;48:11–23.
- 14 Hosein AN, Brekken RA, Maitra A. Pancreatic cancer stroma: an update on therapeutic targeting strategies. *Nat Rev Gastroenterol Hepatol* 2020;17:487–505.
- 15 Su S, Chen J, Yao H, et al. CD10<sup>+</sup>GPR77<sup>+</sup> Cancer-Associated Fibroblasts Promote Cancer Formation and Chemoresistance by Sustaining Cancer Stemness. *Cell* 2018;172:841–56. e16.
- 16 Khan MA, Srivastava SK, Zubair H, et al. Co-targeting of CXCR4 and hedgehog pathways disrupts tumor-stromal crosstalk and improves chemotherapeutic efficacy in pancreatic cancer. *J Biol Chem* 2020;295:8413–24.
- 17 Aldaz P, Otaegi-Ugartemendia M, Saenz-Antoñanzas A, et al. SOX9 promotes tumor progression through the axis BMI1-p21<sup>CIP</sup>. *Sci Rep* 2020;10:357.
- 18 Feldman RJ, Sementchenko VI, Watson DK. The epithelial-specific ETS factors occupy a unique position in defining epithelial proliferation, differentiation and carcinogenesis. *Anticancer Res* 2003;23:2125–31.
- 19 Zhao T, Jiang W, Wang X, et al. ESE3 inhibits pancreatic cancer metastasis by upregulating E-cadherin. *Cancer Res* 2017;77:874–85.
- 20 Liu J, Jiang W, Zhao K, et al. Tumoral EHF predicts the efficacy of anti-PD1 therapy in pancreatic ductal adenocarcinoma. *J Exp Med* 2019;216:656–73.
- 21 Albino D, Civenni G, Rossi S, et al. The ETS factor ESE3/EHF represses IL-6 preventing STAT3 activation and expansion of the prostate cancer stem-like compartment. *Oncotarget* 2016;7:76756–68.
- 22 Dallavalle C, Albino D, Civenni G, et al. MicroRNA-424 impairs ubiquitination to activate STAT3 and promote prostate tumor progression. *J Clin Invest* 2016;126:4585–602.
- 23 Albino D, Longoni N, Curti L, et al. ESE3/EHF controls epithelial cell differentiation and its loss leads to prostate tumors with mesenchymal and stem-like features. *Cancer Res* 2012;72:2889–900.
- 24 Wang L, Xing J, Cheng R, et al. Abnormal localization and tumor suppressor function of epithelial tissue-specific transcription factor ESE3 in esophageal squamous cell carcinoma. *PLoS One* 2015;10:e0126319.
- 25 Lim JH, Cho J-Y, Park YB, et al. ESE-3 transcription factor is involved in the expression of death receptor (DR)-5 through putative Ets sites. *Biochem Biophys Res Commun* 2006;350:736–41.
- 26 Hamada S, Masamune A, Takikawa T, et al. Pancreatic stellate cells enhance stem cell-like phenotypes in pancreatic cancer cells. *Biochem Biophys Res Commun* 2012;421:349–54.
- 27 Cave DD, Di Guida M, Costa V, et al. TGF- $\beta$ 1 secreted by pancreatic stellate cells promotes stemness and tumorigenicity in pancreatic cancer cells through L1CAM downregulation. *Oncogene* 2020;39:4271–85.
- 28 Barbato L, Bocchetti M, Di Biase A, et al. Cancer stem cells and targeting strategies. *Cells* 2019;8:926.
- 29 Seino T, Kawasaki S, Shimokawa M, et al. Human pancreatic tumor organoids reveal loss of stem cell niche factor dependence during disease progression. *Cell Stem Cell* 2018;22:454–67.
- 30 Öhlund D, Handly-Santana A, Biffi G, et al. Distinct populations of inflammatory fibroblasts and myofibroblasts in pancreatic cancer. *J Exp Med* 2017;214:579–96.
- 31 Wang T, Notta F, Navab R, et al. Senescent carcinoma-associated fibroblasts upregulate IL8 to enhance prometastatic phenotypes. *Mol Cancer Res* 2017;15:3–14.
- 32 Wei L, Ye H, Li G, et al. Cancer-associated fibroblasts promote progression and gemcitabine resistance via the SDF-1/SATB-1 pathway in pancreatic cancer. *Cell Death Dis* 2018;9:1065.
- 33 Albino D, Civenni G, Dallavalle C, et al. Activation of the Lin28/let-7 axis by loss of ESE3/EHF promotes a tumorigenic and stem-like phenotype in prostate cancer. *Cancer Res* 2016;76:3629–43.
- 34 Righetti A, Giulietti M, Šabanović B, et al. Cxcl12 and its isoforms: different roles in pancreatic cancer? *J Oncol* 2019;2019:1–13.
- 35 Jung Y, Cackowski FC, Yumoto K, et al. CXCL12 $\gamma$  promotes metastatic castration-resistant prostate cancer by inducing cancer stem cell and neuroendocrine phenotypes. *Cancer Res* 2018;78:2026–39.
- 36 Janani C, Ranjitha Kumari BD. PPAR gamma gene--a review. *Diabetes Metab Syndr* 2015;9:46–50.
- 37 Wang Z, Shen W, Li X, et al. The PPAR $\gamma$  agonist rosiglitazone enhances the radiosensitivity of human pancreatic cancer cells. *Drug Des Devel Ther* 2020;14:3099–110.
- 38 Bunt SK, Mohr AM, Bailey JM, et al. Rosiglitazone and gemcitabine in combination reduces immune suppression and modulates T cell populations in pancreatic cancer. *Cancer Immunol Immunother* 2013;62:225–36.
- 39 Li Y, Zhang D-W, Lin D-Q, et al. Peroxisome proliferator-activated receptor- $\gamma$  inhibits pancreatic cancer cell invasion and metastasis via regulating MMP-2 expression through PTEN. *Mol Med Rep* 2015;12:6255–60.
- 40 Galli A, Ceni E, Crabb DW, et al. Antidiabetic thiazolidinediones inhibit invasiveness of pancreatic cancer cells via PPAR $\gamma$  independent mechanisms. *Gut* 2004;53:1688–97.
- 41 Fujita M, Hasegawa A, Yamamori M, et al. In vitro and in vivo cytotoxicity of troglitazone in pancreatic cancer. *J Exp Clin Cancer Res* 2017;36:91.
- 42 Zhao T, Jin F, Xiao D, et al. IL-37/STAT3/ HIF-1 $\alpha$  negative feedback signaling drives gemcitabine resistance in pancreatic cancer. *Theranostics* 2020;10:4088–100.
- 43 Jesnowski R, Fürst D, Ringel J, et al. Immortalization of pancreatic stellate cells as an in vitro model of pancreatic fibrosis: deactivation is induced by matrigel and N-acetylcysteine. *Lab Invest* 2005;85:1276–91.



**Supplementary figure 1.** (A) The objective quantified method for EHF. Mean nucleus intensity of EHF, positive rate of EHF and EHF staining grade were quantified by PerkinElmer Advanced Image Analysis Software-in Form 2.4 Viewer. Tumor areas were manually outlined to exclude stromal nuclei. Nuclei, cytoplasm and membrane were segmented and DAPI was used to identify nuclei. (B) Single cell suspensions were prepared from 18 cases of fresh PDAC tissues and CD133<sup>+</sup> population were detected by flowcytometry. Anti-CD133 antibody (Miltenyi Biotec) was used. Representative histograms were shown (left) and Spearman correlation analysis between EHF IHC score and the proportions of CD133<sup>+</sup> cells (right);  $n=18$ ,  $P<0.01$ . (C-D) Prognostic significance of CD133<sup>+</sup> PCSCs for overall survival (C) and recurrence free survival (D) in a series of 93 cases of PDAC. Kaplan-Meier OS and RFS for different levels of CD133<sup>+</sup> PCSCs accumulation based on the log-rank statistic test. (E-F) Prognostic significance of ALDH1<sup>+</sup> PCSCs for overall survival (E) and recurrence free survival (F) in a series of 93 cases of PDAC. Kaplan-Meier OS and RFS for different levels of ALDH1<sup>+</sup> PCSCs accumulation based on the log-rank statistic test.

**Supplementary table1: Correlation of ESE3/EHF expression to clinicopathological features in PDAC.**

Parameters		ESE3(n)		$\chi^2$	<i>P</i>	<i>r</i>
		low	high			
<b>Age(years)</b>	<60	33	16	0.205	0.601	0.042
	≥60	30	14			
<b>Gender</b>	Male	35	12	0.106	0.435	0.032
	Female	36	10			
<b>Histological grade</b>	G1, G2	45	20	5.472	<b>0.020<sup>a</sup></b>	-0.324
	G3	25	3			
<b>p TNM stage</b>	IA, IB	33	19	3.276	<b>0.031<sup>a</sup></b>	-0.137
	IIA, IIB	28	13			
<b>Tumor size</b>	T1≤3.5cm	25	22	2.725	0.231	-0.456
	T2>3.5cm	30	16			
<b>LN metastasis</b>	N0	25	24	5.782	0.075	-0.443
	N1	30	14			

Note: Data was based on IHC assay. Statistical data on EHF expression in relation to clinic-histopathologic features for surgical PDAC specimens. *P* values were calculated using the chi-square test. <sup>a</sup> Statistically significant (*P*<0.05). <sup>b</sup> Here EHF expression was divided into high-EHF and low-EHF according to staining scores.

**Supplementary table2: Univariate and multivariate Cox proportional hazards analysis of clinicopathological factors for median overall survival and relapse free survival.**

Variables	Overall survival		Relapse free survival	
	HR (95.0% CI)	P	HR (95.0% CI)	P
<b>Univariate analysis</b>				
Age	0.989(0.631-1.550)	0.962	1.108(0.707-1.737)	0.655
Gender	0.934(0.606-1.438)	0.756	1.008(0.654-1.552)	0.973
Differentiation	0.762(0.451-1.287)	<b>0.031<sup>a</sup></b>	0.710(0.420-1.199)	<b>0.020<sup>a</sup></b>
Tumor size	1.582(1.007-2.487)	<b>0.046<sup>a</sup></b>	1.589(1.011-2.507)	<b>0.045<sup>a</sup></b>
p TNM stage	2.493(1.602-3.891)	<b>0.000<sup>a</sup></b>	2.439(1.550-3.830)	<b>0.000<sup>a</sup></b>
LN metastasis	0.862(0.505-1.472)	0.586	0.781(0.457-1.335)	0.366
EHF expression	0.253(0.156-0.409)	<b>0.000<sup>a</sup></b>	0.268(0.164-0.437)	<b>0.002<sup>a</sup></b>
<b>Multivariate analysis</b>				
Differentiation	0.571(0.332-0.982)	<b>0.043<sup>a</sup></b>	0.581(0.551-1.579)	<b>0.049<sup>a</sup></b>
p TNM stage	1.886(1.094-3.251)	<b>0.022<sup>a</sup></b>	2.099(1.209-3.645)	<b>0.008<sup>a</sup></b>
EHF expression	0.274(0.161-0.495)	<b>0.000<sup>a</sup></b>	0.303(0.180-0.509)	<b>0.000<sup>a</sup></b>

NOTE: Data was based on IHC assay. EHF staining score was determined by two independent pathologists who were blinded to the patients' clinical features and outcomes. Multivariate Cox proportional hazards analysis used backward selection model. Abbreviations: HR, hazard ratio; CI, confidence interval; LN, lymph node. <sup>a</sup> Statistically significant ( $P < 0.05$ ).

Supplementary table3: a list of drug library used for ESE3/EHF targeting screening

list of drug library										
	1	2	3	4	5	6	7	8	9	10
<b>A</b>	Vonoprazan	Peritoinin	Tomivosertib	Faropenem daltosate	Flavopiridol	Flavopiridol (Hydrochloride)	Semagacestat	Mitoquinone (mesylate)	Taranabant	Delpazolid
<b>B</b>	Nevaniribe hydrochloride	K-604 dihydrochloride	Limaprazan	BFH772	Odenacatib	Cadazolid	Treprostiniil	Paquinimod	AEE788	Plerixafor
<b>C</b>	Dihydroxidine (hydrochloride)	Velparib (dihydrochloride)	<b>Allopurinol riboside</b>	<b>Gestrinone</b>	<b>Ralfinamide</b>	<b>Rosiglitazone</b>	<b>Zanubrutinib</b>	<b>Ibuprofen piconol</b>	<b>AZD-5991</b>	<b>Linrodostat</b>
<b>D</b>	Ilaprazole	Aticaprant	GSK2982772	Ziritaxestat	EDO-S101	Danusertib	Dasatinib	Dasatinib (hydrochloride)	BMS-986142	Minde sap
<b>E</b>	Triciclib hydrochloride	Nitromide	Fosfomycin	Ganciclovir	Doramectin	Capreomycin	Nafitine	Tegobuvir	Novobocin	Daclatasvir
<b>F</b>	Niclosamide	Ronidazole	Ciclopirox	Sulfamerazine	Cloxacillin	Ivermectin	Ceftazidime	Moxidectin	Bekanamycin	Dihydrostreptomycin
<b>G</b>	Sertaconazole	Ciprofloxacin	Micalungin	Sulfathiazole	Valganciclovir	Cefdinir	Tohalate	Tizoxanide	Radezolid	Chlortetracycline
<b>H</b>	Valacyclovir	Arbidol	Triconazole	Butoconazole	Vancromycin	Isoniazid	Atazanavir	Mezocillin	Elvitegravir	Pipemidic acid
<b>I</b>	Chloroxine	Azocillin	ABT-333	Tobramycin	Ritonavir	Oxfendazole	Nafcilin	Chloquinol	Proflavine	Cinoxacin
<b>J</b>	Pentamidine	Subactam	Doripenem	Atovaquone	Besifloxacin	<b>Zanamvir</b>	<b>idoxuridine</b>	<b>Butenafine</b>	Ketoconazole	Moxifloxacin
<b>K</b>	Methacycline	Lopinavir	Ethambutol	Rientine	Norfloxacin	Anidulafungin	Erythromycin	Osetamvir	<b>Roxithromycin</b>	<b>Saquinavir</b>
<b>L</b>	Sulfanilamide	Artemisinin	Oxacillin	Saquinavir	<b>Letemovir</b>	Levofloxacin	Cefpramide	BAY57-1293	GS-7340	Dapirvine
<b>M</b>	Cidofovir	Fenbendazole	Bifonazole	Sulfadoxine	Boceprevir	Furagin	HygromycinB	Ceflitoren	Rimantadine	Salinomycin
<b>N</b>	Eprinomectin	(S)-Tedizolid	Darunavir	Succinylsulfathiazole	Bla penem	Ribostamycin	Cefamandole	HIV-1 integrase inhibitor	Abacavir	Ceftazoxime
<b>O</b>	Cefetamet pivoxil	Cephalothin	Clotofcol	CDK9-IN-1	Actinomycin D	PSI-6130	Acyclovir	Amprolium	Cloxiquine	GS-7340
<b>P</b>	Clarithromycin	Cefradine	Tolcofos-methyl	Diniconazole	Cefonicid	Lumefantrine	Chloroxylenol	Ceftriaxone	Permethrin	tamoxifen
<b>Q</b>	Betulinaldehyde	Kasugamycin	Paromomycin	Tazobactam	Vidarabine	Penicillin	Valnemulin	Amikacin	Itraconazole	metformin
<b>R</b>	MinocyclineR	Ribavirin/Ripovirin	Cefmetazole	Nifursiol	AZithromycin	Omidazole	Toltrazunil	Amantadine	Pyrazinamide	Famciclovir
<b>S</b>	Demeclocycline	Limomin	Neomycin	Retapamulin	Naphthoquine	Cefsulodin	Hexetidine	HV-1 integrase inhibitor 2	Omidazole	Rufloxacin

**Supplementary table4: detailed information of two patients whose specimens were used for isolation of primary cancer cells.**

	Patient1#	Patient2#
Primary cell name	PDX1#	PDX2#
Gender	male	female
age	65	64
Date of admission	2016-03-23	2016-11-09
Date of operation	2016-04-06	2016-11-28
Date of recurrence	2016-12-05	2017-09-02
Date of death	2017-03-02	2017-12-05
Surgical option	pancreaticoduodenectomy	pancreaticoduodenectomy
Pathological diagnosis	PDAC	PDAC
Histologic grade	G2	G2
Tumor size	3.0cm	4.0cm
LN metastasis	yes	yes
Vessel invasion	yes	yes
Nerve invasion	yes	yes

**Supplementary table5: Genomic background of two primary cancer cells PDX1# and PDX2#.**

Sample	Gene name	Spliced variant	Function	Mutation type	AA change
PDX1#	KRAS	NM_004985,NM_03336 0	exonic	missense SNV	KRAS:NM_004985:exon2:c.G35C:p.G12A,KRAS:NM_033360:exon2:c.G35C:p.G12A
	TP53	NM_000546,NM_001126112,NM_001126113,NM_001126114,NM_001126115,NM_001126116,NM_001126117,NM_001126118,NM_001276695,NM_001276696,NM_001276697,NM_001276698,NM_001276699,NM_001276760,NM_001276761	exonic	missense SNV	TP53:NM_001126115:exon3:c.G347A:p.R116Q,TP53:NM_001126116:exon3:c.G347A:p.R116Q,TP53:NM_001126117:exon3:c.G347A:p.R116Q,TP53:NM_001276697:exon3:c.G266A:p.R89Q,TP53:NM_001276698:exon3:c.G266A:p.R89Q,TP53:NM_001276699:exon3:c.G266A:p.R89Q,TP53:NM_001126118:exon6:c.G626A:p.R209Q,TP53:NM_000546:exon7:c.G743A:p.R248Q,TP53:NM_001126112:exon7:c.G743A:p.R248Q,TP53:NM_001126113:exon7:c.G743A:p.R248Q,TP53:NM_001126114:exon7:c.G743A:p.R248Q,TP53:NM_001276695:exon7:c.G626A:p.R209Q,TP53:NM_001276696:exon7:c.G626A:p.R209Q,TP53:NM_001276760:exon7:c.G626A:p.R209Q,TP53:NM_001276761:exon7:c.G626A:p.R209Q
	SMAD4	NM_005359	Intronic mutation		
	P16	No mutation was found			
PDX2#	KRAS	NM_004985,NM_03336 0	exonic	missense SNV	KRAS:NM_004985:exon2:c.G35A:p.G12D,KRAS:NM_033360:exon2:c.G35A:p.G12D
	TP53	NM_000546,NM_001126112,NM_001126115,NM_001126118,NM_001276697,NM_001276760,NM_001276761	exonic	missense SNV	TP53:NM_001126115:exon6:c.G683C:p.G228A,TP53:NM_001276697:exon6:c.G602C:p.G201A,TP53:NM_001126118:exon9:c.G962C:p.G321A,TP53:NM_000546:exon10:c.G1079C:p.G360A,TP53:NM_001126112:exon10:c.G1079C:p.G360A,TP53:NM_001276760:exon10:c.G962C:p

					.G321A,TP53:NM_001276761: exon10:c.G962C:p.G321A
	TP53	NM_000546,NM_00112 6112,NM_001126113,N M_001126114,NM_0011 26115,NM_001126116, NM_001126117,NM_00 1126118,NM_00127669 5,NM_001276696,NM_ 001276697,NM_001276 698,NM_001276699,N M_001276760,NM_001 276761	exonic	stopgain	TP53:NM_001126115:exon2:c. C241T:p.R81X,TP53:NM_0011 26116:exon2:c.C241T:p.R81X,T P53:NM_001126117:exon2:c.C 241T:p.R81X,TP53:NM_001276 697:exon2:c.C160T:p.R54X,TP 53:NM_001276698:exon2:c.C1 60T:p.R54X,TP53:NM_0012766 99:exon2:c.C160T:p.R54X,TP5 3:NM_001126118:exon5:c.C52 0T:p.R174X,TP53:NM_000546: exon6:c.C637T:p.R213X,TP53: NM_001126112:exon6:c.C637T: p.R213X,TP53:NM_001126113: exon6:c.C637T:p.R213X,TP53: NM_001126114:exon6:c.C637T: p.R213X,TP53:NM_001276695 :exon6:c.C520T:p.R174X,TP53: NM_001276696:exon6:c.C520T :p.R174X,TP53:NM_00127676 0:exon6:c.C520T:p.R174X,TP5 3:NM_001276761:exon6:c.C52 0T:p.R174X
	SMAD4	NM_005359	exonic	stopgain	SMAD4:NM_005359:exon3:c.C 403T:p.R135X
	SMAD4	NM_005359	Intronic mutation		
	P16	No mutation was found			

**Supplementary table6: shRNA sequences for stable knockdown cell lines**

Human EHF shRNA1 (most efficient)	Top: ccggGCCAATTGTATCCCTTTCCAACCTCGAGTTGGAAAGGGATACAATTG GCtttt
	Bottom: aataaaaaGCCAATTGTATCCCTTTCCAACCTCGAGTTGGAAAGGGATACA ATTGGC
Human EHF shRNA2	Top: ccggGGGAGTTCATCCGAGACATTCTCGAGGAATGTCTCGGATGAACT CCCtttt
	Bottom: aataaaaaGGGAGTTCATCCGAGACATTCTCGAGGAATGTCTCGGATG AACTCCC
Human EHF shRNA2	Top: ccggAGTCCGCACACAATGTCATTGCTCGAGCAATGACATTGTGTGCGG ACtttt
	Bottom: aataaaaaAGTCCGCACACAATGTCATTGCTCGAGCAATGACATTGTGTG CGGAC
Human CXCR4 shRNA1	Top ccggCCATCATCTTCTTAACTGGCAtttt
	Bottom aataaaaaCCATCATCTTCTTAACTGGCA
Human CXCR4 shRNA2 (most efficient)	Top ccggCCTGCTATTGCATTATCATCTtttt
	Bottom aataaaaaCCTGCTATTGCATTATCATCT
Human CXCR4 shRNA 3	Top ccggGGAGAGTTGTAGGATTCTACA tttt
	Bottom aataaaaaGGAGAGTTGTAGGATTCTACA

**Supplementary table7: Primers used for genotyping of KPC mice model**

<b>Primer name</b>	<b>Sequence(5'-3')</b>
Trp53-primer1	CTT GGA GAC ATA GCC ACA CTG
Trp53-primer2	AGC TAG CCA CCA TGG CTT GAG TAA GT
Trp53-primer3	CAA CTG TTC TAC CTC AAG AGC C
Kras-primer1	GTC TTT CCC CAG CAC AGT GC
Kras-primer2	CTC TTG CCT ACG CCA CCA GCT C
Kras-primer3	AGC TAG CCA CCA TGG CTT GAG TAA GTC TGC A
Pdx1-Cre-internal positive control forward	AGA TGG AGA AAG GAC TAG GCT ACA
Pdx1-Cre-internal positive control reverse	CTG TCC CTG TAT GCC TCT GG
Pdx1-Cre-transgene forward	CCT GGA CTA CAT CTT GAG TTG C
Pdx1-Cre-transgene reverse	AGG CAA ATT TTG GTG TAC GG

**Supplementary table8: PCR procedure for genotyping of KPC mice model**

Trp53	Step1: 94°C 3min; Step2: 94°C 1min, 60°C 30s, 72°C 30s (34 repeats for step2); Step3: 72°C 5min; End.
Kras	Step1: 94°C 5min; Step2: 94°C 30s, 61°C 30s, 72°C 30s (34 repeats for step2); Step3: 72°C 10min; End.
Pdx1-Cre	Step1: 94°C 3min; Step2: 94°C 30s, 65°C 1min(-0.5°C per cycle decrease), 68°C 30s (10 repeats for step2); Step3: 94°C 30s; Step4: 94°C 30s, 60°C 1min, 72°C 30s (28 repeats for step4); Step5: 72°C 5min; End.

**Supplementary table9: Antibodies used in this study**

Antibodies name	Dilution	Source	Cat #
Anti-human EHF antibody (for WB)	1:5000	LSBio	LS-B11884
Anti-human EHF antibody (for IHC and Ch-IP)	1:1000	abcam	ab220113
Anti-human Sox9 antibody (for WB and IHC)	1:1000	abcam	ab185230
Anti-human Sox2 antibody (for WB and IHC)	1:1000	Proteintech	66411-1-Ig
Anti-human Nanog antibody (for WB and IHC)	1:1000	abcam	ab109250
Anti-human Oct4 antibody (for WB and IHC)	1:1000	abcam	ab18976
Anti-human CXCR4 antibody (for WB and IHC)	1:1000	abcam	ab124824
Anti-human CD133 antibody (for mIHC)	1:100	Miltenyi Biotec	130-118-143
Anti-human tubulin antibody (for WB)	1:5000	abmart	M20005
Anti-human ALDH1 antibody (for mIHC)	1:1000	BD	611194
Anti-human PPAR $\gamma$ antibody (for Ch-IP)	1:10	abcam	ab45036
Anti-human carbonic anhydrase2 antibody (for WB)	1:1000	abcam	ab124687
Anti-human CK19 antibody (for WB)	1:1000	abcam	ab7755
Anti-human E-cadherin antibody (for WB)	1:1000	abcam	ab1416
PE/Cy7 anti-human EpCAM antibody (for FCM)	5 $\mu$ l/test	Biolegend	324222
FITC anti-human CD24 antibody (for FCM)	5 $\mu$ l/test	Biolegend	101805
PE anti-human CD24 antibody (for FCM)	5 $\mu$ l/test	Biolegend	311106
APC anti-human CD44 antibody (for FCM)	5 $\mu$ l/test	Biolegend	338806
APC/Cy7 anti-human CXCR4 antibody (for FCM)	5 $\mu$ l/test	Biolegend	306528
PE anti-human CD133 antibody (for FCM)	5 $\mu$ l/test	Biolegend	372804
Anti-human IL6 antibody (for neutralizing)	5 $\mu$ g/ml	R&D	MAB206

Anti-human IL8 antibody (for neutralizing)	5µg/ml	R&D	MAB208
Anti-human GRO antibody (for neutralizing)	5µg/ml	R&D	AF275
Anti-human CSF2 antibody (for neutralizing)	5µg/ml	R&D	MAB215
Anti-human MCP1 antibody (for neutralizing)	5µg/ml	R&D	MAB279
Anti-human PDGF antibody (for neutralizing)	5µg/ml	R&D	AF-220-NA
Anti-human CXCL12/SDF-1 antibody (for neutralizing)	5µg/ml	R&D	MAB310
Anti-human activin-A antibody (for neutralizing)	5µg/ml	R&D	AF338
Anti-human periostin antibody (for neutralizing)	5µg/ml	R&D	MAB35483
Anti-human CTGF antibody (for neutralizing)	5µg/ml	Fibrogen	FG-3019
Anti-human endothelin antibody (for neutralizing)	5µg/ml	R&D	MAB34401
Mouse IgG1 isotype control (for matching with anti-IL6, anti-IL8, anti-CXCL12, anti-CSF-2, anti-MCP1, anti-periostin, anti-CTGF and anti-endothelin)	5µg/ml	R&D	MAB002
Polyclonal Goat IgG isotype control (for matching with anti-GRO, anti-PDGF, anti-activin-A)	5µg/ml	R&D	AB-108-C

**Supplementary table10: Primers used for RT-PCR and Ch-IP in this study**

Gene name	Forward	Reverse
<b>h EHF</b>	TGCAGCATCTGAAGTGGA AC	AGGAAGGTGACTGGTGGTTG
<b>hSox9</b>	GCTCTGGAGACTTCTGAA CGA	CCGTTCTTCACCGACTTCCT
<b>hSox2</b>	ACACCAATCCCATCCACAC T	GCAAACCTTCCTGCAAAGCTC
<b>h Nanog</b>	TTCCTTCTCCATGGATCT G	ATCTGCTGGAGGCTGAGGTA
<b>hOct4</b>	GAAGGATGTGGTCCGAGT GT	GTGAAGTGAGGGCTCCCATA
<b>hCXCR4</b>	GAACCCTGTTTCCGTGAA GA	AGGGAAGCGTGATGACAAAG
<b>hCXCR7</b>	CAAAACAGGGCTCACCAA GC	GCCGGTACAAAACACCACAC
<b>h Actin</b>	ACCCTGAAGTACCCCATC GAG	AGCACAGCCTGGATAGCAAC
<b>EHFCh-IP-Sox9-1</b>	AGAGCCCTGGATACGAAG	TCCCAAATAAACGCACAG
<b>EHFCh-IP-Sox9-2</b>	GCCGATTCACCACAACAA	GCACCACCGCAGACAAAA
<b>EHFCh-IP-Sox2-1</b>	GCGTGGGAGGGAGTTTGT	AGAAGGGTTTTCGGTCTGTG
<b>EHFCh-IP-Nanog-1</b>	CCCACCTAACAAACTGTGC	TCCTTCCTATTCCCAAAC
<b>EHFCh-IP-Nanog-2</b>	TTGAATGTTGGGTTTGGG	TAGGGTGATTTCTTGATTTGA G
<b>EHFCh-IP-Oct4-1</b>	GCATTCCGTTGGCTATTC	GGGCAGCTCTAACCCATAA
<b>EHFCh-IP-CXCR4-1</b>	GGGATGTCTTGGAGCGAG TT	CCCTCTGCCTACTGTGCTG
<b>PPAR <math>\gamma</math> Ch-IP-EHF-1</b>	GGTTAATCTCAGGCAATG	AGACAAATCAGGCACAAC
<b>PPAR <math>\gamma</math> Ch-IP-EHF-2</b>	ACAGTCACCACCAAATCA	TAAGCAATAAGCCACCAA

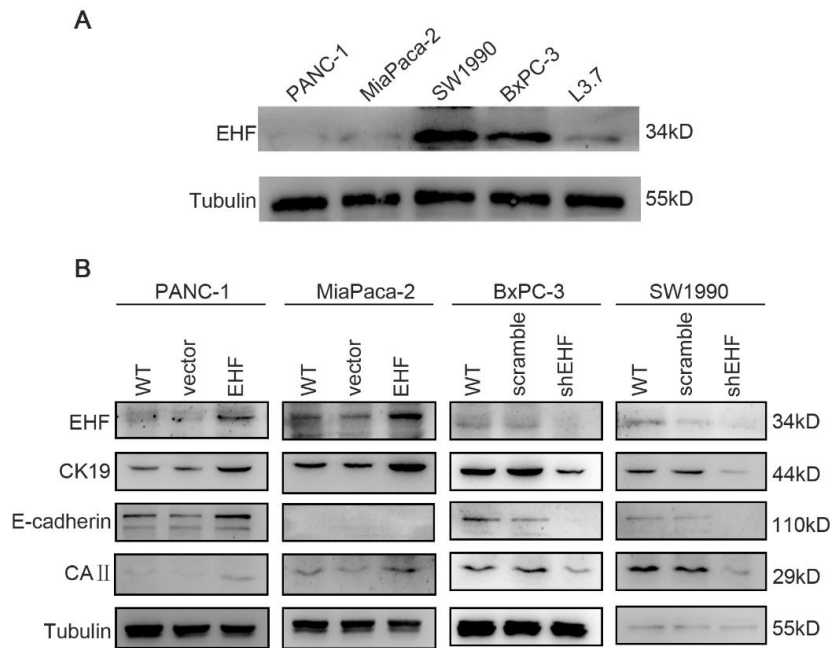
**Supplementary table11: Sequence of the vectors for luciferase analysis**

CXCR4 promoter-EBS1-wt (yellow region stands for EBS1-wt sequence)
<p>tccccaccccgcttctccctccccgcccagcggcgcatgcgccgctcggagcgtgttttataaaagt  ccggccgcccagaaacttcagtttgttggctgcggcagcaggtagcaaagtgacgccgagggcctgagtgc  tccagtagccaccgcatctggagaaccagcggttaccatggaggggatcagtgtaagtccagtttcaacctgc  tttgcataaatgtacaaacgtttgaacttagagcgcagcccctctccgagcgggcagaagcggccaggacat  tggaggtaccgtactccaaaaagggtcaccgaaaggagttttcttgaccatgcctatatagtgcggtggg  tggggggggagcaggattggaatcttttctctgtgagtcgaggagaaacgactggaagagcgttccagtg  ctgatgtgtctcccccttgagtcgccgcgcgggcggcttgacgctgtttgcaaactgaagaacattct  gtgcacaagtgcagagaaggcgtgcgctgcctcgggactcagaccaccggtctcttccttggggaagcggg  gatgtcttggagcagttacattgtctgaatttagaggcggagggcggtgctgctgggctgagttccaggag  gagattgccccgcttt<b>aacttcggggtt</b>aagcgcctgggtgactgttcttgacactgggtgctgtttgttaa  actctgtgcccgcagggagctgtgcccagtcctccagcacagtaggacagggcgaggagggcgggtggacc  accgcccgatcctctgaggggatcagtggtggcagcagctaggagttgatccgccgcgctttgggtt  gagggggaaaaccttcccgcgtccgaagcgcctcttccccacggccgcgagtgggctcctgcagttcgaga  gtttgggctgagcagaggtcagcggagtggttgacctcccccttgacacgcgagctgcagccctgaga  tttgcgctcggggataggagcgggtacgggtgagggcgggggcggttaagaccgcacctgggctccagg  tcgccgcccgaagactggcaggtgcaagtgggaaaccgtttggctctctccgagtcagttgtgatgttta  accgtcgggtgtttccagaaacctttgaaacctcttgctagggagttttggtttctgcagcggcgca  attcaaagacgctcggcgagccgccagtcgctccccagcaccctgtgggacagagcctggcgtgcgcc  cagcggagcccctgcagcgtgcttgcccggcgggtggcgtgggtgtagtgggcagccgcccggccgggct  ggacgaccggcccccgctgcccacgcctggaggcttccagctgcccacctccggcgggtaactggat  cagtgccgggtaattgggaagccaccgggagagtgaggaaatgaaactggggcaggaccaggggtcaga  ccccgttaccttccaccaggaaaatgcccgcctccctaactcccaaaccgccaagtataaacacgag  gatggcaagagaccacacacggagagcgccttgggggaggaggtgcccgtttgttattttctgacac  tcccgcccaatatacccaagcaccgaaggccttctgttttaagaccgattctctttaccactacaagt  tgcttgaagcccagaatggttgtatttaggcaggcgtgggaaaattaagttttgctttaggagaatgag  tctttgcaacgccccgcccctccccgtgatcctccttctcccccttctccctccctgggcgaaaaactct  tcaaaaaagttaatcactgcccctctagcagaccaccaccacccccacgccctgggagtgcccttt  gtgtgtatttttttttctcctaaggaagg</p>
CXCR4 promoter-EBS1-mut (yellow region stands for EBS1-mut sequence)
<p>Tccccaccccgcttctccctccccgcccagcggcgcatgcgccgctcggagcgtgttttataaaagt  ccggccgcccagaaacttcagtttgttggctgcggcagcaggtagcaaagtgacgccgagggcctgagtgc  tccagtagccaccgcatctggagaaccagcggttaccatggaggggatcagtgtaagtccagtttcaacctgc  tttgcataaatgtacaaacgtttgaacttagagcgcagcccctctccgagcgggcagaagcggccaggacat  tggaggtaccgtactccaaaaagggtcaccgaaaggagttttcttgaccatgcctatatagtgcggtggg  tggggggggagcaggattggaatcttttctctgtgagtcgaggagaaacgactggaagagcgttccagtg  ctgatgtgtctcccccttgagtcgccgcgcgggcggcttgacgctgtttgcaaactgaagaacattct  gtgcacaagtgcagagaaggcgtgcgctgcctcgggactcagaccaccggtctcttccttggggaagcggg  gatgtcttggagcagttacattgtctgaatttagaggcggagggcggtgctgctgggctgagttccaggag  gagattgccccgcttt<b>tttttttttt</b>aagcgcctgggtgactgttcttgacactgggtgctgtttgttaa  actctgtgcccgcagggagctgtgcccagtcctccagcacagtaggacagggcgaggagggcgggtggacc  accgcccgatcctctgaggggatcagtggtggcagcagctaggagttgatccgccgcgctttgggtt  gagggggaaaaccttcccgcgtccgaagcgcctcttccccacggccgcgagtgggctcctgcagttcgaga</p>

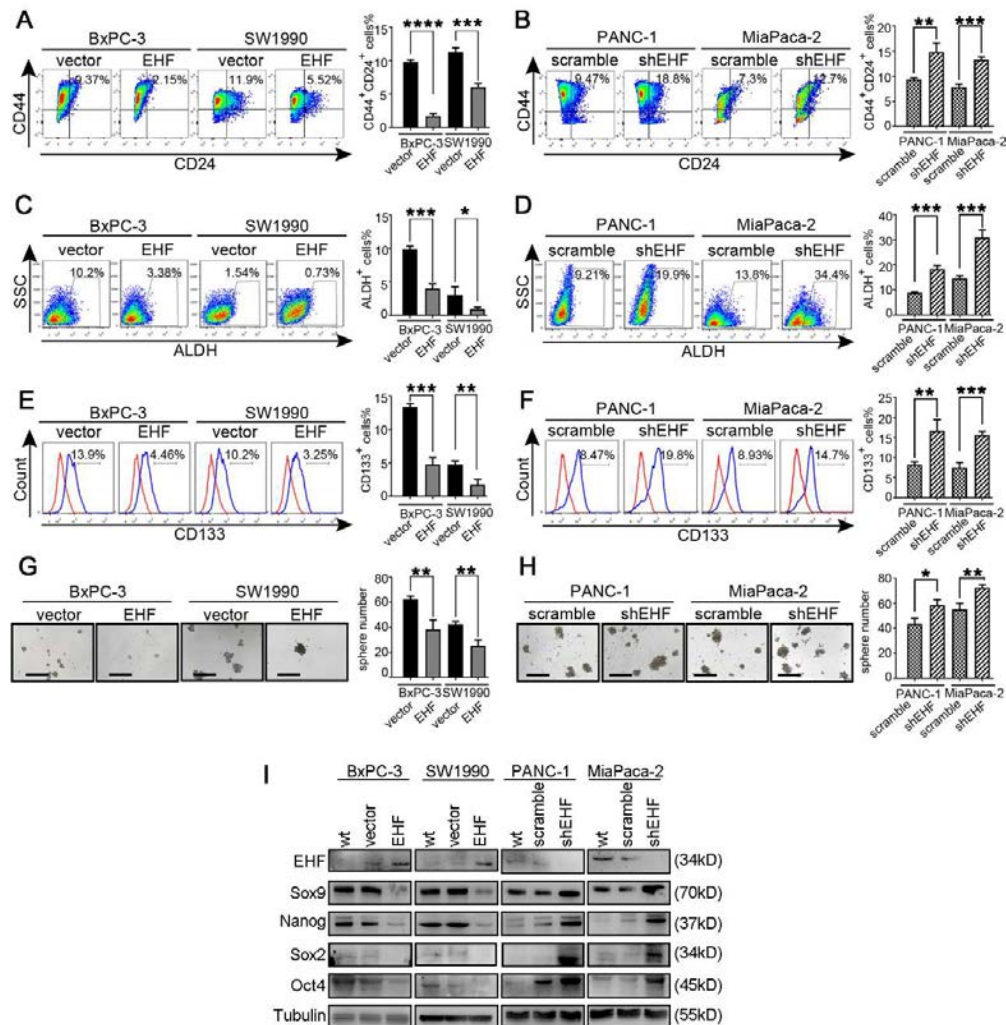
gtttggggtcgtgcagagggtcagcggagtggtttgacctcccccttgacaccgcgcagctgccagccctgaga  
 tttgcgctccggggataggagcgggtacggggtgaggggccccgggtaagaccgcacctgggctgccagg  
 tcgccgccgaagactggcagggtgcaagtggggaaaccgtttggctctctccgagtcagttgtgatgttta  
 accgtcgggtggtttcagaaacctttgaaacctcttctagggagttttggttctcgcagcggcgcgca  
 attcaaagacgctcgcggcggagcccccagtcgctccccagcacctgtgggacagagcctggcgtgcgcc  
 cagcggagcccctgcagcgtgcttgcggcggttggtgtagtgggagccgcggcggccccggggct  
 ggacgaccggccccgcgtgccaccgctggaggcttccagctgccacctccggcgggtaactggat  
 cagtgccgggtaatgggaagccaccgggagagtgaggaaatgaaactggggcaggaccacgggtgcaga  
 cccggttaccttctccaccaggaaatgccccgctcctaactccaaacgcgccaagtataaacacgag  
 gatggcaagagaccacacacggaggagcggcgttgggggaggaggtgccgtttgttattttctgacac  
 tcccgccaatataccccaagcaccgaaggccttctgttttaagaccgattctctttaccactacaagt  
 tgcttgaagcccagaatggtttgtatttaggcaggcgtgggaaaattaagtttttgcgttttaggagaatgag  
 tctttgcaacgccccgccccgtgatcctccttctccctcttccctccctgggcgaaaaacttct  
 tacaaaaagttaatcactgcccccttagcagcaccacccccaccccgccctgggagtgccctcttt  
 gtgtgtatttttttttctcctaaggaagg

#### EHF promoter-PPRE1/2-wt

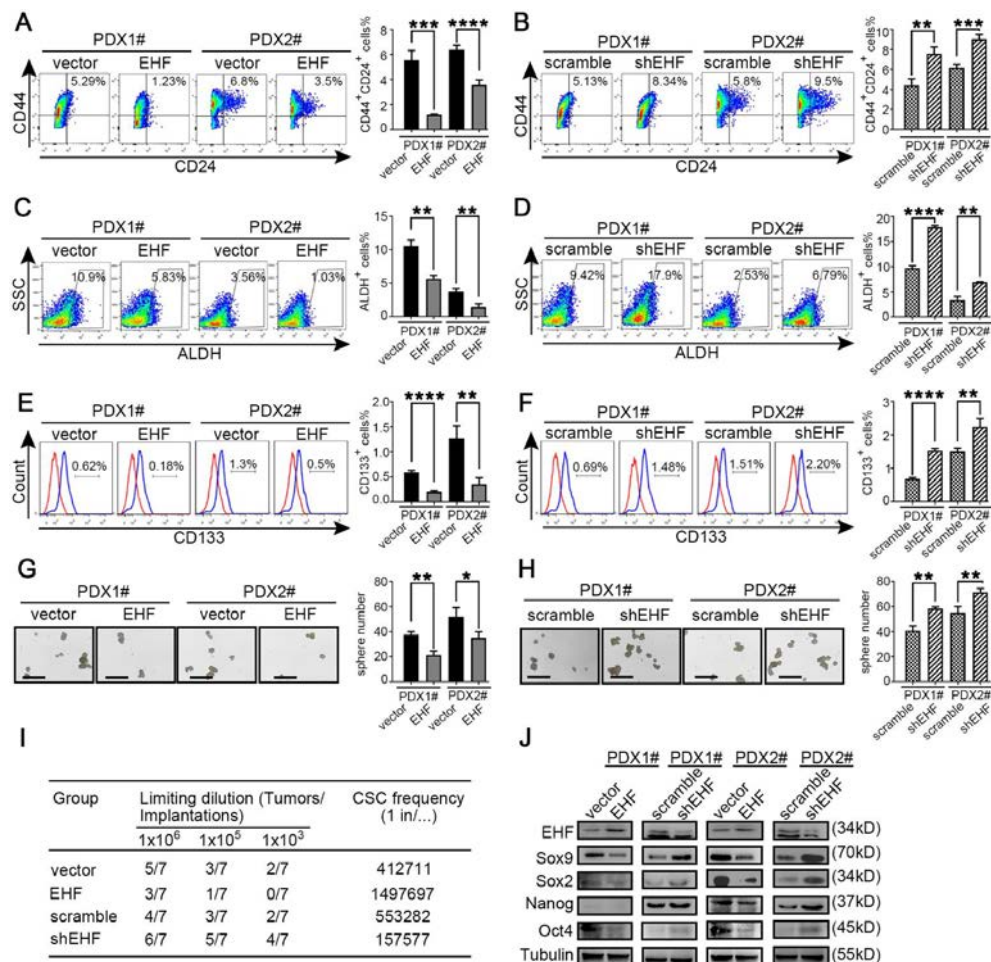
tggtcagagagccacatcacttttgggttcatttgaagttcactatctcttgaccacacaaccctagccc  
 ttctactcccaccctgctgtctcaggtaaatctcaggcaatggtgtaaagaaggccaagttgtttccctgga  
 gtcccacgggctctagcaataatgcttccctttctcagtgagtgccccgcaccaccccccttcaccatcat  
 acacacaaatgccctgcagtggtggaatgtagttacttcagggtgtgcctgatttgtctctcaagcaaaact  
 ccagcaggcattccctcagggccctgctctcagatctggaactgatagactaattggggctaatgtgataat  
 gggaaataatgaaattgttttttatcagtggtatgaggggggggttacatttgcattttcacagggc  
 ccttgcaagttcacagggtgaacagttgggaagggtgggaatgctggggcagggttagggaggcagaggga  
 tttattagaactcccctaaactgcactgaccaaagcctcaagccttctcaagactgccagcttccaaga  
 ccttccaagtccacccttgttttccactgagcttttacactttcagaaacctgtaattgtgtagaac  
 tagaaaaataagtaagaaaagactaataactactgcacactcactgttcccccttaataataaccagttt  
 tatctattcagtcagcctttgaccataagcagaccttttttttcttttaacacaagtaacttcttggtt  
 tgatcaciaaatctttatctctgcaaatctcaacttcccttccctctcccaaaaaggaggcccgttgagt  
 caaagaatctgcttagacactttgctcatgccaggccagtgctcctggaaggttcaacagagaaagttaatgg  
 ttgggggatggtattttcttgctaggagcagtcattcaccgtagggagaaggtacatttgtgaccaggt  
 gaagcaggtacaggttaactcccataatgtcccttgcccaagggaatagaggttgcctgggtatttgaatccg  
 tagatcctccctaataattccacttcttctgtccaaactgtgctttttatttccagtttcagcattttggt  
 ctctcatcttaactcttataggagtgtaataaaccttttaaaaagatcatgtaagtcaagaggaag  
 tgaagaactagataatccaccaaccggataatcagctcttgcatatttgagagttgactgcttgacctaac  
 atctctcataaggtaccctccctccaggaccttcccttcaaacctctcaaggctttacctggggccagg  
 ggagataggctttcaagtcattgaattgccaagagctctgtcaagaaggcagtcaggtgcctggagag  
 ggaacttgctgggagccccctcagagcctggtacttatagagctagggaaaagatcttgatgcaaaagcagg  
 tggactaaatacagactaataaatgagacaggtgctcaagaggccccctcataccatcatctcctcagatt  
 tggacttctactcatttgcctttacattcccttccgatggtgtctttggtagcagggtgcttttacc  
 tgaacagcctctgagctgaaaagaacagtcaccaccaaatcaattcctcatcattaacaggttctctct  
 gttcttgagacacaggcattacctggttagacctgtttgtttgaaactaacgtgtgagttggcaaatgca  
 aatgagccagtggttgaatcctttatttttttaagggtgggttagcaatcagaagggggaagt  
 gacttagggaattccgggttggtgcttattgcttaacatcctacaaaatgattttaaattattgttatatgc  
 atttatcttactctgatgagggtcag



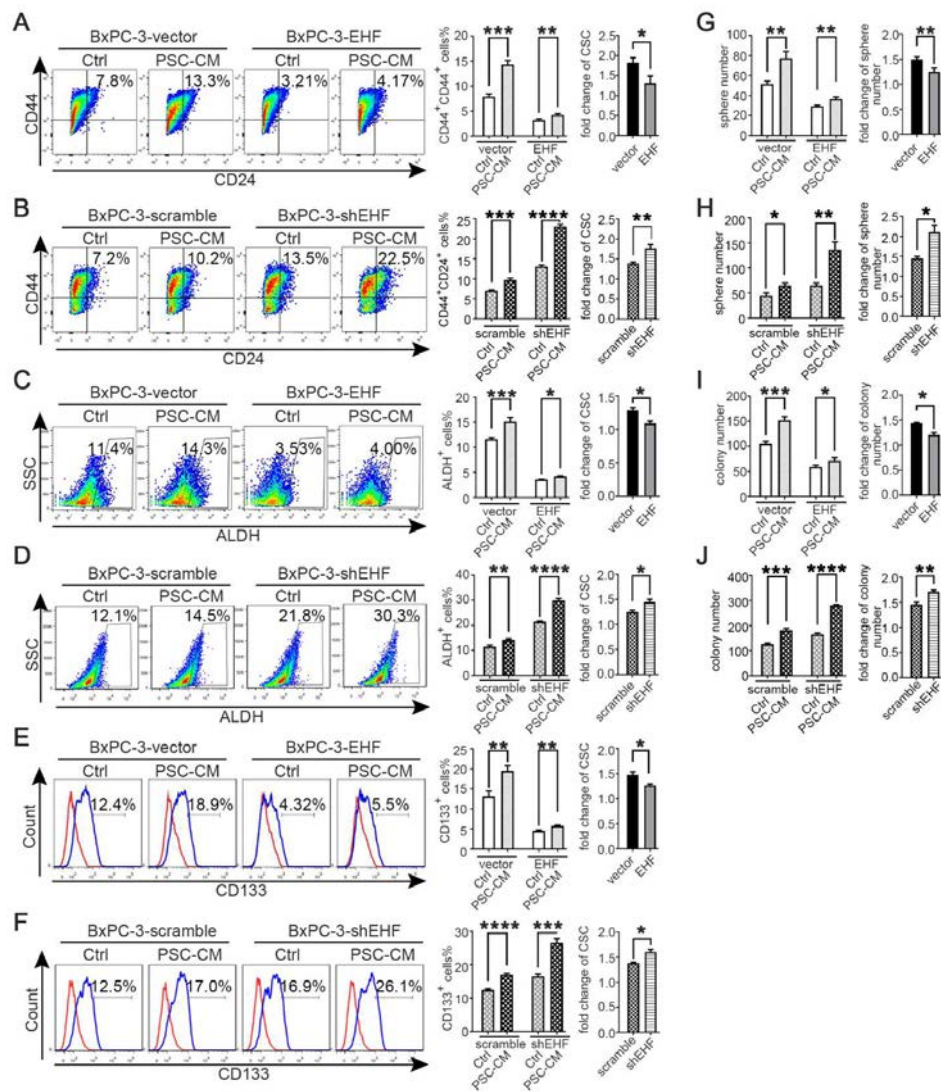
**Supplementary figure 2.** (A) Western blot for the basal expression of ESE3/EHF in five PDAC cancer cell lines (B) Western blot for the expression of differentiation markers (CA II , E-cadherin and CK19) in PANC-1-vector/EHF, MiaPaca-2-vector/EHF, BxPC-3-scramble/shEHF and SW1990-scramble/shEHF cell lines.



**Supplementary figure 3.** Tumoral EHF regulates pancreatic cancer stemness in PANC-1-scramble/shEHF, MiaPaca-2-scramble/shEHF, BxPC-3-vector/EHF and SW1990-vector/EHF cell lines. (A-B) The proportion of CD44<sup>+</sup>CD24<sup>+</sup> cells in indicated cell lines were analyzed using flow cytometry. Representative dot plots (A, left; B, left) and percentage of CD44<sup>+</sup>CD24<sup>+</sup> cells (A, right; B, right) were shown. (C-D) The proportion of ALDH<sup>+</sup> cells in indicated cells were analyzed using flow cytometry. Representative dot plots (C, left; D, left) and percentage of ALDH<sup>+</sup> cells (C, right; D, right) were shown. (E-F) The proportion of CD133<sup>+</sup> cells in indicated cells were analyzed using flow cytometry. Representative histograms (E, left; F, left) and percentage of CD133<sup>+</sup> cells (E, right; F, right) were shown. (G-H) Sphere formation assays were performed in indicated cell lines. Representative images (G, left; H, left) and sphere number analysis (G, right; H, right) were shown. Bars:100 $\mu$ m. (K) Western blot on EHF, Sox9, Sox2, Nanog and Oct4 were analyzed in indicated cell lines.  $\beta$ - tubulin was used as loading control. Representative results were shown. All experiments were repeated three times independently. Paired Student's t-test was used as statistical analysis. \* $P$ <0.05, \*\* $P$ <0.01, \*\*\* $P$ <0.001 and \*\*\*\* $P$ <0.0001.

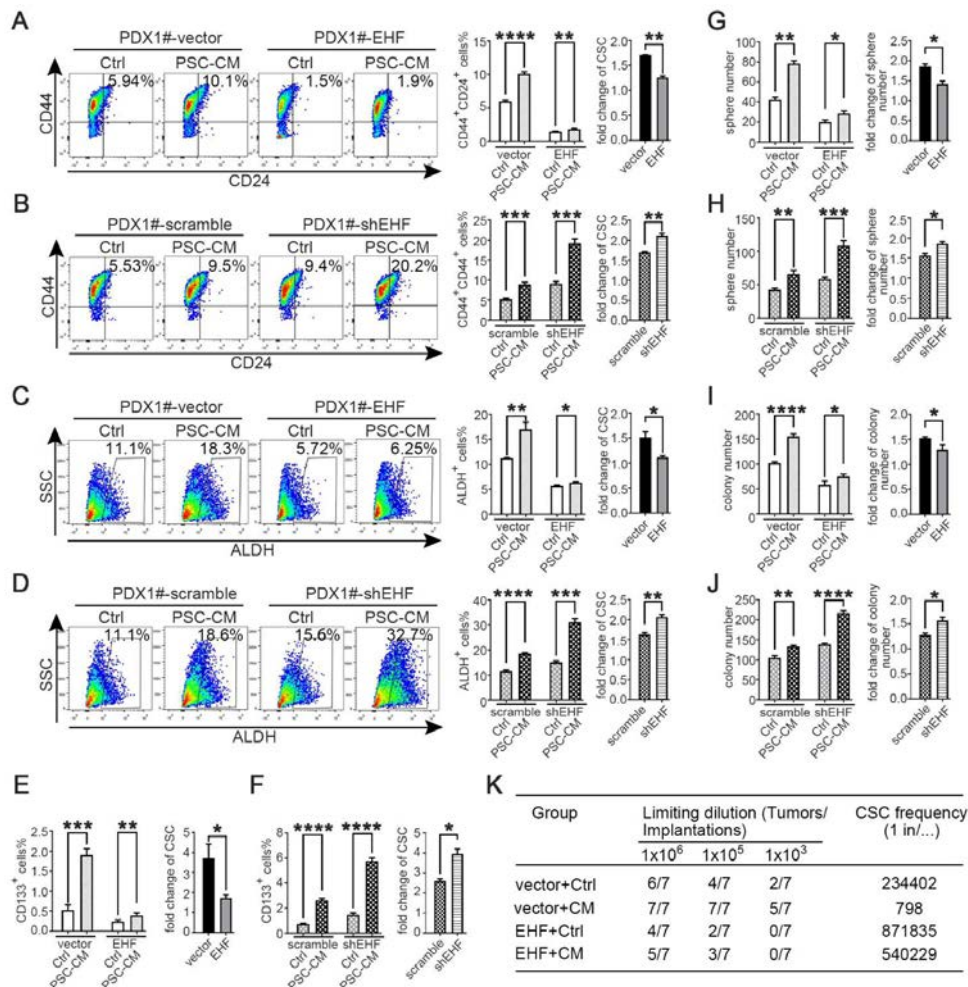


**Supplementary figure 4.** Tumoral EHF regulates pancreatic cancer stemness in PDX1#-vector/EHF, PDX1#-scramble/shEHF, PDX2#-vector/EHF and PDX2#-scramble/shEHF. (A-B) The proportion of CD44<sup>+</sup>CD24<sup>+</sup> cells in indicated cell lines were analyzed using flow cytometry. Representative dot plots (A, left; B, left) and percentage of CD44<sup>+</sup>CD24<sup>+</sup> cells (A, right; B, right) were shown. (C-D) The proportion of ALDH<sup>+</sup> cells in indicated cells were analyzed using flow cytometry. Representative dot plots (C, left; D, left) and percentage of ALDH<sup>+</sup> cells (C, right; D, right) were shown. (E-F) The proportion of CD133<sup>+</sup> cells in indicated cells were analyzed using flow cytometry. Representative histograms (E, left; F, left) and percentage of CD133<sup>+</sup> cells (E, right; F, right) were shown. (G-H) Sphere formation assays were performed in indicated cell lines. Representative images (G, left; H, left) and sphere number analysis (G, right; H, right) were shown. Bars:100μm. (I) In vivo limited dilution assays for PDX1#-vector/EHF and PDX1#-scramble/shEHF cell lines were performed. Representative tumor incidence and CSC probabilities were shown. (J) Western blot on EHF, Sox9, Sox2, Nanog and Oct4 were analyzed in indicated cell lines. β-tubulin was used as loading control. Representative results were shown. All experiments were repeated three times independently. Paired Student's t-test were used for in vitro experiments. \**P*<0.05, \*\**P*<0.01, \*\*\**P*<0.001 and \*\*\*\**P*<0.0001.



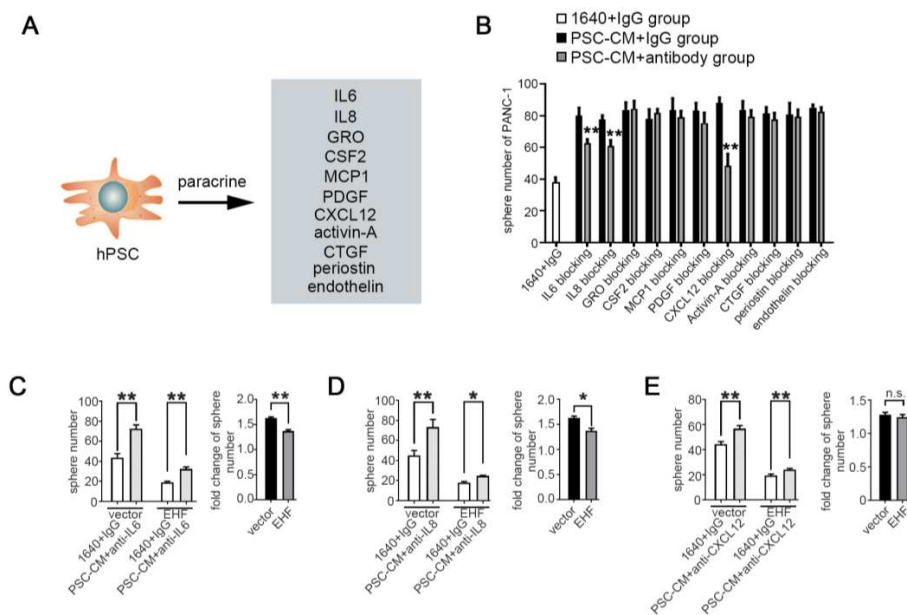
**Supplementary figure 5.** Data from another BxPC-3-vector/EHF and BxPC-3-scramble/shEHF cell lines culturing with PSC-CM. (A-F) BxPC-3-vector, BxPC-3-EHF, BxPC-3-scramble and BxPC-3-shEHF were cultured with PSC-CM or the control medium. The percentage of PCSCs in each cell line under each treatment were shown, the fold change of the percentage of PCSCs in each cell line after culturing with PSC-CM was calculated: (A-B) CD24<sup>+</sup>CD44<sup>+</sup> cells, (C-D) ALDH<sup>+</sup> cells, (E-F) CD133<sup>+</sup> cells. Representative dot plots/ histogram (left), the statistical analysis of CSC percentage of each group (medium) and the statistical analysis of the fold change in each cell line (right) (G-H) Statistical analysis of the sphere number of each cell line under the treatment of serum-free medium and serum-free medium with PSC-CM added (left), statistical analysis of the fold change of sphere number after culturing with serum-free medium containing PSC-CM in each cell line(right). (I-J) Statistical analysis of the soft agar colony number of each cell line under the treatment of control medium and PSC-CM (left). Statistical analysis of the fold change of colony number after culturing with PSC-CM in each cell line (right).

All experiments were repeated three times independently. Paired Student's t-test was used for statistical analysis. \* $P < 0.05$ , \*\* $P < 0.01$ , \*\*\* $P < 0.001$ , \*\*\*\* $P < 0.0001$  and n.s. means non-significant.

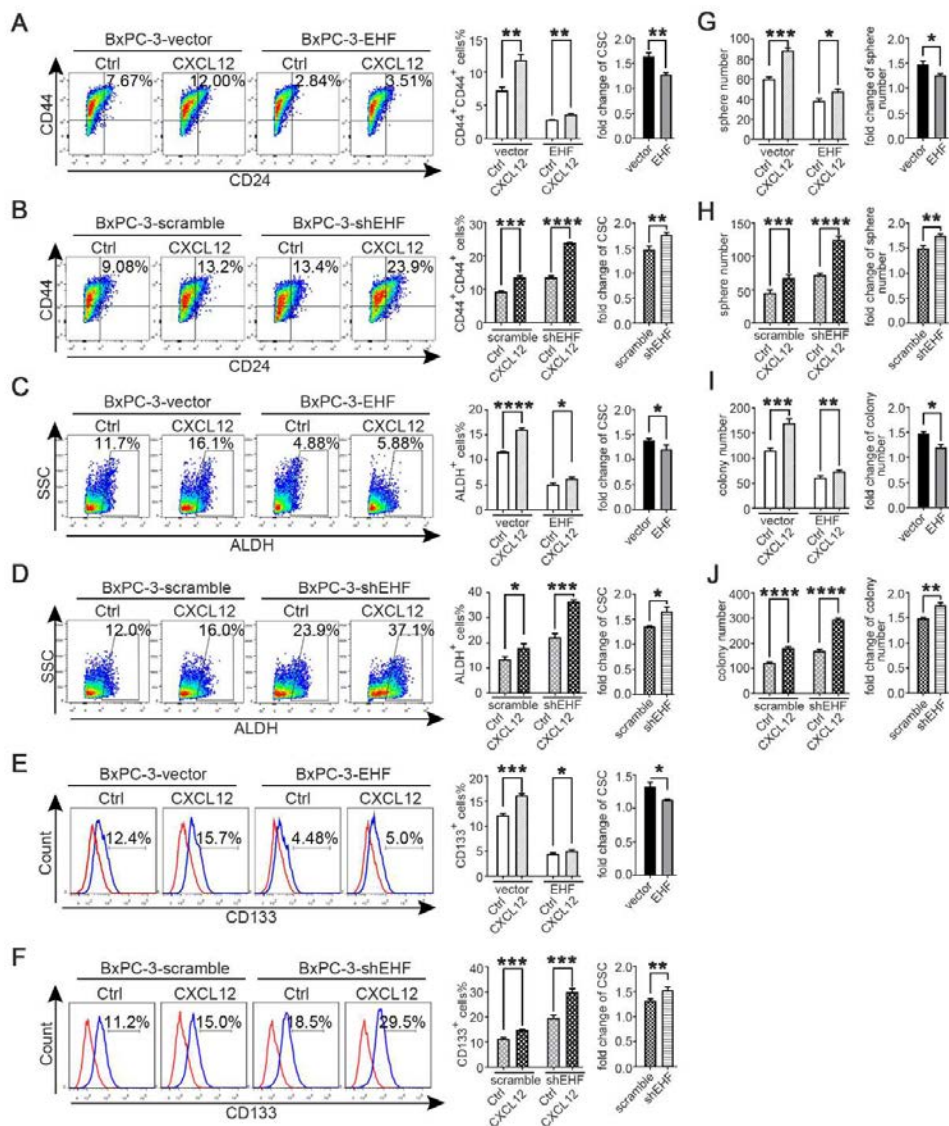


**Supplementary figure 6.** Data from another primary PDX1#-vector/EHF or PDX1#-scramble/shEHF cell lines culturing with PSC-CM. (A-F) PDX1#-vector, PDX1#-EHF, PDX1#-scramble and PDX1#-shEHF were cultured with PSC-CM or the control medium. The percentage of PCSCs in each cell line under each treatment were shown, the fold change of the percentage of PCSCs in each cell line after culturing with PSC-CM was calculated: (A-B) CD24<sup>+</sup>CD44<sup>+</sup> cells, (C-D) ALDH<sup>+</sup> cells, (E-F) CD133<sup>+</sup> cells. Representative dot plots (for CD24<sup>+</sup>CD44<sup>+</sup> cells and ALDH<sup>+</sup> cells), the statistical analysis of CSC percentage of each group and the statistical analysis of the fold change in each cell line. (G-H) Statistical analysis of the sphere number of each cell line under the treatment of serum-free medium and serum-free medium with PSC-CM added (left), statistical analysis of the fold change of sphere number after culturing with serum-free medium containing PSC-CM in each cell line (right). (I-J) Statistical analysis of the soft agar colony number of each cell line under the treatment of control medium and PSC-CM (left). Statistical analysis of the fold change of colony number after culturing with PSC-CM in each cell line (right). (K) In vivo limited dilution assay was performed to determine the effects of PSC-CM on CSC self-renewal of PDX1#-vector/EHF. Representative tumor incidence and CSCs probabilities were shown. All experiments were repeated three times

independently. Paired Student's t-test was used for statistical analysis. \* $P < 0.05$ , \*\* $P < 0.01$ , \*\*\* $P < 0.001$ , \*\*\*\* $P < 0.0001$  and n.s. means non-significant.

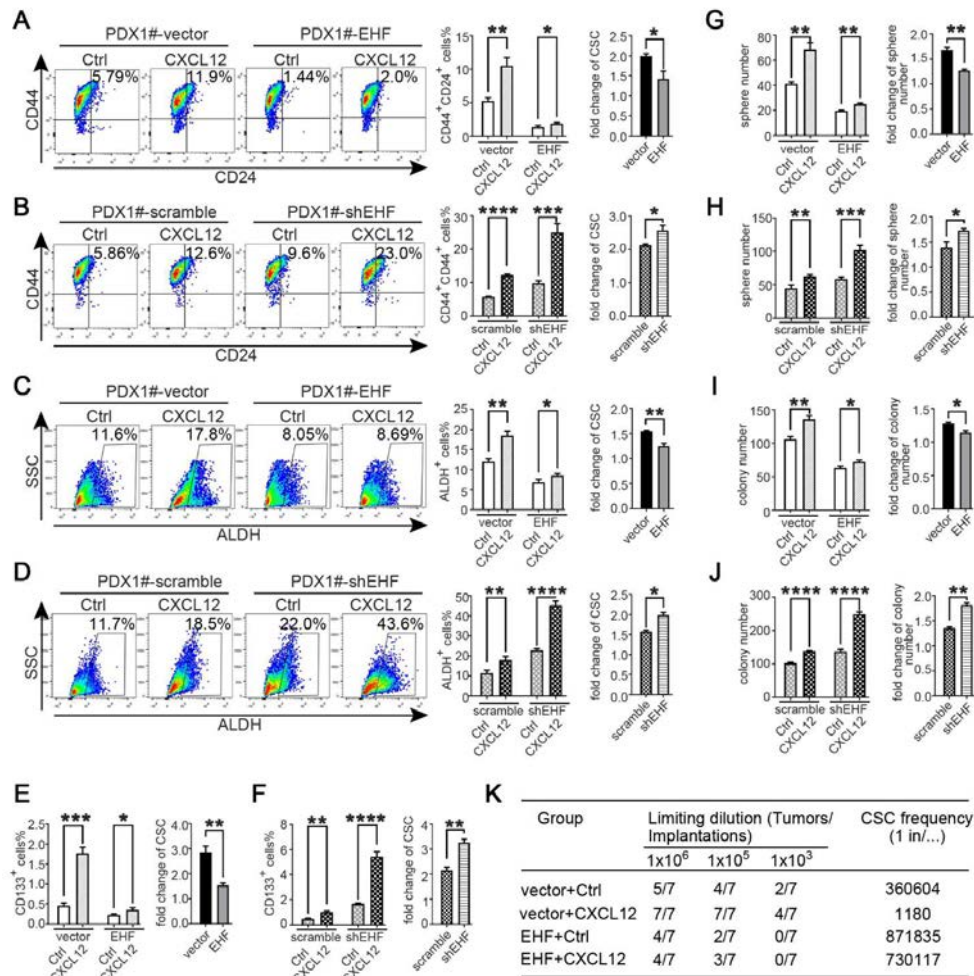


**Supplementary figure 7.** (A) Illustration of cytokines secreted by PSCs. (B) Sphere formation capacity of PANC-1 cells cultured in PSC-CM derived serum-free medium after blocking with series of cytokine antibodies, respectively. Anti-IL6, anti-IL8, anti-GRO, anti-CSF2, anti-MCP1, anti-PDGF, anti-CXCL12, anti-activin-A, anti-CTGF, anti-periostin and anti-endothelin antibodies were used. IgG isotype were used as control. (C) The actual sphere number (left) and the fold change of sphere number (right) in PANC-1-vector/EHF after culturing with PSC-CM derived serum-free medium neutralized with anti-IL6 antibody. (D) The actual sphere number (left) and the fold change of sphere number (right) in PANC-1-vector/EHF after culturing with PSC-CM derived serum-free medium neutralized with anti-IL8 antibody. (E) The actual sphere number (left) and the fold change of sphere number (right) in PANC-1-vector/EHF after culturing with PSC-CM derived serum-free medium neutralized with anti-CXCL12 antibody. \* $P < 0.05$ , \*\* $P < 0.01$  and n.s. means non-significant.



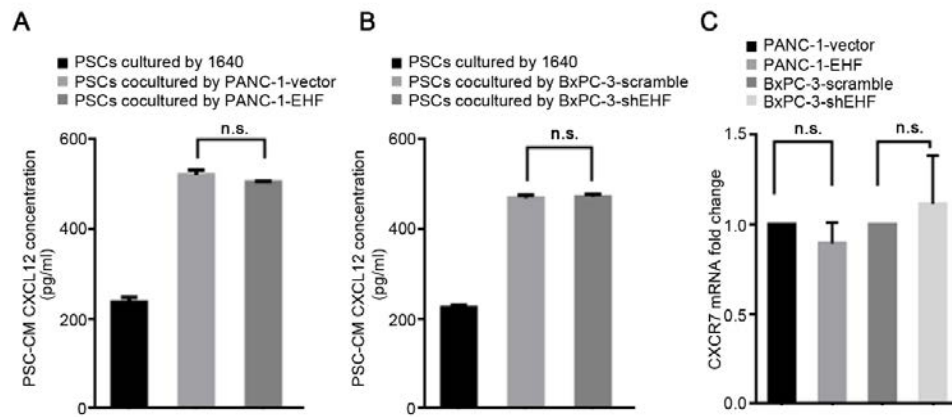
**Supplementary figure 8.** Data from another BxPC-3-vector/EHF and BxPC-3-scramble/shEHF cell lines treating with recombinant human CXCL12/SDF-1 $\alpha$ . (A-F) BxPC-3-vector, BxPC-3-EHF, BxPC-3-scramble and BxPC-3-shEHF were cultured with medium containing CXCL12 or the control medium. The percentage of PCSCs in each cell line under each treatment were shown, the fold change of the percentage of PCSCs in each cell line after culturing with medium containing CXCL12 was calculated: (A-B) CD24<sup>+</sup>CD44<sup>+</sup> cells, (C-D) ALDH<sup>+</sup> cells, (E-F) CD133<sup>+</sup> cells. Representative dot plots/histogram (left), the statistical analysis of CSC percentage of each group (medium) and the statistical analysis of the fold change in each cell line (right). (G-H) Statistical analysis of the sphere number of each cell line under the treatment of serum-free medium and serum-free medium with CXCL12 added (left), statistical analysis of the fold change of sphere number after culturing with serum-free medium containing CXCL12 in each cell line (right). (I-J) Statistical analysis of the soft agar colony number of each cell line under

the treatment of control medium and medium containing CXCL12 (left), statistical analysis of the fold change of colony number after culturing with medium containing CXCL12 in each cell line (right). All experiments were repeated three times independently. Paired Student's t-test was used for statistical analysis. \* $P < 0.05$ , \*\* $P < 0.01$ , \*\*\* $P < 0.001$ , \*\*\*\* $P < 0.0001$  and n.s. means non-significant.

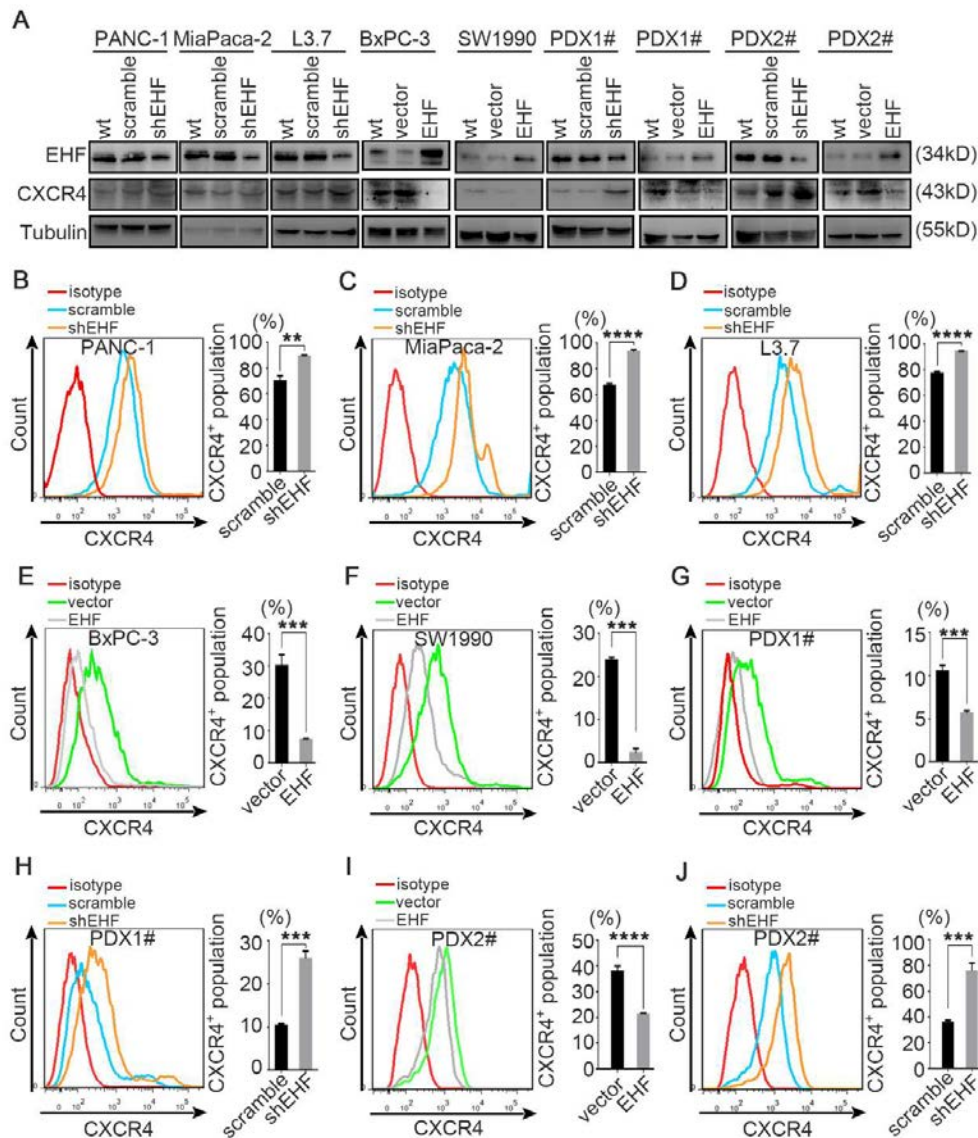


**Supplementary figure 9.** Data from another primary PDX1#-vector/EHF or PDX1#-scramble/shEHF cell lines treating with recombinant human CXCL12/SDF-1 $\alpha$ . (A-F) PDX1#-vector, PDX1#-EHF, PDX1#-scramble and PDX1#-shEHF were cultured with medium containing CXCL12 or the control medium. The percentage of PCSCs in each cell line under each treatment were shown, the fold change of the percentage of PCSCs in each cell line after culturing with medium containing CXCL12 was calculated: (A-B) CD24<sup>+</sup>CD44<sup>+</sup> cells, (C-D) ALDH<sup>+</sup> cells, (E-F) CD133<sup>+</sup> cells. Representative dot plots (for CD24<sup>+</sup>CD44<sup>+</sup> cells and ALDH<sup>+</sup> cells), the statistical analysis of CSC percentage of each group and the statistical analysis of the fold change in each cell line. (G-H) Statistical analysis of the sphere number of each cell line under the treatment of serum-free medium and serum-free medium with CXCL12 added (left), statistical analysis of the fold change of sphere number after culturing with serum-free medium containing CXCL12 in each cell line(right). (I-J) Statistical analysis of the soft agar colony number of each cell line under the treatment of control medium and medium containing CXCL12 (left), statistical analysis of the fold change of colony number after culturing with medium containing CXCL12 in each cell line(right). (K) In vivo limited dilution assay was performed to determine the effects of human recombinant CXCL12 on CSC self-renewal of PDX1#-vector/EHF. Control

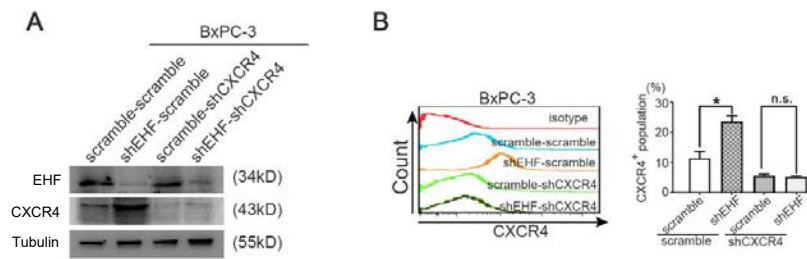
medium was used as the control of CXCL12. Tumor incidence and CSCs probabilities were shown. All experiments were repeated three times independently. Paired Student's t-test was used for statistical analysis. \* $P < 0.05$ , \*\* $P < 0.01$ , \*\*\* $P < 0.001$ , \*\*\*\* $P < 0.0001$  and n.s. means non-significant.



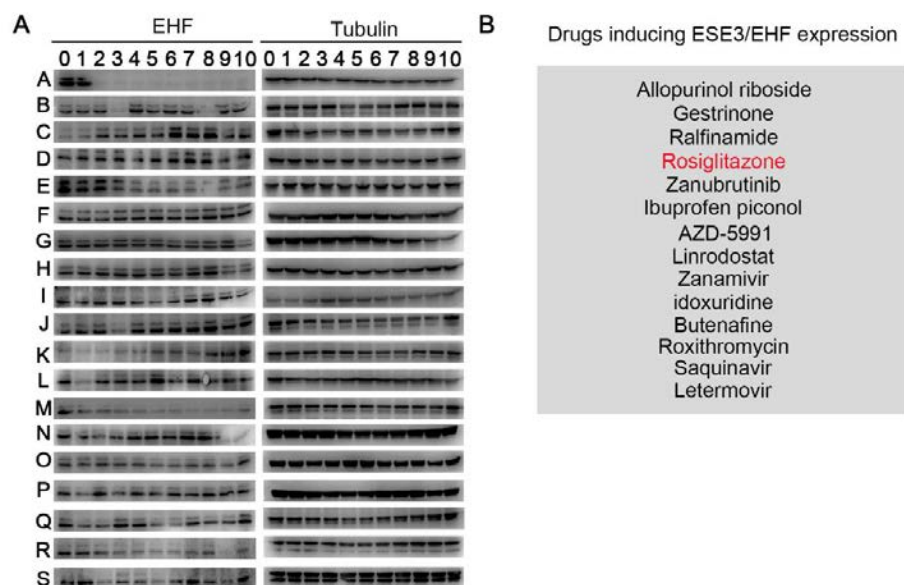
**Supplementary figure 10.** (A-B) ELISA assay for CXCL12 protein in conditioned medium of PSCs indirectly cocultured by PANC-1-vector/EHF and BxPC-3-scramble/shEHF cell lines (1640 was used as control). Representative results were shown (PANC-1, A; BxPC-3, B). (C) CXCR7 mRNA expression was determined in PANC-1-vector/EHF and BxPC-3-scramble/shEHF cell lines. All experiments were repeated three times independently. Paired Student's t-test was used as statistical analysis and n.s. means non-significant.



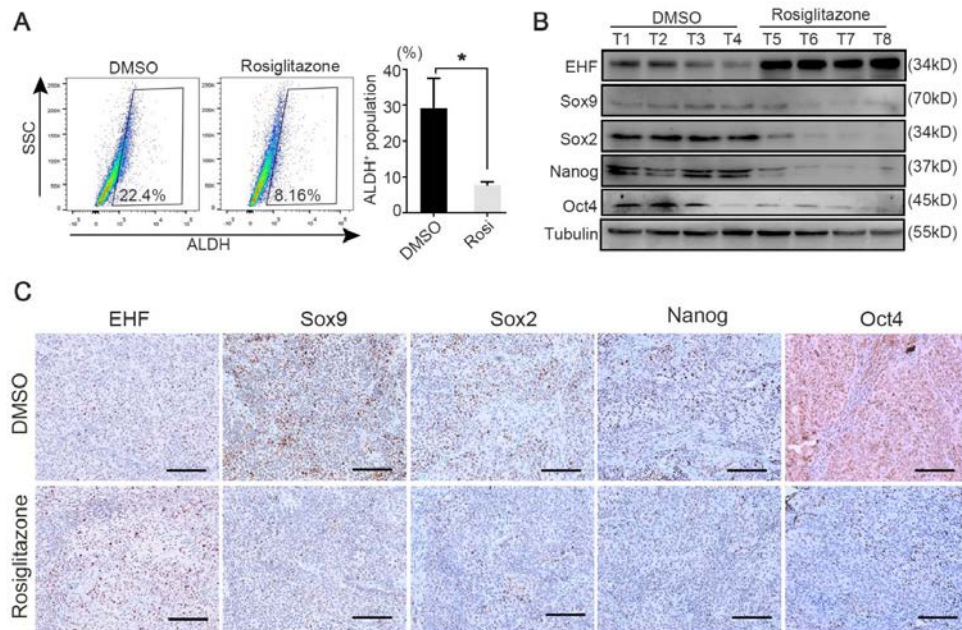
**Supplementary figure 11.** EHF negatively regulated the expression of CXCR4 in newly established PDAC cell lines. (A) Total protein expression of EHF and CXCR4 were validated in indicated cell lines by western blot. Tubulin was used as loading control. Representative results were shown. (B-J) Percentage of CXCR4<sup>+</sup> population in indicated cell lines were analyzed by flowcytometry. Isotype was used as negative control. Representative histogram and statistical analysis were shown. All experiments were repeated three times independently. Paired Student's t-test were used for statistical analysis. \*P<0.05, \*\*P<0.01, \*\*\*P<0.001, \*\*\*\*P<0.0001.



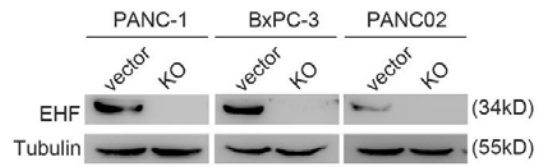
**Supplementary figure 12.** (A) Protein expression of EHF and CXCR4 were detected in BxPC-3-scramble-scramble/shCXCR4 and BxPC-3-shEHF-scramble/shCXCR4 cell lines by western blot. Representative results were shown. (B) Percentage of CXCR4<sup>+</sup> population were analyzed in indicated cell lines by flow cytometry. Representative histograms (left) and percentage of CXCR4<sup>+</sup> population (right) were shown.



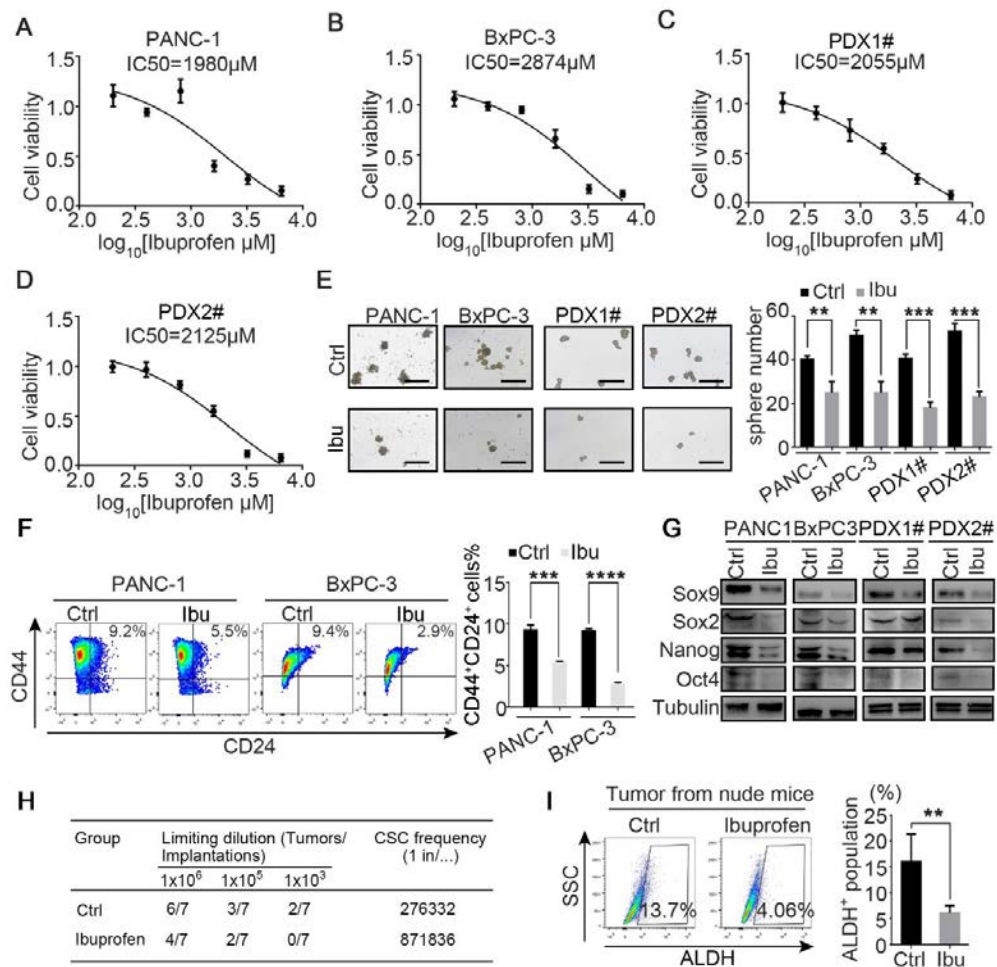
**Supplementary figure 13.** (A) PANC-1 cells were treated with total 190 compounds (10 $\mu$  M; 24h) from our drug library for screening potential ESE3/EHF agonists. A0, B0, C0, D0, E0, F0, G0, H0, I0, J0, K0, L0, M0, N0, O0, P0, Q0, R0 and S0 mean groups treated with DMSO. Western blot was taken to detect EHF protein expression.  $\beta$ -tubulin was used as a loading control for western blot. Experiments were repeated three times independently. Representative results were shown. (B) The list of drugs which induced ESE3/EHF protein expression in PANC-1 cells.



**Supplementary figure 14.** Rosiglitazone suppresses PDAC stemness in orthotopic mouse model. (A) BALB/C nude mice were orthotopically implanted with  $5 \times 10^5$  PANC02 cells. Rosiglitazone was injected intraperitoneally three times a week. Mice were sacrificed at day 28 after drug administration and single cell suspension of pancreatic orthotopic tumors were prepared for ALDH<sup>+</sup> CSCs detection. PI was used to exclude dead cells and CD45 was used to exclude leukocytes and DEAB was used as negative control. Representative dot plots (left) and statistical analysis (right) were shown. (B) Western blot of EHF and stemness markers in tissue proteins from murine pancreatic orthotopic tumors were performed. Tubulin was used as loading control and representative results were shown. (C) IHC of EHF and stemness markers in pancreatic orthotopic tumors were carried out. Bar, 200 $\mu$ m. All experiments were repeated three times independently. Non-paired Student's t-test was used for statistical analysis. \* $P < 0.05$ .

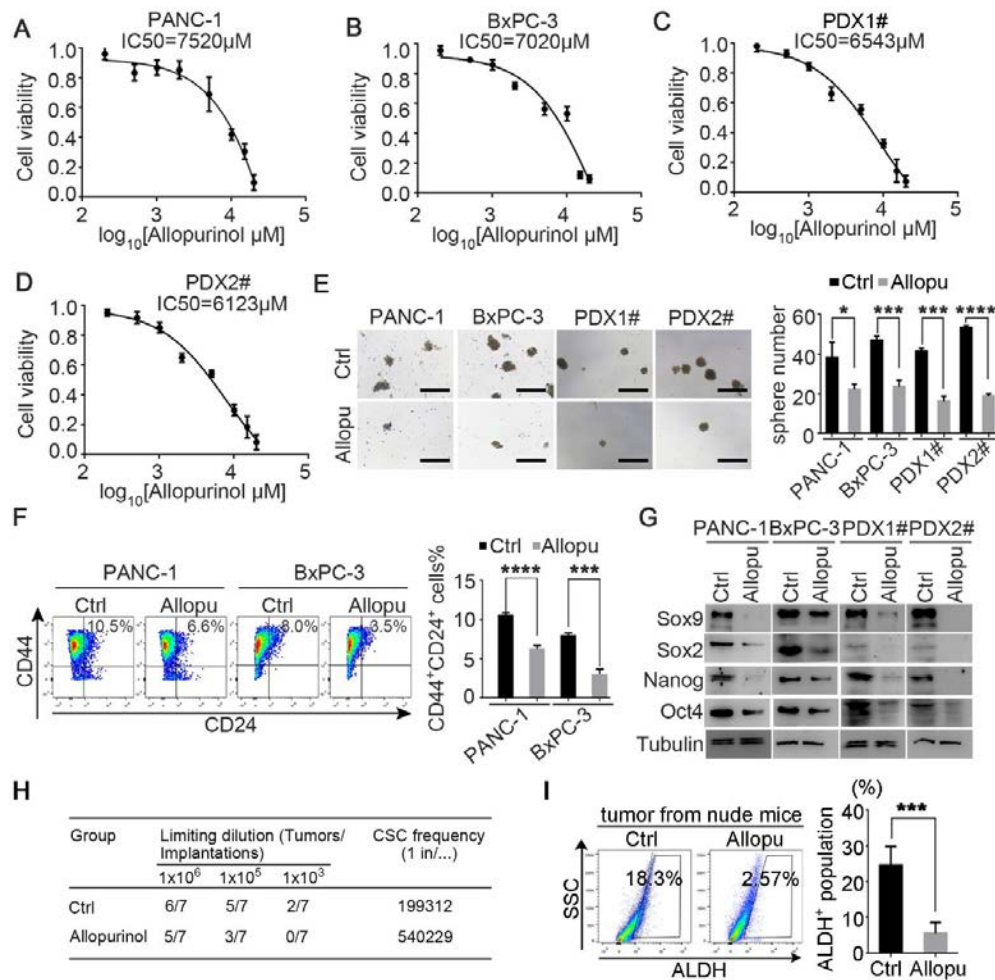


**Supplementary figure 15.** Validation of EHF expression in PANC-1-vector/EHF-KO, BxPC-3-vector/EHF-KO and PANC02-vector/Ehf-KO cell lines by western blot.



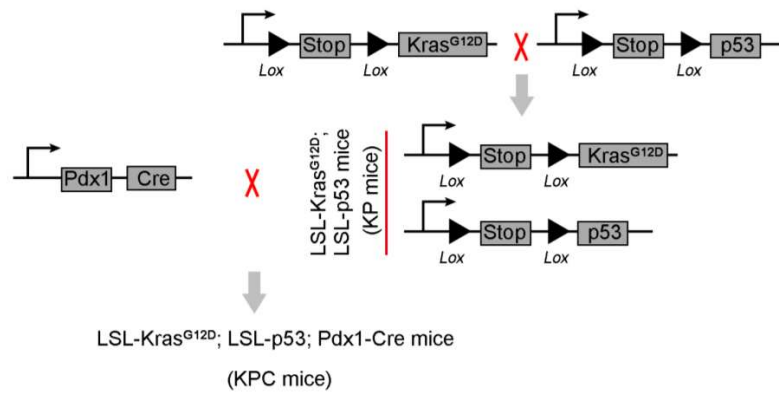
**Supplementary figure 16.** Ibuprofen suppresses cellular stemness in PDAC. (A-D) IC<sub>50</sub> of ibuprofen in PANC-1 and BxPC-3 cell lines and PDX1# PDX2# primary cell lines were detected by CCK-8. 1mM ibuprofen was used in following experiments. (E) Adherent PDAC cell lines were pre-treated with 1mM ibuprofen for 48 hours (DMSO was used as control); and then cells were collected and cultured with serum-free medium for the following sphere formation assays. Ibuprofen abbreviated as Ibu in following experiments. Representative images were shown (left) and statistical analysis were shown (right). (F) Percentage of CD44<sup>+</sup>CD24<sup>+</sup> population were detected in indicated cell lines treated with 1mM ibuprofen by flow cytometry. Representative dot plots were shown (left) and statistical analysis were presented (right). (G) Western blot for stemness markers (Sox9, Sox2, Nanog and Oct4) were performed on indicated cell lines treated with 1mM ibuprofen. (H) In vivo limited dilution assay was performed to determine the effects of ibuprofen on CSC self-renewal of PANC-1 cells. Tumor incidence and CSCs probabilities were shown. (I) Percentage of ALDH<sup>+</sup> cells in harvested tumor tissues from panel H. PI was used to exclude dead cells and CD45 was used to exclude leukocytes and DEAB was used as negative control. Representative dot plots were shown (left) and statistical analysis were shown (right). Paired Student's t-test was used for statistical analysis of in vitro experiments

and non-paired Student's t-test was used for statistical analysis of in vivo murine experiments. \*\*P<0.01, \*\*\*P<0.001 and n.s. means non-significant.



**Supplementary figure 17.** Allopurinol suppresses cellular stemness in PDAC. (A-D) IC50 of allopurinol in PANC-1 and BxPC-3 cell lines and PDX1# PDX2# primary cell lines were detected by CCK-8. 5mM allopurinol was used in following experiments. (E) Adherent PDAC cell lines were pre-treated with 5mM allopurinol for 48 hours (DMSO was used as control); and then cells were collected and cultured with serum-free medium for the following sphere formation assays. Allopurinol abbreviated as Allopu in following experiments. Representative images were shown (left) and statistical analysis were shown (right). (F) Percentage of CD44<sup>+</sup>CD24<sup>+</sup> population were detected in indicated cell lines treated with 5mM allopurinol by flow cytometry. Representative dot plots were shown (left) and statistical analysis were presented (right). (G) Western blot for stemness markers (Sox9, Sox2, Nanog and Oct4) were performed on indicated cell lines treated with 5mM allopurinol. (H) In vivo limited dilution assay was performed to determine the effects of allopurinol on CSC self-renewal of PANC-1 cells. Tumor incidence analysis and CSCs probabilities were shown. (I) Percentage of ALDH<sup>+</sup> cells in harvested tumor tissues from panel H. PI was used to exclude dead cells and CD45 was used to exclude leukocytes and DEAB was used as negative control. Representative dot plots were shown (left) and statistical analysis were shown (right). Paired Student's t-test was used for statistical

analysis of in vitro experiments and non-paired Student's t-test was used for statistical analysis of in vivo murine experiments. \*\*P<0.01, \*\*\*P<0.001, \*\*\*\*P<0.0001 and \*\*\*\*P<0.0001.



**Supplementary figure 18.** The breeding strategies for KPC mice models.

## Materials and method

### Patients and samples collection

A total of 93 patients who had received radical surgery R0 resection with histological diagnosis of PDAC at the Tianjin Medical University Cancer Institute and Hospital, China from July 2011 to January 2015 were retrospectively collected in this study. Until the last follow-up date of October 23, 2019, the follow-up rate was 100%. Clinicopathological data of the 93 consecutive PDAC patients, including age, sex, tumor size, regional lymph node status, TNM stage, histological grade, differentiation and regional vessel invasion status were obtained. None of the patients had received neoadjuvant chemotherapy or radiotherapy before tissue samples were collected. Systemic gemcitabine-based chemotherapy was given to all the patients.

From January 2018 to November 2019, 39 consecutive cases of fresh PDAC tissues were prospectively collected during operation. The PDAC tissue mass was cut into two parts, one parts were grinded and digested into single cell suspension for flowcytometry, the paired parts were used for IHC detection of ESE3/EHF expression. The usage of these specimens and the patients' information were approved by the Ethics Committee of the Tianjin Medical University Cancer Institute and Hospital (Tianjin, China). All patients provided written consent for the use of their specimens and disease information for future investigations according to the ethics committee and in accordance with recognized ethical guidelines of Helsinki.

### Cell culture

Human PDAC cell lines PANC-1, BxPC-3 and SW1990 were obtained from the Type Culture Collection Committee of the Chinese Academy of Sciences (Shanghai, China) and the MiaPaca-2 cell line was obtained from ATCC in 2013. The murine PDAC cell line PANC02 was a gift from Prof. Yang SY (Moffitt Cancer Center, Tampa, FL, USA). The immortalized human PSC cell line ihPSC was established by retrovirus-mediated gene transfer for simian virus 40(SV40) T antigen and human telomerase reverse transcriptase (hTERT) into the human PSCs isolated from the resected pancreas tissue of a patient undergoing operation for pancreatic cancer. *Mycoplasma* contamination was excluded in these cell lines at the beginning of this study. These cells were cultured in DMEM and RPMI1640 basic medium supplemented with 10% Fetal Bovine Serum(FBS) at 37°C in a humidified atmosphere of 95% air and 5% CO<sub>2</sub>.

### Plasmid construction and lentiviral transduction

shCXCR4 sequences were designed by GeneCopeia Company (China) and three recommended sequences for CXCR4 genes were synthesized and cloned into the psi-nU6.1 Vectors. Human CRISPR/dCas9-EHF knockout virus and murine CRISPR/dCas9-Ehf-knockout viruses were purchased from Genechemat company (China) and PANC-1-vector/EHF-KO, BxPC-3-vector/EHF-KO and PANC02-vector/Ehf-KO cell lines were constructed according to the manufacturer's instructions.

### The establishment of primary cancer cell lines in pancreatic cancer

Fresh human PDAC tissues were obtained during surgery and immediately washed by PBS three times. Blood clots, dead tissues and other connective tissues were removed. PDAC tissues were cut into small pieces (1mm<sup>3</sup>) and then PDAC pieces were transferred into 15ml Conical centrifugal tube(Corning) resuspended with a mix of 5ml enzymes buffer containing 1 mg/ml collagenase(Sigma-Aldrich,C2799), 2.5 U/ml hyaluronidase(Sigma-Aldrich, H3506) and 0.1 mg/ml DNase(Sigma-Aldrich DN25) in 37°C water bath for 4~6 h. The mix were then filtrated in a 30um strainer (MACS Smart Strainer) to obtain single cell suspension. The primary cancer cells were centrifuged, cell pellet was re-suspended with fresh medium and seeded in 6-well plates. Genomic sequencing (including four highly mutated genes: TP53, KRAS, SMAD4 and p16) were performed to investigate the genomic background of primary cancer cell lines and detailed information of PDX1# and PDX2# were listed in supplementary table 4-5. Low-passage (<10 passages) primary cancer cells were used for later experiments.

### **Immunohistochemistry (IHC)**

IHC analysis was performed in PDAC tissues using a DAB substrate kit (ORIGENE, ZLI-9019). All antibodies used in this study were list in supplementary table 9. The intensity of the staining was evaluated using the following criteria: 0, negative; 1, low; 2, medium; and 3, high. The extent of staining was scored as 0, 0% stained; 1, 1%–25% stained; 2, 26%–50% stained; and 3, 51%–100% stained. Five random fields (100×magnification) were evaluated under a light microscope. The final scores were calculated by multiplying the scores of the intensity with those of the extent and dividing the samples into four grades: 0, negative (-); 1–2, low staining (+); 3–5, medium staining (++); and 6–9, high staining (+++). IHC score was determined by two independent pathologists who were blinded to the patients' clinical features and outcomes.

### **Multiplex fluorescent IHC and Multispectral imaging**

Two sets of 93 PDAC tissues were used for immunological assessment of EHF, CD133 and ALDH1. All antibodies used in this study were list in supplementary table 9. CD133 or ALDH1 was labeled by Opal 520(494nm-525nm), EHF was labeled by Opal 650(627nm-650nm) (Perkin Elmer, 2395285). Isotype controls were used for all assays. Stained slides were scanned over the whole slide using the Vectra Polaris system (PerkinElmer). Phenochart slide reviewer (PerkinElmer) was used to systematically capture tissue heterogeneity in an unbiased manner. The selected images were then captured with a 20× lens using the Vectra Polaris system. Form cell Analysis software 2.4 (PerkinElmer) was used to evaluate the counts of EHF, ALDH1 and CD133 positive points per high power field (HPF; 200x). Tumor areas were manually outlined to exclude stromal nuclei. DAPI was used to identify nuclei. EHF was then measured on a cell-nucleus based mode. Five random fields (200×magnification) were evaluated. The count of EHF-positive points per high power field (HPF; 200X) ranged from 0 to 260, mean ± SD, 108.05 ± 65.13. EHF-positive counts/HPF > 108.05 was considered as high-EHF group; EHF-positive counts/HPF < 108.05 was considered as low-EHF group. The count of ALDH1-positive points per high power field (HPF; 200X) ranged from 0 to 30, mean ± SD, 17.61 ± 7.37. ALDH1-positive counts/HPF > 17.61 was considered as high-ALDH1 group; ALDH1-

positive counts/HPF < 17.61 was considered as low-ALDH1 group. The count of CD133-positive points per high power field (HPF; 200X) ranged from 0 to 52, mean  $\pm$  SD, 27.99  $\pm$  13.35. CD133-positive counts/HPF > 27.99 was considered as high-CD133 group; CD133-positive counts/HPF < 27.99 was considered as low-CD133 group.

### **Sphere formation assay**

PDACs (5000 cells/ml) were cultured in ultra-low adhesion plates (Corning) in serum-free DMEM/F12 medium (GIBCO), which contains B27 (1:50, Invitrogen), 20ng/ml EGF (Proteintech), 10ng/ml FGF2 (Proteintech), 0.4% Bovine Serum Albumin (Sigma) and 5 $\mu$ g/ml insulin (Sigma). After 2 weeks, tumor spheres with diameter >75 $\mu$ m were counted.

### **CCK8 cell viability and cytotoxicity assay**

PANC-1, BxPC-3, PDX1# and PDX2# cells were seeded in clear, flat-bottom 96-well plates (Corning) at a density of 1000 cells per well. The following day, cancer cells were treated with dilution range of ibuprofen (sigma, I4833) (0, 0.2mM, 0.4mM, 0.8mM, 1.6mM, 3.2mM and 6.4mM) or allopurinol (sigma, PHR1377) (0, 0.2mM, 0.5mM, 1mM, 2mM, 5mM, 10mM, 15mM and 20mM) (6 duplications for each concentration) for 72h. And then, culture media were replaced with fresh DMEM containing 10% CCK8 (Bimake, B34302) and plates were incubated for 3 h in an incubator. The absorbance was read at 595nm and the IC50 for ibuprofen or allopurinol were calculated.

### **Anchorage-independent growth assay**

A total of 5000 cells were individualized through 40- $\mu$ m porous strainers and seeded in a medium solution with 0.7% agar settled on a solidified 1.2% agar layer. Once solidified, fresh medium was added above the cell-containing layer and replaced 3 times a week. Cells were maintained in a humidified atmosphere with 5% CO<sub>2</sub> at 37°C. After 3 weeks in culture, medium was removed and replaced with 1 mg/mL 3-(4, 5-dimethylthiazolyl-2)-2 (MTT, M2128, Sigma-Aldrich) solution. Only the colonies formed by cells with metabolic activity are able to reduce MTT to formazan, forming dark blue crystals. Colonies with a diameter <100  $\mu$ m were excluded from the analysis.

### **ALDEFLUOR assay**

The ALDEFLUOR™ kit (STEMCELL Technologies, 01700) was used to analyze the subpopulation with the high ALDH enzymatic activity which has been considered as the marker of pancreatic CSCs. The assay follows the protocols suggested by the manufacturer.  $1 \times 10^6$  cells were suspended in ALDEFLUOR assay buffer containing ALDH substrate (BAAA) and incubated in a cell incubator for 60 min at 37°C. For the negative control, each sample aliquot was treated with diethylamino benzaldehyde (DEAB), a specific ALDH inhibitor. The cell flow cytometric sorting gates were established using DEAB treated cells as negative controls.

### **Flowcytometry**

To explore the relationship between the expression of EHF and percentages of pancreatic CSCs subsets in PDAC tissues, fresh PDAC specimens were collected and

divided into two parts, one part was immediately fixed in formalin buffer and embedded in paraffin for IHC of EHF; the other part were immediately prepared into the single cell suspension with 1 mg/ml collagenase (Sigma-Aldrich, C2799), 2.5 U/ml hyaluronidase (Sigma-Aldrich, H3506) and 0.1 mg/ml DNase (Sigma-Aldrich DN25). To determine the percentages of CSCs subsets of tumor tissues, single cell suspension was divided into three parts, three different combination of CSCs markers were used, including ESA<sup>+</sup>CD44<sup>+</sup>CD24<sup>+</sup> CSCs, CD133<sup>+</sup> CSCs and ALDH<sup>+</sup> CSCs. Related antibodies were used according the instructions.

The percentages of CSCs subsets in human pancreatic cancer cell lines were also detected by flowcytometry. Three different combination of CSCs markers was used, including CD44<sup>+</sup>CD24<sup>+</sup> CSCs, CD133<sup>+</sup> CSCs and ALDH<sup>+</sup> CSCs.

Besides, the percentages of CXCR4<sup>+</sup> (biolegend, 306528) population in fresh PDAC specimens and pancreatic cancer cell lines were also determined by flowcytometry. Isotype controls were used as negative controls. The data were analyzed using soft Flow Jo 10.0.

#### **In vivo limited dilution assay**

Female 4–6-week-old NOD/SCID mice were purchased from SPF (Beijing) Biotechnology Company. All mice were maintained in specific pathogen-free conditions, and animal experiment procedures were approved by the Ethics Committee of Tianjin Medical University Cancer Institute and Hospital, in compliance with the principles and procedures of the NIH Guide for the Care and Use of Laboratory Animals.

To validate the effects of EHF on PDAC stemness, mice were randomized into four groups: (A) PANC-1-vector group, (B) PANC-1-EHF group, (C) PANC-1-scramble group, (D) PANC-1-shEHF group. In each group, cancer cells at a dilution range of  $1 \times 10^3$ ,  $1 \times 10^5$  and  $1 \times 10^6$  were suspended in a 60  $\mu$ l mix of Matrigel plug (Corning,356234) and PBS at a 1:1 ratio and then subcutaneously injected into contralateral flanks of the mice. Primary PDX1#-vector, PDX1#-EHF, PDX1#-scramble and PDX1#-shEHF cell lines was also used to repeat the experiment. Xenograft tumors were observed and measured twice a week using a caliper. All the mice were euthanized at the end of two months. Subcutaneous tumors were harvested and tumor incidence were analyzed. Stem cell frequency were calculated on website <http://bioinf.wehi.edu.au/software/elda/>.

#### **Reverse transcription PCR (RT-PCR)**

The total RNA of the cells was extracted with TRizol (Invitrogen) according to the manufacturer's instructions. Then, the mRNA was reverse transcribed to single-stranded cDNAs using a Reverse Transcription PCR (RT-PCR) System (Takara Bio Inc.). Then, real-time fluorescent quantitative PCR was used to analyze the cDNA levels. Actin was used as a loading control. Related primers were listed in supplementary table10.

#### **Western blotting**

Whole-cell extracts were prepared by lysing the cells with SDS protein lysis buffer supplemented with proteinase inhibitor cocktail (bimake, B14001). Protein lysate was separated by SDS-PAGE, and then, the target proteins were detected by Western blotting with the following primary antibodies: anti-EHF (LSBio, LS-B11884,1:5000), anti-

Sox9(abcam,ab185230,1:1000), anti-Sox2(proteintech,66411-1-Ig,1:1000), anti-Nanog(abcam, ab109250,1:1000), anti-Oct4(abcam, ab18976,1:1000), anti-CXCR4(abcam, ab124824,1:1000), anti-E-cadherin(abcam,ab1416, 1:1000), anti-CK19(abcam,ab52625,1:1000) and anti-CA II (abcam,ab124687,1:1000).  $\beta$ -tubulin (Abmart,1:5000) was used as a loading control. Secondary antibodies: Goat anti-rabbit or mouse antibody at 1:5000(Abmart).

### Cell Sorting

To determine the effects of EHF on CSCs and non-CSCs, primary pancreatic cancer cell lines were used for cell sorting. PDX1# and PDX2# primary cell lines were stained with anti-human CD133 antibody (Miltenyi Biotec, 130-118-143) and ALDEFUOR detection kit (STEMCELL Technologies, 01700), respectively; Then, CD133<sup>-</sup>, CD133<sup>+</sup>, ALDH<sup>-</sup> and ALDH<sup>+</sup> cells were sorted by FACS. The purities of sorted CD133<sup>+</sup> cells and ALDH<sup>+</sup> cells were both higher than 95%. The purities of sorted CD133<sup>-</sup> cells and ALDH<sup>-</sup> cells were both nearly 100%. Cell viability was checked by Trypan blue dye exclusion. The sorted CD133<sup>+</sup>/CD133<sup>-</sup> cells and ALDH<sup>+</sup>/CD133<sup>-</sup> cells were transfected with EHF-overexpression plasmids or siEHF. 72 hours later, cells were collected for further experiments.

### Preparation of PSC-conditioned medium

PSCs were grown to 70% to 80% confluence in 10cm dishes in complete culture media. Then the medium was replaced with FBS-free DMEM/F12 (1:1), and the cells were cultured for additional 48 h. The medium was collected, centrifuged at 1200 rpm for 5 min, and the supernatant was filtrated through a 0.22  $\mu$ m filter (Millipore Corp., Billerica, MA, USA). PSC-CM was stored at -80 °C until further use.

To obtain the serum free single cytokine depletion conditional medium, PSCs were pre-treated with serum-free medium for 48h and then the PSCs-CM was collected. The serum free PSC-CM was incubated with the neutralizing antibody of IL6, IL8 and CXCL12, etc. for 48 h at 4 °C to obtain the serum free single cytokine-depleted PSC-CM. Isotype IgG was used as control. Related information of antibodies used was listed in supplementary table 9.

### The evaluation of the increasement of PDAC stemness after treating by PSC-CM

For the medium in sphere formation assay, PSCs-CM was added into serum free medium (1:1), then the stem cells culture factors, including B27 (1:50), 20ng/ml EGF, 10ng/ml FGF2, 0.4% Bovine Serum Albumin and 5 $\mu$ g/ml insulin were added. For the control group, the medium was serum free medium with the stem cells culture factors of the same concentration. The increasement of the sphere between PSCs-CM group and control group was calculated in each cell lines. (PDAC-vector, PDAC-EHF, PDAC-scramble and PDAC-shEHF)

In order to investigate the increasement of the ability of PDACs to grow in suspension under the stimulation of PSCs-CM, their capacity to form colonies in solid agar was assessed. 500ul PSCs-CM was added to 500ul top agar, which was used to suspend PDAC-vector/ PDAC-EHF/ PDAC-scramble/ PDAC-shEHF. Control medium was used as control. The increasement of the number of clones between PSCs-CM group and control

group was calculated in each cell lines.

For the cell using in flowcytometry, PDAC-vector, PDAC-EHF, PDAC-scramble, PDAC-shEHF were seeded in 6-well plates ( $1 \times 10^5$  cells/well). The following day, the PDAC culture medium was replaced by a mix of PSC-CM and fresh 1640 medium (at a ratio of 1:1). Pure fresh 1640 medium was used as control. 48 hours later, cancer cells were collected for flowcytometry.

To validate the different effects of PSCs-CM on PDAC stemness in PDAC with different EHF expression, NOD/SCID mice were randomized into PANC-1-vector-control medium group, PANC-1-vector- PSCs-CM group, PANC-1-EHF-control medium group and PANC-1-EHF-PSCs-CM group. In each group, indicated PDAC cells at a dilution range of  $1 \times 10^3$ ,  $1 \times 10^5$  and  $1 \times 10^6$  were suspended in a 60 $\mu$ l mix of Matrigel and PBS at a 1:1 and then subcutaneously injected into the contralateral flanks. Eight mice for each dilution. 200  $\mu$ l PSCs-CM or culture medium were injected intratumorally three times a week. PDX1#-vector and PDX1#-EHF were also used to repeat the experiment. Seven mice for each dilution.

To determine EHF decreased the sensitivity of PDACs to PSCs derived CSC-supporting stimulus through CXCR4, cell lines of BxPC3-scramble-scramble, BxPC3-shEHF-scramble, BxPC3-scramble-shCXCR4, BxPC3-shEHF-shCXCR4 were set up. Mice were randomized into BxPC3-scramble-scramble-control medium, BxPC3-scramble-scramble-PSCs-CM, BxPC3-shEHF-scramble-control medium, BxPC3-shEHF-scramble-PSCs-CM, BxPC3-scramble-shCXCR4-control medium, BxPC3-scramble-shCXCR4-PSCs-CM, BxPC3-shEHF-shCXCR4-control medium, BxPC3-shEHF-shCXCR4-PSCs-CM. The increasements of the tumorigenicity between PDAC-PSCs-CM and PDAC-control medium were compared between cell lines.

### **The evaluation of the increasement of PDAC stemness after stimulated by CXCL12**

To explore the difference of the effects of CXCL12 on sphere formation promoting in PDAC with different EHF expression, human recombinant CXCL12 were added into the serum-free medium for cancer cell sphere formation assay. The final concentration of CXCL12 was 100ng/ml.

To explore the difference of the effects of CXCL12 on promoting anchorage-independent growth in PDAC and PDAC-EHF, human recombinant CXCL12 (100ng/ml) was added into RPMI 1640 containing 20% FBS for further culture system. Cells were incubated for 3 weeks and the conditional medium was replaced every 3 times a week.

For the cell using in flowcytometry, PDAC-vector, PDAC-EHF, PDAC-scramble, PDAC-shEHF were seeded in 6-well plates ( $1 \times 10^5$  cells/well). The following day, the PDAC culture medium was replaced by a mix of 1640 contained with 100ng/ml CXCL12. 1640 medium was used as control. 48 hours later, cancer cells were collected for flowcytometry and western blot.

To validate the different effects of CXCL12 on PDAC stemness in PDAC with different EHF expression, NOD/SCID mice were randomized into PANC-1-vector-control medium group, PANC-1-vector-CXCL12 group, PANC-1-EHF- control medium group and PANC-1-EHF-CXCL12 group. In each group, indicated PDAC cells at a dilution range of  $1 \times 10^3$ ,  $1 \times 10^5$  and  $1 \times 10^6$  were suspended in a 60 $\mu$ l mix of Matrigel and PBS at a 1:1 and then

subcutaneously injected into contralateral flanks. Eight mice for each dilution. Human recombinant CXCL12 or culture medium were injected intratumorally three times a week. PDX1#-vector and PDX1#-EHF were also used to repeat the experiment. Seven mice for each dilution. Tumor proliferation was monitored twice a week. Mice were sacrificed after 2 months. Subcutaneous tumors were harvested and tumor incidence were analyzed. Stem cell frequency was calculated on website. <http://bioinf.wehi.edu.au/software/elda/>.

### **Chromatin immunoprecipitation (Ch-IP) and luciferase analysis**

Ch-IP assays were performed using Ch-IP kit (Millipore) according to the manufacturer's instructions. To detect if EHF directly bound to de promoter region of Sox2, Sox9, Nanog, Oct4, CXCR4, PANC-1 were immunoprecipitated with anti-EHF antibody (abcam, ab220113). Then the immunoprecipitated products were detected by PCR. Related primers were listed in supplementary table 10. To detect if EHF directly suppressed the transcriptional activity of CXCR4, luciferase analyses were conducted using dual-luciferase reporter assay kit (Promega, E1910). PANC-1 and 293T cells were transfected with pCDH-EHF plasmid or control vector (pCDH-vector), which were subsequently transfected with pGL3-CXCR4-EBS1-wt and pGL3-CXCR4-EBS1-mut, respectively. Forty-eight hours later, cells were subjected to dual luciferase analysis. Related sequences of the vectors for luciferase analysis were listed in supplementary table 11.

Similarly, to elucidate if PPAR $\gamma$  directly bound to the promoter region and suppressed the transcriptional activity of EHF, PANC-1 were immunoprecipitated with anti-PPAR  $\gamma$  (abcam, ab45036). The immunoprecipitated products were detected by PCR. PANC-1 was transfected with pGL3-EHF-PPRE(WT) plasmid or control vector(pGL3-vector).Then PANC-1 were treated with 10 $\mu$ M rosiglitazone for 24 hours. DMSO was used as negative control. Renilla reporter plasmid was used as internal control. Forty-eight hours later, cells were subjected to dual luciferase analysis.

The information of the related Ch-IP primers was listed in supplementary table 10. The results of luciferase analysis were expressed as a fold induction relative to the cells transfected with the control vector after normalization to Renilla activity.

### **In vitro drug-screening for EHF agonists among drugs of routine medication**

For EHF agonists screening, 1 $\times$ 10<sup>5</sup> PANC-1 were suspended with DMEM (10%FBS) and seeded in 6-well plates. 12 hours later, PANC-1 was adherent to the bottom of the plate, the medium was replaced with 1ml DMEM (10%FBS) with 10  $\mu$  M compounds added, the cells were cultured for additional 24 h. Then cells were collected for evaluating EHF expression by western blot. Detailed compounds information was listed in supplementary table 3.

### **In vitro evaluation of the therapeutic effect of rosiglitazone**

To evaluate the effects of rosiglitazone on the maintenance of the stemness of PDACs, adherent cancer cells were pre-treated with 5 $\mu$ M rosiglitazone(Sigma,R2408) for 48 hours (DMSO was used as control) , which were collected for sphere formation assays. To avoid cellular toxicity, no continuous infusion of rosiglitazone was added into sphere formation system. After 2 weeks, tumor spheres with diameter>75 $\mu$ m were counted.

### **In vivo evaluation of the therapeutic effect of rosiglitazone**

To evaluate the effects of rosiglitazone on PDAC stemness under the stimulus of CXCL12, NOD/SCID mice were randomized into four groups (DMSO was used as the control for rosiglitazone, culture medium was used as the control for CXCL12): (A) control medium +DMSO, (B) control medium +rosiglitazone, (C) CXCL12+DMSO, (D) CXCL12+rosiglitazone. In each group, PANC-1 cells at a dilution range of  $1 \times 10^3$ ,  $1 \times 10^5$  and  $1 \times 10^6$  were suspended in a 60  $\mu$ l mix of Matrigel and PBS at a 1:1 ratio and then subcutaneously injected into mice. One week later, rosiglitazone (100mg/kg/day; DMSO was used as control) and human recombinant CXCL12 protein (20  $\mu$ g/mouse/day; control medium was used as control) were intratumorally injected three times a week. Tumor proliferation was monitored twice a week. Mice were sacrificed after 2 months; subcutaneous tumors were harvested and tumor incidence were analyzed. Stem cell frequency were also calculated on website <http://bioinf.wehi.edu.au/software/elda/>.

To better determine the effects of rosiglitazone on PDAC,  $5 \times 10^5$  PANC02-luc cell was resuspended using a 40  $\mu$ l mix of matrigel plug and PBS(1:1) per mouse for the establishment of orthotopic tumor models. BABL/C nude were randomized into two groups :(A) DMSO control group(n=8), (B) rosiglitazone treatment group(n=8). One week after tumor inoculation, rosiglitazone (100mg/kg/day) or DMSO were injected intraperitoneally three times a week and continued to one month. Tumour growth was analysed by bioluminescent imaging (BLI) twice a week. Pancreatic tumours were harvested for further experiments at the end of one month. To evaluate the effects of rosiglitazone on ALDH<sup>+</sup> cells, fresh tumour tissues were prepared into the single cell suspension with 1 mg/ml collagenase, 2.5 U/ml hyaluronidase and 0.1 mg/ml DNase and then cells were stained with ALDEFUOR kit for flowcytometry analysis (PI was used to exclude dead cells and CD45 was used to exclude leukocytes). IHC and western blot on tumor tissues were carried out to detect the expression of EHF and stemness markers (Sox9, Sox2, Nanog and Oct4). Another cohort of orthotopic tumor models were also established which received the same treatment in each groups Motilities of the mice were recorded and survival curves were plotted.

To determine if rosiglitazone suppressed the stemness of PDAC mostly via EHF, PANC02-ctrl-luc and PANC02-EHF-KO-luc cell lines were established. BABL/C nude mice were randomized into two groups: (A) DMSO control group, (B) rosiglitazone treatment group. In each group, pancreatic orthotopic tumor models was established using a 40  $\mu$ l mix of matrigel plug and PBS(1:1) per mouse containing  $5 \times 10^5$  PANC02- ctrl-luc(n=8) or PANC-EHF-KO(n=8) cell lines. One week later, rosiglitazone (100mg/kg/day) or DMSO were injected intraperitoneally three times a week and drug treatment was continued to one month. Tumour growth was analysed by bioluminescent imaging (BLI) twice a week. Motilities of mice was recorded and survival curves were plotted.

### **Breeding and genotyping analysis for KPC mice model**

LSL-KrasG12D/+ mice, LSL-Trp53R172H/+ and Pdx1-Cre mouse model was a gift from the Stephen J. Simpson Lab (Broadway Research Building at Johns Hopkins University, USA) and mice were maintained in specific pathogen-free conditions. The breeding

strategy to get KPC mice often started with crossing LSL-Kras<sup>G12D/+</sup> mice with LSL-Trp53<sup>R172H/+</sup> mice to obtain LSL-Kras<sup>G12D/+</sup>; LSL-Trp53<sup>R172H/+</sup> (KP) mice. LSL-Kras<sup>G12D/+</sup>; LSL-Trp53<sup>R172H/+</sup> mice (KP) male mice were then crossed with Pdx-1-Cre female mice to generate LSL-Kras<sup>G12D/+</sup>; LSL-Trp53<sup>R172H/+</sup>; Pdx-1-Cre (KPC) mice. Genomic DNA of mice tails were purified by Mouse direct PCR kit (Bimake, B40013) and then polymerase chain reaction (PCR) was performed for the genotyping of KPC mice. The primer sequences and PCR conditions for the genotyping of KPC mice were listed in supplementary table 7-8. All animal experiment procedures were approved by the Ethics Committee of Tianjin Medical University Cancer Institute and Hospital, in compliance with the principles and procedures of the NIH Guide for the Care and Use of Laboratory Animals.

### Ultrasound imaging for pancreatic tumor in KPC mice

Pancreatic tumor of KPC mice were monitored by the VEVO2100 ultrasound imaging system (Visual Sonics). KPC mice were anesthetized and taped to the imaging stage. KPC mice were imaged in supine position; then, images of pancreas were captured using the abdominal package in B-Mode and long diameter/short diameter of pancreatic tumor were measured. Tumor volume(V) was calculated by the following formula:  $V = (\text{long diameter}) \times (\text{short diameter})^2/2$ .

### Preclinical animal cohorts

Pancreatic tumor volume of KPC mice were monitored twice a week by the VEVO2100 ultrasound imaging system (Visual Sonics). When pancreatic tumor of KPC mice initiated and reached 20~60mm<sup>3</sup>, mice were then randomized into four groups: (A) vehicle (Corn oil purchased from Sigma, C8267; 1.0ml/kg once a day by oral gavage), (B) gemcitabine (purchased from MCE, HY-17026; 25mg/kg intraperitoneally once a week), (C) rosiglitazone (purchased from Sigma, C2408; rosiglitazone were pre-dissolved in olive oil; 100mg/kg once a day by oral gavage), (D) gemcitabine +rosiglitazone. Mice were separated in 2 sets. For set 1(8 mice per group), drug was administrated when the tumor reached 20~60mm<sup>3</sup> until death. In set 2 (6 mice per group), mice were treated like in set 1 but killed after 8 weeks of treatment to compare tissues. The volume of pancreatic tumor was monitored twice a week by the VEVO2100 ultrasound imaging system. For mice in set 2, pancreatic tumor tissues were harvested and weighed. Tumor tissues were divided into three parts: first part was immediately made into single cell suspensions and prepared for detection of ALDH activity by flow cytometry (PI was used to exclude dead cells and CD45 was used to exclude leukocytes); second part of the tumor tissues were immediately fixed in buffered formalin and embedded in paraffin and another part were kept at -80°C for protein extraction and western blot analysis. Tissue slides(5μm) were prepared and Hematoxylin & Eosin (H&E) staining were performed for histopathological analysis according to instructions. IHC of Ki67 (abcam, ab16667) staining were performed to evaluate proliferation status of tumor tissues. Tissues protein from vehicle group and rosiglitazone group were prepared for western blot to analyze the expression of EHF and stemness markers (Sox9, Sox2, Nanog and Oct4).

### In vitro evaluation of the therapeutic effect of ibuprofen and allopurinol

To evaluate the effects of ibuprofen and allopurinol on the maintenance of the stemness of PDACs, adherent cancer cells were pre-treated with 1mM ibuprofen (sigma, I4833) or 5 mM allopurinol (sigma, PHR1377) for 48 hours (DMSO was used as control), which were collected for flowcytometry analysis of CD44<sup>+</sup>CD24<sup>+</sup> cells, western blot of stemness genes (Sox9, Sox2, Nanog and Oct4) and sphere formation assays. To avoid cellular toxicity, no continuous infusion of ibuprofen or allopurinol was added into sphere formation system. After 2 weeks, tumor spheres with diameter >75µm were counted.

#### **In vivo evaluation of the therapeutic effect of ibuprofen and allopurinol**

To evaluate the effects of ibuprofen or allopurinol on PDAC stemness, NOD/SCID mice were randomized into two groups (DMSO was used as the control): (A) DMSO group (B) ibuprofen or allopurinol group, PANC-1 cells at a dilution range of  $1 \times 10^3$ ,  $1 \times 10^5$  and  $1 \times 10^6$  were suspended in a 60µl mix of Matrigel and PBS at a 1:1 ratio and then subcutaneously injected into 4-6-week-old NOD/SCID mice. One week later, ibuprofen (45mg/kg/day; DMSO was used as control) or allopurinol (30mg/kg/day; DMSO was used as control) were peritumorally injected three times a week. Tumor proliferation was monitored twice a week. Mice were sacrificed after 2 months; subcutaneous tumors were harvested and tumor incidence were analyzed. Stem cell frequencies were also calculated on website <http://bioinf.wehi.edu.au/software/elda/>. Proportion of ALDH<sup>+</sup> cells in subcutaneous tumors were analyzed by flowcytometry.